THE UNIVERSITY OF QUEENSLAND

AUSTRALIA

Exploring engineered solid-state single-photon emitter as multi-photon sources

Nor Azwa Zakaria

M.Sc.

iD

0000-0001-6486-5247

A thesis submitted for the degree of Doctor of Philosophy at
The University of Queensland in 2020
School of Mathematics and Physics

ABSTRACT

Recent years has seen a breakthrough in developing photon sources based on artificial atom semiconductor quantum dots (QDs). New fabrication techniques have allowed to structure photonics to be manufactured around single quantum dots, enabling spatial, temporal and frequency control of the photon emission properties. In this thesis I presented two generations of such devices, where the quantum dots are respectively embedded in passively and actively controlled micropillar cavities. Each device is driven by different optical pumping schemes; non-resonant, quasi-resonant and resonant excitations. The first-generation device produced single photons with near-unity indistinguishability, and high brightness of 14% at the output of the single mode fibre. The first generation device also demonstrated long stream of photons exhibiting high two-photon interference—even when the photons are produced more than 400ns apart. The performance of the device brings solid-state sources into a regime suitable for scalable implementations. With such brightness I created a multi spatial-mode photon source using active spatial and temporal photonic demultiplexing. The second-generation device was driven by a coherent pumping scheme where the transition energy of the dot can be controlled via the induced electric-field Stark shift. Using independent single photons from the second-generation device, I realised an event-ready entangled photon pairs using linear photonics via Type II fusion gate operation. In this gate conditional detection of photons at the ancilla output ports prepares the photons 2 and 3 in a maximally entangled state. This technique allows a single-photon source to be converted into an event-ready source of polarization-entangled photon pairs with much brightness that previous possible. I investigate the effect of single-photon indistinguishability on the entanglement generated by the gate, and I also characterise the generated entangled states using quantum state tomography. This is a scalable architecture for producing entangled photons, important for quantum information processing and fundamental test of quantum mechanics.

DECLARATION BY AUTHOR

This thesis is composed of my original work, and contains no material previously published or written by another person except where due reference has been made in the text. I have clearly stated the contribution by others to jointly-authored works that I have included in my thesis.

I have clearly stated the contribution of others to my thesis as a whole, including statistical assistance, survey design, data analysis, significant technical procedures, professional editorial advice, financial support and any other original research work used or reported in my thesis. The content of my thesis is the result of work I have carried out since the commencement of my higher degree by research candidature and does not include a substantial part of work that has been submitted to qualify for the award of any other degree or diploma in any university or other tertiary institution. I have clearly stated which parts of my thesis, if any, have been submitted to qualify for another award.

I acknowledge that an electronic copy of my thesis must be lodged with the University Library and, subject to the policy and procedures of The University of Queensland, the thesis be made available for research and study in accordance with the Copyright Act 1968 unless a period of embargo has been approved by the Dean of the Graduate School.

I acknowledge that copyright of all material contained in my thesis resides with the copyright holder(s) of that material. Where appropriate I have obtained copyright permission from the copyright holder to reproduce material in this thesis and have sought permission from co-authors for any jointly authored works included in the thesis.

PUBLICATIONS INCLUDED IN THIS THESIS

Publications included in this thesis

1. J.C. Loredo, **N. A. Zakaria**, N. Somaschi, C. Anton, L. de. Santis, V. Giesz, T. Grange, M. A. Broome, O. Gazzano, G. Coppola, A. Sagnes, A. Lemaitre, A. Auffeves, P. Senellart, M. P. Almeida, and A. G. White, Scalable performance in solid-state single-photon sources, *Optica*, 3(4), 433-440, 2016. This is incorporated as Chapter 3 in this thesis.

Contributor	Statement of contribution	% Contribution
N. A. Zakaria (Candidate)	Design and construction of experiment	25%
	Preliminary and final data acquisition	50%
	Contribution to the manuscript	10%
J. C. Loredo	Initial development of the concepts	50%
	Design and construction of experiment	50%
	Final draft of the manuscript	70%
	Referee replies and final manuscript revision	50%
N. Somaschi	Design and construction of experiment	5%
	Preliminary and final data acquisition	5%
C. Anton	Design and construction of experiment	5%
	Preliminary and final data acquisition	5%
L. De Santis	Design and construction of experiment	5%
	Preliminary and final data acquisition	5%
V. Giesz	Design and construction of experiment	5%
	Preliminary and final data acquisition	5%
T. Grange	Theoretical model	70%
M. A. Broome	Design and construction of experiment	5%
	Preliminary and final data acquisition	5%
O. Gazzano	Design and construction of experiment	5%
	Preliminary and final data acquisition	5%
G. Coppola	Design and construction of experiment	5%
	Preliminary and final data acquisition	5%
I. Sagnes	Etching of micropillar cavities	100%
A. Lemaitre	Growth of quantum dots	100%
A. Auffeves	Theoretical model	30%
P. Senellart	Initial development of concept	25%
	Data analysis and interpretation	10%
	Complete first draft of manuscript	15%

Contributor	Statement of contribution	% Contribution
	Final draft of manuscript	15%
	Referee replies and final manuscript revision	30%
M. P. Almeida	Initial development of concept	25%
	Design and construction of experiment	10%
	Data analysis and interpretation	10%
	Referee replies and final manuscript revision	10%
A. G. White	Initial development of concept	30%
	Data analysis and interpretation	10%
	Complete first draft of manuscript	15%
	Final draft of manuscript	15%
	Referee replies and final manuscript revision	10%

2. F. Lenzzini, B. Haylock, J. C. Loredo, R. A. Abrahao, **N. A. Zakaria**, S. Kasure, I. Sagnes, A. Lemaitre, H-P. Phan, D. V. Dao, P. Senellart, M. P. Almeida, A. G. White, and M. Lobino, Active demultiplexing of single photons from a solid-state source, *Lasers & Photonics Review*, 11, 1600297, 2017. This is incorporated as Chapter 4 in this thesis.

Contributor	Statement of contribution	% Contribution
Contributor	Statement of contribution	% Contribution
N. A. Zakaria	Design and construction of experiment	25%
(Candidate)	Preliminary and final data acquisition	50%
	Contribution to the manuscript	10%
F. Lenzzini	Initial development of the concepts	50%
	Device fabrication	50%
	Final draft of the manuscript	70%
	Referee replies and final manuscript revision	50%
B. Haylock	Design and construction of experiment	50%
	Device fabrication	50%
	Preliminary and final data acquisition	50%
	Contribution to the manuscript	25%
J. C. Loredo	Design and construction of experiment	25%
	Preliminary and final data acquisition	50%
	Contribution to the manuscript	25%
R. A. Abrahao	Design and construction of experiment	5%
	Preliminary and final data acquisition	5%
S. Kasure	Growth of quantum dots	100%
I. Sagnes	Etching of micropillar cavities	100%
A. Lemaitre	Growth of quantum dots	100%
H-P. Phan	Growth of quantum dots	100%
D. V. Dao	Growth of quantum dots	100%

P. Senellart	Final draft of manuscript	15%
	Referee replies and final manuscript revision	20%
M. P. Almeida	Data analysis and interpretation	10%
	Final draft of manuscript	15%
	Referee replies and final manuscript revision	20%
A. G. White	Data analysis and interpretation	10%
	Final draft of manuscript	15%
	Referee replies and final manuscript revision	30%
M. Lobino	Initial development of concept	25%
	Data analysis and interpretation	10%
	Complete first draft of manuscript	15%
	Final draft of manuscript	15%
	Referee replies and final manuscript revision	30%

Submitted manuscripts included in this thesis

None

OTHER PUBLICATIONS DURING CANDIDATURE

Conference abstracts

1. **N. A. Zakaria** *et al.,* Solid-state single photons for quantum photonics, Annual Workshop of the ARC Centre of Excellence for Engineered Quantum System (EQUS), Noosa, Australia, 2016. *Poster presentation.*

2. **N. A. Zakaria** *et al.,* Scalable performance in solid-state single -photon sources, APPC-AIP Congress 2016 (Joint 13th Asian Pacific Physics Conference and 22nd Australian Institute of Physics Congress incorporating the Australian Optical Society Conference), Brisbane, Australia, 2016. *Poster presentation.*

3. **N. A. Zakaria** *et al.,* Scalable performance in solid-state single -photon sources, 3rd Australian and New Zealand Conference on Optics and Photonics (ANZCOP), Queenstown, New Zealand, December, 2017. *Poster presentation*

4. **N. A. Zakaria** *et al.,* Scalable performance in solid-state single -photon sources, Annual Workshop of the ARC Centre of Excellence for Engineered Quantum System (EQUS), Sydney, Australia, 2017. *Poster presentation.*

5. **N. A. Zakaria** *et al.,* Solid-state single photons for quantum photonics, 23nd Australian Institute of Physics Congress (AIP), Perth, Australia, December, 2018. *Oral presentation.*

Contributions by others to the thesis

Prof. Andrew White and Dr. Marcelo De Almeida supervised throughout my candidature. Prof. Andrew White provided critical feedback, editing, proof-reading and supervision of this thesis. Prof. Jacquiline Romero revised the Abstract of this thesis.

Statement of parts of the thesis submitted to qualify for the award of another degree

None.

Research involving human or animal subjects

No animal or human subjects were involved in this research

ACKNOWLEDGEMENTS

Alhamdulillah for the times when His blessings are so obvious. For the times when it's hard to see the good but you know it's there. For the challenges that come with an opportunity to grow. For the trials in this life that elevate us in the next. *Alhamdulillah* for it all.

This thesis is dedicated specially for both of my parents—**Zaiton Abu Bakar** & **Zakaria Abdullah**. You two are the pillar of my strength.

My PhD journey started with my advisor, Andrew White. Thank you for being my constant encouragement source during my roller coaster journey. From our first interview until the completion of this thesis, your endless supports is beyond a PhD candidate could ever asked for. It shapes me into a confident and resilience person that I never imagine. Thank you for the opportunities given to me exploring physics while just being "present". You made my gloomy winter less lonely and scorching summer enjoyable! I would like to extend my appreciation to Marcelo De Almeida; for letting me explored the QT lab while enjoying the cringing sound of cryostat. Thank you for trusting me with the dot and had me as your side kicked during major operation; aligning the Ti:Sap laser, installing new electrically tunable dot. Those priceless experiences are something that I could never get out of a manual book. I can proudly call myself an experimentalist!

Not to mention Till and Jacqui for always checking on me throughout my time at UQ. I will surely miss our coffee time together, Jacqui! Now I have more time and zero excuses to do yoga. Life as a Phd student will not be fun without my QT-labers; Kaumudi, Jihun, Micheal, Leo, Ming Su, and Lewis. It has been a great pleasure to work and endless discussion with you guys. Kaumudi, Jihun, and Micheal, thank you for always keeping your door open and letting me ranting on my long tedious days in the lab. Being the only female experimentalist in the last two years certainly hard but I know I can count on your shoulders. To the kind soul—Christina Giarmatzi—I can't thank you enough for the mental health support you offered me. Knowing that someone who also there for me is comforting. Not to mention, Sarah Lau; I will cherish our memories in kayaking, shared room during workshops, Boost sessions and obviously between-the-break-coffee. You surely make my journey less lonely. You words on *"Your PhD doesn't define who you are"* will be forever craved in my heart.

What would i do without my Brisbane-family; Effa, Najaa, Nora, Zan, and Kak Jah. Thank you for all the helps offered during tough times. You guys spoiled me with scrumptious home-cooked meals when I was homesick, celebrated my birthdays and slept-over when I needed company. I will surely miss our hiking days; Mount Coot-Tha, Mount Tohey, Mount Nebo, Whiterock, Mount Glorious. I am glad we made the all the trips back in those years. Effa, I

am finally out of the dark space! Najaa, we should go on more hiking in the future. Zan, you have no idea how you are my source of inspiration. I will see you at the end tunnel! Nora, your thirst in knowledge amazed me. Kak Jah, thank you for showering me with love and constant supports.

To my better half—Muhammad Shahazmi Zambri, I am forever grateful for you to take this journey with me. We built our early years of marriage in Brisbane and that was the most important chapter in my life. You are the light during my darkest day and I could not have done without you. Thank you for your tremendous help around the house when the hours in the lab were longer than I thought. Our late night conversation when my laser in the lab broken proves how great listener you are. I love you. Maybe we can start watching of your favourite movies; Star Wars from back to back?

For my family in Kemaman; Ayah, Mak. I am extremely grateful for your infinite prayers and unconditional love. I am forever indebted to you two for encourage me to go with my own journey and create my own path. This path would not have been possible if not for you two, and for that, I dedicate this milestone to you two.

For my siblings; Hussein Zakaria, Nor Ain Zakaria, and Zharfan Zakaria. You guys know how to keep me sane while being away from our family for such a long period time. To Tokwan and Ciksu, for the warm loving thoughts even from far away. Not to forget my parents in law; Abah and Mak. Thank you for be so understanding during my thesis writing months. Last not least, my two oldest friends; Nadiah Zainudin and Hilawati Hamzah. I still can not believe you two came visit me no matter I where was. True friend last even if you've not met for months or years, or when distance apart. When we meet again, you continue from where you last left off. Finally, to myself, you've made it, Azwa!

Done and dusted!

Financial support

Keywords

Keywords: photonics, quantum information, quantum optics, solid-state single-photon source, entangled photons

Australian and New Zealand Standard Research Classifications (ANZSRC)

1. ANZSRC code: 020603 Quantum Information, Computation and Communication 80%

2. ANZSRC code: 020604 Quantum Optics, 20%

Fields of Research (FoR) Classification

FoR code: 0206 Quantum Physics, 80%
FoR code: 0205 Optical Physics, 20%

x

CONTENTS

LIST OF FIGURES

LIST OF TABLES

LIST OF ABBREVIATIONS AND SYMBOLS

Abbreviations	
SPDC	spontaneous parametric down conversion
QD	quantum dots
DBR	Distributed Brag Reflectors
TTM	Time-tangging measurement
SE	spontaneous emission
HOM	Hong-Ou-Mandel
MBE	molecular-beam epitaxy
APD	avalanche photodiode
FWHM	full width at half maximum
HWP	half wave plate
QWP	quarter wave plate
LN	Lithium niobate
MuChOS	Multiple Channel Optical Switch
FGPA	field programmable gate array
PLL	phase-locked loops
PBS	polarising beam splitter
RPBS	rotating polarizing beam splitter

Symbols	
$g^{(2)}$	second-order correlation
$\hat{a}$	annihilation operators
$\hat{a}^\dagger$	creation operators
V	visibility
V_{HOM}	HOM visibility
$C_\perp$	coincidence count
R	Hong-Ou-Mandel
B_{exp}	brightness at first lens
I_x	photon count rate for X line
τ_x	lifetime of the X line
F_p	Purcell factor
β	spontaneous emission
g	coupling strength
e	electron charge
ϵ_0	permittivity of free space
ϵ	elective dielectric constant of the host

m_0	free-space mass of electron
f	QD exciton's oscillator strength
V_m	mode volume of the cavity
E_0	energy level
γ_x	full width at half maximum of exciton
γ_c	full width at half maximum of photon
$\hbar$	Plank's constant
Q	cavity quality factor
γ	radiative decay rate
γ_0	isotropic rate
R_0	asymptotic rate value
P_0	saturation power
P	power
T	temperature
X	neutral exciton
η_{setup}	efficiency of setup collection
$\Delta\tau_e$	temporak distance
$\mathcal{R}$	reflectivity of the beam splitter
$\mathcal{T}$	transmissivity of the beam splitter
δt	time-bins
N	integration constant
γ_i^*	pure dephasing rate
$\delta\omega$	frequency detuning
ω	frequency
A	average area under peaks
$\triangle\beta$	phase mismatch
$S_{DM}(n)$	scale efficiency of demultiplexer
η_{DM}	switching efficiency
H	horizontal polarisation
V	vertical polarisation
α, β	complex number
$|\psi|^2$	probability amplitude
$\hat{\rho}$	density-matrix operator
ψ_i	probability light field
$\hat{O}$	observable
$\hat{a}_H, \hat{b}_H, \hat{b}_V, \hat{b}_V$	transformation of the beam splitters
U	matrix of the beam splitter
D	diagonal polarisation
C	concurrence
λ_i	eigenvalues
F	fidelity

To every cup of coffee—Hussein

And Ayah, this is for you.

CHAPTER 1

INTRODUCTION

Advances in fabrication technology have seen quantum photonics rapidly move from proof-of-concept to engineered systems. The ideal platform will combine single-photon sources and detectors in one optoelectronic device. Those platforms will be compact, robust, and enable quantum applications from sensing through communication to computation. A fundamental element of the platform is the single-photon source. Single photons are desirable in quantum information because of their: intrinsic low decoherence; multiple available degrees of freedom for encoding information— polarisation, path, transverse spatial mode; obvious advantages for communication [1]; and their high error threshold in quantum communication [2]. Over the last half a century, various techniques have been studied to generate single photons. Kimble et al., (1977)[3] were the first to observe single photons, seeing anti-bunching from the sodium atomic transition, albeit with very low efficiency. Photons from such atomic resources require complex set-ups and the operating rate is low due to the dynamic of atom-based sources.

Fast forward to today and we recently have become able to control atoms—both natural [4, 5] and artificial [6, 7]—and hence generate photons on demand with near-identical wave packets. Previously, the preferred source for generating photons was using a nonlinear process such as spontaneous parametric down conversion [8] (SPDC). This is the most widely used nonclassical light source, where the process generates two single photons into different spatial modes where one down-converted photon is used to herald the other one. This source is a well established in generating near ideal Fock states of n=1, i.e with photon indistinguishability close to unity, albeit by conditioning on detector. However, the probability to collect one photon per laser pulse is extremely low, in the range between 10^{-4} to 10^{-2} and this is a strong limiting factor for scaling their use in more complicated quantum information experiments. Increasing the pump power does increase the probability but reduces the multiphoton suppression of the emitted photons. Furthermore, the probabilistic nature ensures that photons are emitted at random. This in particular makes it difficult to perform complex information processing task using single photons from multiple down conversion sources.

One of the most promising types of single-photon sources today are solid-state quantum emitters [9] such as quantum dots (QDs), colour centres in diamond [10], defects in solid [11], two-dimensional hosts [12] and carbon nanotubes [13]. Quantum dots also known as artificial atoms display outstanding optical properties as well as having properties desirable for scalable system integration. Semiconductor quantum-dot single-photon sources now out

perform downconversion by simultaneously achieving high brightness, singe photon purity, and indistinguishability. They have been used in pivotal applications such as quantum teleportation [14, 15] and Boson Sampling [16].

In a bulk material, photon emission occurs in random directions, resulting in poor single-photon collection efficiencies. This problem can be circumvented by embedding the quantum dot in a cavity [17, 18]. For example, Figure 1.1 shows a micropillar cavity formed by a thick cylindrical layer of two highly reflective mirrors called Distributed Brag Reflectors (DBRs). With the presence of the cavity, the emission is directed into a well-defined frequency and propagation mode—the cavity mode—leading to high collection efficiencies. Additionally, in a weak coupling regime, the Purcell effect enhances the spontaneous emission from the dot and minimises dephasing process known to degraded single-photon indistinguishability.

This thesis encompasses two generations of device based on InGaAs quantum dots deterministically embedded into photonic cavities. The first device is InGaAs quantum-dots in micro-cavities where we optimised the optical delivery and collection of the photon source, achieving a then record brightness of 14%. This brightness allowed an improvement in applications by other authors — e.g 10^3 more efficient in Boson Sampling [16] as well as a fast demultiplexer [19]. As a results, Boson sampling protocol can be completed with faster than other devices [20–23] due to rich photon influx. The ability to establish those parameters in the first generation device gave us a strong platform experimental and theoretical platform to move forward with the second generation of devices. The second generation is the latest technology, combining deterministic fabrication [6, 24] QD with electricaly tunable cavities. This tuning means that charge noise in the surrounding QD can be controlled, resulting in higher photon extraction efficiency and allowing us to achieve event-ready entanglement using single photons from our source.
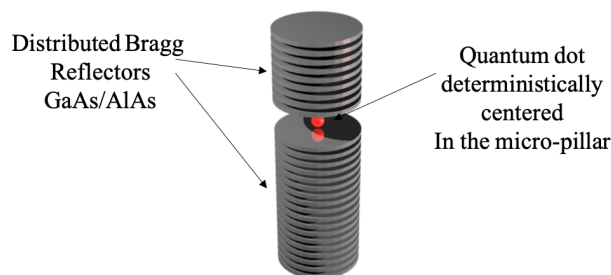
Figure 1.1: Semiconductor QD inserted in a micropillar cavity

1.1 Thesis outline

This thesis is structured as follows:

Chapter 2 discusses ideal single-photon sources. Next, I will explain the figures of merit for an ideal single photon that are commonly use in the quantum dot community. In order to introduce our devices it is necessary to discuss the fundamentals of cavity-based coupling and different types of excitation schemes. Ultimately, I will introduce to our two generations of

quantum-dot devices, respectively embedded in passive and active tuned micropillar cavities.

Chapter 3 is the work done with collaborators [25] using our first generation of devices during the first year of my PhD. Investigation on the long-time indistinguishability between consecutively emitted photon is the core of this chapter. Our first generation of device resulted in approximately one in seven laser pulses containing a high quality single-photon that can be sent directly to another multiphoton experiment such as Boson Sampling [16].

Chapter 4 presents a scheme for active demultiplexing using an integrated waveguide device. Owing to our high indistinguishability and brightness, we were able to demonstrate temporal-to-spatial demultiplexing. The performance of the device enabled a six-photon rate three-orders-of magnitude higher than the equivalent downconversion source.

Chapter 5 will begin with a short overview on quantum entanglement and how entangled pairs are generated. I then will outline a scheme that generates entangled photon pairs using measurement. Using this scheme, we realised event-ready entangled photons using the deterministic second-generation devices and linear-optical elements. Next, I discuss the effect of single-photon indistinguishability on the entanglement generated by the gate. We also characterise the generated entangled states using quantum state tomography

Chapter 6 concludes the works done, discusses the future steps in order to enable the full scalability of quantum dot-based single-photon sources for quantum technologies.

REFERENCES

[1] Chaiwongkhot, P. *et al.* Enhancing secure key rates of satellite qkd using a quantum dot single-photon source. *arXiv preprint arXiv:2009.11818* (2020).

[2] Gisin, N. & Thew, R. Quantum communication. *Nature Photonics* **1**, 165 (2007).

[3] Kimble, H. J., Dagenais, M. & Mandel, L. Photon antibunching in resonance fluorescence. *Physical Review Letters* **39**, 691 (1977).

[4] Bloch, I. Quantum coherence and entanglement with ultracold atoms in optical lattices. *Nature* **453**, 1016 (2008).

[5] Udem, T., Holzwarth, R. & Hänsch, T. W. Optical frequency metrology. *Nature* **416**, 233 (2002).

[6] Somaschi, N. *et al.* Near-optimal single-photon sources in the solid state. *Nature Photonics* **10**, 340 EP – (2016).

[7] He, Y.-M. *et al.* On-demand semiconductor single-photon source with near-unity indistinguishability. *Nature Nanotechnology* **8**, 213 (2013).

[8] Pan, J.-W. *et al.* Multiphoton entanglement and interferometry. *Reviews of Modern Physics* **84**, 777 (2012).

[9] Senellart, P., Solomon, G. & White, A. High-performance semiconductor quantum-dot single-photon sources. *Nature Nanotechnology* **12**, 1026 (2017).

[10] Neu, E. *et al.* Single photon emission from silicon-vacancy colour centres in chemical vapour deposition nano-diamonds on iridium. *New Journal of Physics* **13**, 025012 (2011).

[11] Siyushev, P. *et al.* Coherent properties of single rare-earth spin qubits. *Nature Communications* **5**, 3895 (2014).

[12] Chakraborty, C., Kinnischtzke, L., Goodfellow, K. M., Beams, R. & Vamivakas, A. N. Voltage-controlled quantum light from an atomically thin semiconductor. *Nature Nanotechnology* **10**, 507 (2015).

[13] Ma, X., Hartmann, N. F., Baldwin, J. K., Doorn, S. K. & Htoon, H. Room-temperature single-photon generation from solitary dopants of carbon nanotubes. *Nature Nanotechnology* **10**, 671 (2015).

[14] Fattal, D., Diamanti, E., Inoue, K. & Yamamoto, Y. Quantum teleportation with a quantum dot single photon source. *Physical Review Letters* **92**, 037904 (2004).

[15] Gao, W. *et al.* Quantum teleportation from a propagating photon to a solid-state spin qubit. *Nature Communications* **4**, 2744 (2013).

[16] Loredo, J. *et al.* Boson sampling with single-photon fock states from a bright solid-state source. *Physical Review Letters* **118**, 130503 (2017).

[17] Pelton, M. *et al.* Efficient source of single photons: a single quantum dot in a micropost microcavity. *Physical Review Letters* **89**, 233602 (2002).

[18] Solomon, G., Pelton, M. & Yamamoto, Y. Single-mode spontaneous emission from a single quantum dot in a three-dimensional microcavity. *Physical Review Letters* **86**, 3903 (2001).

[19] Lenzini, F. *et al.* Active demultiplexing of single photons from a solid-state source. *Laser & Photonics Reviews* **11**, 1600297 (2017).

[20] Broome, M. A. *et al.* Photonic boson sampling in a tunable circuit. *Science* **339**, 794–798 (2013).

[21] Spring, J. B. *et al.* Boson sampling on a photonic chip. *Science* **339**, 798–801 (2013).

[22] Tillmann, M. *et al.* Experimental boson sampling. *Nature photonics* **7**, 540–544 (2013).

[23] Crespi, A. *et al.* Integrated multimode interferometers with arbitrary designs for photonic boson sampling. *Nature photonics* **7**, 545–549 (2013).

[24] Dousse, A. *et al.* Controlled light-matter coupling for a single quantum dot embedded in a pillar microcavity using far-field optical lithography. *Physical Review Letters* **101**, 267404 (2008).

[25] Loredo, J. C. *et al.* Scalable performance in solid-state single-photon sources. *Optica* **3**, 433–440 (2016).

QUANTUM DOT-MICROPILLAR CAVITIES

InGaAs semiconductor quantum-dots in micro-cavities are established as single-photon sources with unprecedented performance [1–4]. InGaAs dots have large optical dipoles, resulting in a large coupling with confined or guided optical modes, a key feature in obtaining a bright source. Their intrinsic properties make them compatible with mature technologies, allowing them to be further integrated into engineered photonic structures such as micro-cavities [5–7] or resonators[8–11]. At present, self-assembled InAs/GaAs dots currently have the highest all-around as QD-based single-photon sources [2, 4, 12–14]. Coupling those emitters into cavities is quite advantageous, since as Purcell demonstrated in 1946 [5], spontaneous emission is also influenced by the atom's surrounding environment. Therefore, inserting the dot into a micro-cavity increases the single-photon emission rates, thus improving efficiency. In this chapter I highlight what is the ideal single photon source, discussing the general figures-of-merit for single-photon sources in the quantum dots community. I then highlight the fundamental principles of cavity-based QD, focusing on photon-emission enhancement and how to enable high extraction efficiencies without comprising two-photon interference. Furthermore, I introduce different type of pumping scheme that I facilitate for our devices. There are two generation of devices InGasAs semiconductor quantum-dots which are deterministically embedded in the centre of their microcavities that will be introduced in this chapter. This first generation device achieved a record of absolute brightness of 14% with a strong suppression of the multiphoton probability $g^2(0)$=0.0130±0.0002. The second generation device is able to produce photons where the degree of entanglement scales up with nonclassical visibility. Throughout this chapter I refer to generation of single photons using both coherent and incoherent excitation of the quantum dot.

2.1 Ideal single-photon source

Single photons are the heart for many quantum technologies for instance quantum key distribution [15], linear optical quantum computing [16, 17], as well as quantum information processing [18–20] and also potential applications in real-world. Tremendous efforts have been spent towards realising a near ideal single-photon source, with demonstrations in solid-state systems transitioning from proof-of-principle to engineering devices. advancement specifically in solid-state systems. Nevertheless, the requirements for a device to achieve a perfect single-

photons are still challenging, namely—growth and fabrication technology. In the quantum-dot community [2, 11] there are three crucial parameters typically considered when characterising single-photon sources. First, the ability to produce one and only one single photon for one excitation pulse. This means near ideal probability of suppressing multiphoton emissions.

Secondly, to achieve a perfect quantum interference, the emitted photons should be indistinguishable, i.e. each emitted photons should have identical wavepackets in terms of polarisation, and spatio-temporal profile. This is a key requirement in applications such as linear optical computing and Boson Sampling [21–24].

Brightness of the device enable a series of new applications in photonics and quantum information technology. The brightness of the source represents the maximum count rate at which single photons can be collected [2, 11]. The measurement for brightness varies on the applications. It can be measured at first collection lens, or at the output of a single mode fibre. The device with high brightness is good for speed in quantum communications.

The final requirement is efficiency: each photon emitted should be collected with minimal optical losses. A few groups have realised devices which can produce single-photons with efficiency of greater than 50% [25, 26]. The state-of-art is work done by Tomm and co-workers [27] where they demonstrate fiber-end-coupling efficiency of 57%. This is achieved by employing a tunable gated quantum-dots in an open Fabry-Perot cavity.

However, the quest to find the ultimate device that posses all above requirements simultaneously is still unmet. In the race towards realising an ideal single-photon source, efforts have been invested into fabrication technology such as: improving quantum dot and cavity growth; increased positioning accuracy to ensure optimal cavity-dot resonance; as well as surface passivation to reduce scattering losses. In the next section, I will discuss the principles of measuring single-photons.

2.2 Measuring single photons

2.2.1 Single photon purity

A purity of a single-photon light field can be determined by the second-order correlation, $g^{(2)}(\tau)$ in the Hanbury Brown and Twiss experiment [28]. It can be described as follows

$$
\begin{aligned}
g^{(2)}(\tau) &= \frac{\langle I(t)I(t+\tau)\rangle^2}{\langle I(t)\rangle} \\
&= \frac{\langle \hat{a}^\dagger(t)\hat{a}^\dagger(t+\tau)\hat{a}(t)\rangle^2}{\langle \hat{a}^\dagger(t)\hat{a}(t)\rangle^2}
\end{aligned}
\tag{2.1}
$$

where $I(t)$ is the emission intensity at time t, $\hat{a}$ and $\hat{a}^\dagger$ are respectively the annihilation and creation operators. Experimentally, $g^{(2)}(\tau)$ can be well approximated—after normalisation— by histogram of the delay time between detection events on the "start" and "stop" channels of Hanbury-Brown and Twiss setup [29]. A schematic diagram of the setup is illustrated in Fig 2.1.

A stream of photons is sent to a beamsplitter and a measurement is made at the output of two single-photon detectors (D1 and D2). The two outputs are sent to correlation electronics (time-tagging measurement, TTM) that measure the difference of arrival time between coincident detection events, that is, events where both detectors clicked. It is more convenient to express Eq. 2.6 in discreet photon-number mode, $\hat{n}$ as follows [30]:

$$g^{(2)}(0) = \frac{\langle \hat{n}(\hat{n}-1) \rangle}{\langle \hat{n} \rangle^2} \tag{2.2}$$

where $\langle \hat{n} \rangle$ is the mean number of photons per pulse. Here we refer as multiphoton suppression, $1-g^{(2)}$, as the source's ability to emit one and only one photon per excitation per pulse—(for a pulsed excitation scheme) i.e $n=2$ and above photons are never emitted. For a thermal state, the emitted photons exhibit *super-Poissonian* statistics, i.e:

$$g^{(2)} = 1 + \frac{(\Delta n)^2 - \langle n \rangle}{\langle n \rangle^2} = 2 \tag{2.3}$$
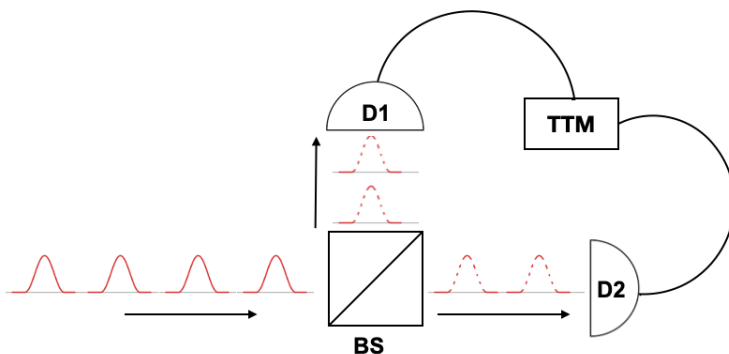
Figure 2.1: A schematic setup based on Hanbury Brown and Twiss experiment containing a beam-splitter (BS) and two output detectors (D1 & D2). The outputs of D1 and D2 are connected to a time tagging module (TTM) that measure the time delay between coincident detections on the "start" and "stop" events.

This is indicates a probability of finding two photons $(n = 2)$ at the same time and they are called *photon bunching*. A coherent state can be modelled by the output of a laser is where the photons are emitted with a constant probability in time. They exhibit *Poissonian* statistics.

$$g^{(2)} = 1 \tag{2.4}$$

Finally, photon-number states aka *Fock* states $|n\rangle$ are a truly nonclassical states where the arrival statistics are *sub-Poissonion*. A Fock state contains a given number of photons, ie. a number of state, $\langle \hat{n}^2 \rangle = \langle \hat{n} \rangle^2$ and the equation becomes:

$$g^{(2)}(0) = 1 - \frac{1}{\langle \hat{n} \rangle} \tag{2.5}$$

For an ideal single photon source $\langle \hat{n} \rangle = 1$ so that $g^{(2)}(0) = 0$. In this state, the emission of

the photon is called *photon antibunching*. This can be further explained when two photons are unlikely to be detected at the same time by the detectors.

2.2.2 Indistinguishability

Photon indistinguishability is an essential figure-of-merit in optical quantum information processing [31, 32]. Indistinguishability can be experimentally quantified by the mean wavepacket overlap of two photons as measured by Hong-Ou-Mandel experiment (Fig. 2.2a)[29]. When two photons are sent to the input of a beam splitter, each with a detector at the output—if they are in the same quantum state, they will exit the beamsplitter at the same output, with only one detector firing. Otherwise, if both photons are indistinguishable, the photons can exit via different outputs of the beamsplitter.

Owing to the bosonic nature of the photons, quantum inference will take place when the two photons arrive simultaneously at the beamsplitter, with four possible outputs as depicted in Figure 2.2. The probability amplitudes of the events "both photons transmitted" (Fig. 2.2b(ii) and Fig. 2.2b(iv)) and "both photons reflected" (Fig. 2.2b(i) and Fig. 2.2(iii)) interfere destructively due to the relations between the reflection and transmission coefficients of the beam splitter. If both of the photons are indistinguishable—identical in all degrees of freedom for example polarisation, spatio-temporal mode and frequency—they will leave the beamsplitter at the same output. This is called *photon bunching* and it can be measured by the HOM visibility, V_{HOM} [2]:

$$V_{HOM} = \frac{(C_\perp - C_\parallel)}{C_\perp} \tag{2.6}$$

where $C_\perp$ and $C_\parallel$ is the second-order coincidence count between two detectors. $C_\parallel$ is measured between two detectors located on two outputs and $C_\perp$ is measured by varying a degree of freedom such as polarisation or delay time between two detectors resulting a destructive quantum interference. The coincidence counts are integrated over the entire pulse temporal duration, as any temporal post-selection artificially increases V_{HOM}. The indistinguishability is defined by [2]:

$$M = V_{HOM}\left(\frac{R^2 + T^2}{2RT}\right) \tag{2.7}$$

where R and T are the transmission and reflection coefficients of the beamsplitter respectively. When $R=T=0.5$, the V_{HOM} visibility is simply the indistinguishability M. If the photon is perfectly overlap in all degree of freedom, the source is a perfect indistinguishability by $M = 1$.

2.2.3 Brightness

The definition of brightness varies somewhat depending on the scientific community and target applications. For instance, the QD community usually refers to the brightness as the amount of photons available just before the collection in the first lens. In this thesis, however, I will define the brightness as the probability of obtaining a single photon coupled into a single mode
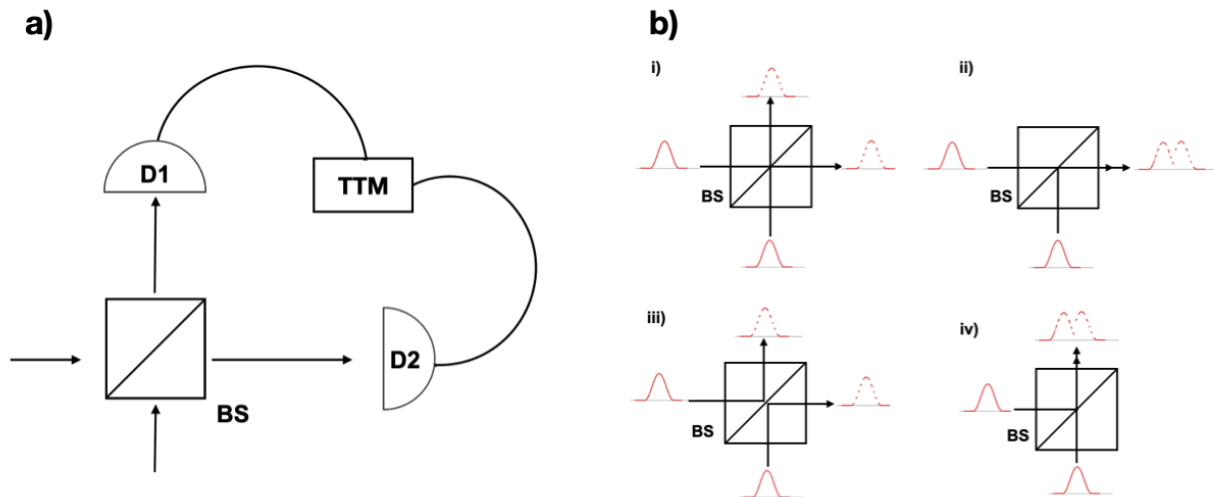
Figure 2.2: a) A schematic diagram of the HOM interference for indistinguishable photons. b) Quantum interference at beam splitter

optical fibre per excitation pulse. This includes the source repetition rate, transmission of the optical elements as well as the detector efficiencies.

According to [2], brightness B can be defined as the probability $P(n)$ of collecting a photon in each light pulse used to pump the source without a vacuum component, $|0\rangle$. In this thesis as well as other communities agree with the brightness metric as such if $P(n)$ is the n-photon number probability, then $B = p(1)$ for $p(1) >> p(p > 1)$ [2, 33]. Experimentally, the imperfect optical elements introduces losses and eventually contribute to the vacuum components. This is true for generation of n-fold single-photons, the probability scales with brightness to the power of n. Nowak [34] measured brightness at the first lens and defined [34] the source brightness as the number of photons collected per excitation cycle of the dot as follows [35]:

$$B_{exp} = I_x \tau_x \sqrt{1 - (g^{(2)}(0))}/\epsilon \tag{2.8}$$

where I_x corresponding to the photon count rate for X line (exciton) and τ_x is the lifetime of the X line (exciton). The square root allows correcting from multiphoton emission [35].

2.3 Cavity Coupling Regime

The cavity confines the field to exist only in a range of modes. In 1998, Gerard et al., [36] demonstrated the enhancement spontaneous emission by inserting QD inside the cavity. Fast forward in early 2000s, several groups realised the accelerations of spontaneous emission for quantum dots in micropillar [37, 38], microdisk [39] and photonic-crystal cavities [40], eventually reaching strong-coupling regime [41–43]. They showed acceleration of photon emission rates up to fivefold when the QD in resonance with the cavity mode. The acceleration is driven by the Purcell factor [5], F_p:

$$F_p = \frac{3}{4\pi^2} \frac{Q}{V} \left(\frac{\lambda}{n}\right)^3 \tag{2.9}$$

where Q is the cavity quality factor, n is the refractive index, and V is the cavity mode volume. According to Migdall [44], the probability of spontaneous emission placing a photon into the cavity is given by $\beta = F_p/(F_p + 1)$ where β is the spontaneous emission coupling factor. If the mode volume of the cavity is sufficiently small, the emitter and cavity couple so strongly that $\beta \simeq 1$, i.e. emissions into the cavity out weight spontaneous emission into free space that with the latest technology several works attained the regime of β-values close to unity experimentally [38, 45–47].

An important parameter to understand the interaction between QD and cavity mode is the coupling strength (g). There are two common regimes [42]—the weak coupling regime and the strong coupling regime. These two regimes can be achieved depending on properties of the particular cavity-emitter system resulting the photon (or light) enters into different regimes. In the perfect system where decoherence processes are negligible, coupling strength can be expressed by the Jaynes-Cummings Hamiltonian [48]. However, when the dot is in resonance with the cavity, one can express the coupling strength, g as follows [48, 49]:

$$g = \sqrt{\frac{e^2}{4\epsilon_0 \epsilon m_0}} \sqrt{\frac{f}{V_m}}, \tag{2.10}$$

where e is the charge of an electron, ϵ_0 is the permittivity of free space, ϵ is the relative dielectric constant of the host, m_0 is the free-space mass of electron, f is the QD exciton's oscillator strength, and V_m is the mode volume of the cavity. The oscillator strength is a dimensionless quantify defined as the ration between the radiative rate of the QD is a homogeneous enviromemnt and the emission rate of a classical harmonic oscillator, and is related to the dipole moment via [50]:

$$f = \frac{m_0}{e^2 \hbar \omega} |\mu|^2 \tag{2.11}$$

The oscillator strength of atoms is of the order of 1 and about 10 for QDs because QDs are larger and interact stronger with light. Conventional QDs are in the strong-confinement regime with a maximum oscillator strength of

$$f_{max} = \frac{E_g}{\hbar \omega}, \tag{2.12}$$

where E_g is the Kane energy, an experimentally accessible quantity.

2.3.1 Strong coupling regime

Strong coupling regime can be achieved when the time scale of coherent coupling between the emitter and cavity field is shorter than that of irreversible decay into various radiative and nonradiative routes [51]. During this process, the emitter and cavity is exchanging energy back and forth leading to Rabi oscillations [52] described as follows

$$2\sqrt{n+1}|g(\vec{r}_A)| \tag{2.13}$$

11

between the states $|e, n\rangle$ and $|g, n+1\rangle$, where $|e, n\rangle$ corresponds to an atom in the excited state and n photons in the cavity, and $|g, n+1\rangle$ corresponds to an atom in the ground state and $n+1$ photons in the cavity. $g(\overrightarrow{r}_A)$ is the coupling parameter between the cavity and emitter:

$$g(\overrightarrow{r}_A) = \frac{|\overrightarrow{\mu}_{eg}|}{\hbar}\sqrt{\frac{\hbar\omega}{2\epsilon_M V_{mode}}}\psi(\overrightarrow{r}_A)\cos(\xi) \tag{2.14}$$

where

$$\psi(\overrightarrow{r}_A) = \frac{E(\overrightarrow{r}_A)}{|E_{max}|} \tag{2.15}$$

and

$$\cos\xi = \frac{\overrightarrow{\mu}_{eg} \cdot \hat{e}}{|\overrightarrow{\mu}_{eg}|} \tag{2.16}$$

where $\overrightarrow{\mu}_{eg}$ = QD dipole moment, V_{mode} = cavity mode volume, ϵ_M = material permittivity at the point of maximum $\epsilon|E|^2$ (where $E = E_{max}$) and $\overrightarrow{r}_A$ = location of the emitter. The relative strength of the dielectric field, ψ is compared to E_{max} at $\overrightarrow{r}_A$ and $\cos(\xi)$ the fraction of the dipole moment along the direction of the electric field, $\hat{e}(\overrightarrow{E} = E \cdot \hat{e})$.

Strong coupling regime, it can be expressed as such:

$$|g| > \kappa/2, \gamma, \tag{2.17}$$

where κ is the cavity field

$$x\kappa = \frac{\omega}{2Q}, \tag{2.18}$$

and γ is the natural emitter decay rate. This can be explained by the unperturbed Hamiltonian of the atom cavity:

$$H = H_A + H_F \tag{2.19}$$

where $H_A = \frac{\hbar v}{2}\hat{\sigma}_z$, $H_F = \hbar\omega(\hat{a}^\dagger\hat{a} + \frac{1}{2})$ and $\hat{a}, \hat{a}^\dagger$ correspond to the annihilation and creation operators for the light field, $\hat{\sigma}_+$, $\hat{\sigma}_-$ are the atom population operators. The bare states are given by $|e, n\rangle$ and $|g, n+1\rangle$ with eigenenergies $\hbar\omega(n + \frac{1}{2})$. The pertubation must be included once the atom-cavity is strongly coupled and cavity must be treated as single system with an anhormonic ladder of states (Jayne-Cummings model) [53]. Thus, Jayne-Cummings Hamiltonian is described as follows

$$H = H_A + H_F + H_{int} \tag{2.20}$$

where

$$H_{int} = i\hbar(g^*(\overrightarrow{r_A})\hat{a}^\dagger\hat{\sigma} - g(\overrightarrow{r_A})\hat{\sigma} + \hat{a}). \tag{2.21}$$

Once the interaction Hamiltonian is turned on, the bare eigenstates are coupled while coupling to other states is neglected by the rotating wave approximation. This results the new eigenstates of the Hamiltonian H, $|1n\rangle$ and $|2n\rangle$, and have corresponding eigenenergies $\hbar(\omega \pm g\sqrt{(n+1)})$. Therefore the dresses states are not degenerate, and exhibit a splitting $2\hbar|g|\sqrt{(n+1)}$, dependent on the photon number n. this splitting is usually used as the indica-

tion that the emitter-cavity system has reached the strong coupling regime. A ladder dresses states is formed in the strong coupling regime. This ladder is anharmonic, i.e. the splitting between dresses states energy levels is not constant. This anharmonicity leads to effects such as photon blockade.

In the presence of detuning between the atom and the cavity, the two lowest order eigenstates have frequencies of $\omega\pm = \hbar\omega\sqrt{(\hbar\delta/2)^2 + (\hbar g)^2}$, where $\delta = v - \omega$, and v and ω are atom and cavity frequencies, respectively. In the presence losses, the resulting eigenfrequencies can be phenomenologically obtained by plugging in $\omega - i\kappa$ and $v - i\gamma$ into this epxression, instead of ω and v respetively. This leads to

$$\omega\pm = \frac{\omega + v}{2} - i\frac{\kappa + \gamma}{2} \pm \sqrt{\left(\frac{\delta - i(\kappa - \delta)}{2}\right)^2 + |g|^2} \tag{2.22}$$

As the system enters the strong coupling regime, for $|g| >> \kappa/2$ and $g >> \gamma$,

$$\omega\pm \rightarrow \frac{\omega + v}{2} \pm |g| - i\frac{\kappa + \gamma}{2} \tag{2.23}$$

Therefore, the eigenstates decay with the rate

$$\Gamma = (\gamma + \kappa)/2 \tag{2.24}$$

This is an upper limit on the decay rate of the emitter, and therefore the highest rate that the single photon source can achieve.

2.3.2 Weak coupling regime

In the weak-coupling case ($\gamma < g < \kappa/2$) the irreversible decay rates dominate over the coherent coupling rate such as the atom-cavity field system does not have enough time to couple coherently before dissipation occurs. This irreversible spontaneous emission process can be viewed as the result of an atom interacting with a large number of modes, and its attempt to start Rabi oscillations at different frequencies. This results a destructive interference of probability amplitudes corresponding to different modes and to irreversible spontaneous emission.

In this Purcell regime, the decay rate of the emitter can also be obtained from Eq. 2.22 with $\kappa >> g >> \gamma$ and is equal to g^2/κ. Multiplying by 2 to give the energy decay rate gives a spontaneous emission rate

$$\Gamma = 2\frac{|g(\overrightarrow{r}_A)|^2}{\kappa} = 2\hbar|\overrightarrow{\mu}_{eg}|^2\frac{Q}{\epsilon_M V_{mode}}\psi^2(\overrightarrow{r}_A)\cos^2(\xi) \tag{2.25}$$

For an imperfect emitter, Γ follows the same $\cos^2(\xi)|\psi|^2$ dependence as g^2 (see Eq. 2.14). Clearly Γ can be increased by increasing Q/V_{mode} of the cavity. Off resonance with the cavity, the spontaneous emission rate follows a Lorentzian lineshape given by the cavity density of states, and the full expression for the modified spontaneous emission rate including detuning

is given by

$$\Gamma = 2\hbar|\vec{\mu}_{eg}|^2 \frac{Q}{\epsilon_M V_{mode}} \psi^2(\vec{r}_A)\cos^2(\xi) \cdot \frac{\Delta\lambda_c^2}{4(\lambda - \lambda_c)^2 + (\Delta\lambda_c)^2} \tag{2.26}$$

where λ_c =cavity resonance wavelength and $\Delta\lambda_c = \lambda_c/Q$ is the cavity linewidth.

2.4 Excitation scheme

Semiconductor quantum-dots can be excited either by optical or electrical pumping. In this thesis, I use pulsed optical excitation to produce single photons. There are three pumping schemes—*non-resonant* excitation, *quasi-resonant* excitation and *resonant* excitation. Non-resonant excitations were used exclusively in the early day of QD research: another term for them is *above-band* excitation. During excitation, the laser is tuned above the GaAs band gap or in the wetting layer (WL) of about 820 nm. The wetting layer is a layer of film form using MBE during the process of the QD growth. In the excitation process, electrons and holes are generated at the wetting layer and subsequently captured by the dot, see Fig 2.3, before relaxing to the lowest energy levels. A typical relaxation time to the lowest energy level is between ~1-100ps. Once inside the dot, they quickly relax to their ground state via a
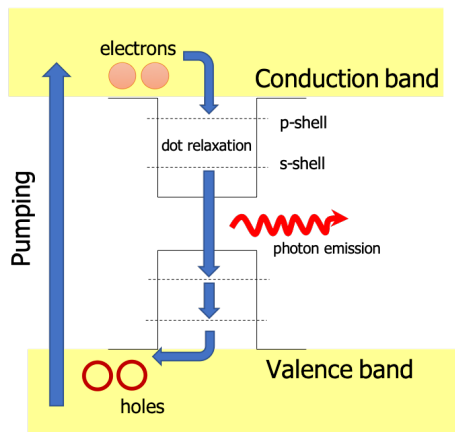
Figure 2.3: A pumping scheme based on above-band excitation

phonon-mediated process, where they then recombine radiatively. With this pumping scheme, several excitons can be injected in the dot resulting in complex photoluminescence. This is the most simple pumping technique because the energy of the pump laser does not have to be precisely controlled. Furthermore, the single photon can be easily selected by filtering, since the wavelength of the pump is very different from the wavelength of the single photon emission. The simplicity of this technique comes at a cost: the purity of the photon emission. When the charge carriers stay longer in the wetting layer, it can result in recombination, causing the re-excitation of the second photon after the first photon has been emitted [66]. In addition, the degree of indistinguishability is limited due to the excitation timing jitter from the incoherent relaxation [67] which consequently leads to a broadening of the peak in the correlation histogram.

Quasi-resonant excitation is performed by tuning the excitation laser to near the emission line of a dot. This type of excitation is used in order to overcome time-jitter from non-resonant

excitation. When the dot is excited into its p-shell, the emission takes place from the s-shell following a fast non-radiative decay (Fig. 2.4). The absence of carrier recapture during quasi-resonant excitation results in an effective reduction of the measured lifetime. In addition, this scheme almost suppress the background light and consequently generate nearly optimal deterministic single photons [25]. Quasi-resonant excitation has been proven to improve the interference visibility of the emitted photons compared to non-resonantly excited QDs [68].
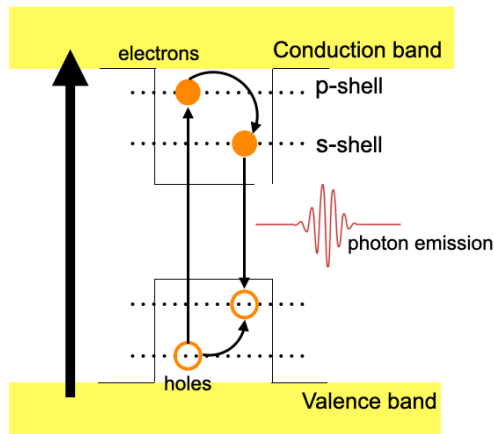
Figure 2.4: A pumping scheme based on quasi-resonant excitation

The ultimate pumping process would be a direct excitation into the s-shell of the dot. This can be executed by tuning the laser wavelength to the s-shell resonant frequency. During this process, a single electron-hole pair is created directly inside s-shell, (Figure 2.5) and can relax to the ground state, thereby preventing creation of unwanted multiple electron-hole pairs in the vacinity of the QDs. In principles, perfect single photons could be produced. This pumping scheme significantly reduces the time jitter, down to solely the radiative lifetime of the emitted photon [31, 66, 69, 70] thus improving single photon indistinguishability. However, this comes at the cost that it cannot be filtered away from the pump without photon loss. For a pulsed resonant excitation, one can observe the coherent control of two-level system via Rabi-oscillations: with a π-pulse, a full population inversion is achieved. There are several
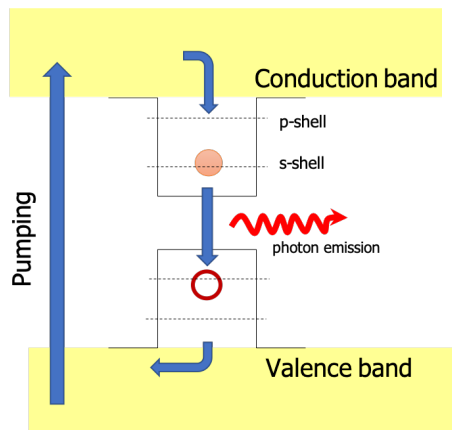
Figure 2.5: A schematic diagram for a strictly resonant excitation scheme

techniques to perform resonant excitations for instance, a phonon-mediated preparation [71],

adiabatic rapid passage [72], spin-flip Raman transition [73], two-photon biexciton excitation [74] or pulsed resonant excitation [75]. In this thesis, I drive the second generation device via pulsed resonant excitation. Although this scheme offers photons with high indistinguishability, it requires a careful technique in order to separate the emitted photon and the laser scattering light. Several methods have been performed in order to suppress the scattering laser such as perpendicular excitation path [76, 77] and polarisation filtering [78].

2.5 First Generation Device

Our quantum dot is formed by an island of GaAs, which acts a barrier material, and creates a three dimensional confinement potential for carriers. A single quantum-dot in a bulk material suffers from poor coupling efficiencies when coupled in a bulk semiconductor. The spontaneous emission (SE) of photons is randomly distributed over full solid angle of 4π radians, hence most of the isotropically-emitted photons are trapped due to total internal reflection. As a result, the photon extraction efficiency optically coupled devices such as a single mode fibre is very low. In order to mitigate this, there are two established techniques. The first is to interface the dot into a photonic waveguide where the emission of the photons are propagating into a lateral mode [79–81]. The second is to place a QD inside a cavity where it modifies the electromagnetic field degrees-of-freedom such as energy, polarisation, and the direction of emission [1, 26, 82]. The latter technique demonstrates high efficiency: with up to 24% collected at the output of a fibre [26]. In this thesis, I showed that our first generation devices achieved a fiber-coupling efficiency of 65%. The long stream of photons emitted by our single dot has high indistinguishability up to 70% when excited non-resonantly, even when pump pulse are separated by 400 ns. Our devices were purchased from Quandela, a company founded by our collaborator Prof. Pascalle Senallart and some members of her team. They used in-situ lithography to deterministically align each cavity to each dot. This will be further elaborated in Chapter 4.

2.6 Second Generation Device

As discussed above, QDs embedded in micropillar cavities have accelerated spontaneous emission via the Purcell effect, allowing single-photons to be produced with high indistinguishability—up to 80%—and high brightness: 40–50%. However our first generation device could not achieve the indistinguishability offered by downconversion sources. First and foremost, the first generation device was only allowed used with non-resonant and quasi-resonant pumping. Therefore, it is impossible to achieve near-unity single-photons with high indistinguishability. Achieving such ideal single-photon production requires resonant excitations, which promises not only highly indistinguishable single-photons, but ones with long coherence times. The first generation device only allowed us to vary the temperature in order to detune the QD cavity resonance. However, detuning the temperature resulted phonons that affected photon indistinguishability. Furthermore, charge noise is a problem not only in semiconductor dots, but also for other single

photon sources like those based on nanowires, because of significant charge noise at the surface [83, 84]. In order to control the charge environment, we moved to a device that reduces charge noise by controlling the electrical environment of the dot. Our second generation device—an electrically tunable quantum-dot micropillar was designed with electric contacts [85] on the photonic microstructure, allowing spontaneous emission of a single photon while applying an electrical field simultaneously [34]. This allow us to perform a resonant excitation pumping and thus control the charge noise of a single QD in a cavity.

2.6.1 Motivation

Dephasing phenomena in solid-states are system is inevitable, especially in a self-assembled QD because of the inhomogeneous growth during the fabrication process. The imperfections of the QD; the presence of impurities and structural defects [86–88], creates localisation sites that can trap the free carriers. These free carriers are the roots of charge noise that limit the coherence properties of the photon emissions. This results in shifts in the optical transition energy of a quantum dot through the d.c. Stark effect [83, 89–91] and a broadening in spectral diffusions by reducing the coherence time [92], both of which are detrimental to the QD performance, particularly the HOM visibility. The charge fluctuations can be substantially reduced to a few μeV, by applying an electrical gate to the diode structure, and performing a resonant excitation pumping [83, 84, 93]. Since 2007, several works have proven that the Stark effect can be used to fine tune a resonance of a dot that is strongly coupled to a micropillar, or to a photonic crystal mode [94–96]. This procedure allows us to control QD-cavity resonance without changing the interaction of QD with its environment; as opposed to temperature detuning [97]. Another advantage that needs to be highlighted is that the process of applying electric fields is reversible, and rather quick compared to changing the temperature where it takes time to see the spectral transitions. This constitutes an important step towards a deterministic spin-photon interface, a building block for a scalable solid-state quantum network.

2.6.2 Electrical Tunable Device

Our second generation devices Fig. 2.6(a), was fabricated by the same group from our first generation device. They used in-situ lithography to deterministically align each cavity to dots with similar wavelengths, positioning the pillar centre within 50nm of each QD, and adjusting the pillar cavity dimensions to ensure spectral resonance between the QD and the cavity [98]. This technique allows them to achieve optimal spatial matching with nanometer accuracy. The pillar in Fig. 2.6(b) is connected with four one-dimensional wires to the surrounding voltage source [34]. To obtain an optimised p-i-n diode with a defined Fermi level around the dot, and to minimise free carrier absorptions in the mirror, the sample was doped during molecular-beam epitaxy (MBE) growth. Our sources are composed of a single semiconductor InGaAs QD embedded in a micropillar λ-cavity with GaAs/AlAs Brag pairs in the top(14) and 28 bottom mirrors [84] respectively. The top mirrors are designed with less reflective layers than
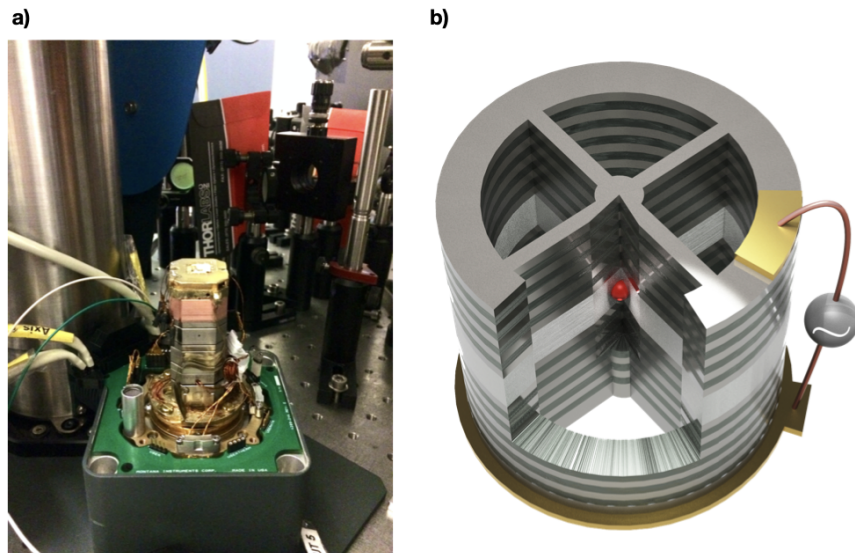
Figure 2.6: a) Second generation device installed in QT Laboratory b) micropillar QD connected to a surrounding circular frame by four one-dimensional wires

the bottom in order to enhance the output efficiency of the photon emission. One of the state-of-art techniques to optically control the QD charge state is by creating an electron-hole pair in the QD with an additional laser. This way traps a hole, since the electron quickly escapes whereas the hole cannot [99]. In the Chapter 5, I show that the second generation device is able to produce entanglement between four single photons emitted by a single dot using only optical elements.

REFERENCES

[1] Somaschi, N. *et al.* Near-optimal single-photon sources in the solid state. *Nature Photonics* **10**, 340–345 (2016).

[2] Senellart, P., Solomon, G. & White, A. High-performance semiconductor quantum-dot single-photon sources. *Nature Nanotechnology* **12**, 1026 (2017).

[3] Santori, C., Pelton, M., Solomon, G., Dale, Y. & Yamamoto, Y. Triggered single photons from a quantum dot. *Physical Review Letters* **86**, 1502 (2001).

[4] Strauf, S. *et al.* High-frequency single-photon source with polarization control. *Nature Photonics* **1**, 704 (2007).

[5] Purcell, E. M. Spontaneous emission probabilities at radio frequencies. In *Confined Electrons and Photons*, 839–839 (Springer, 1995).

[6] Gérard, J.-M. & Gayral, B. Strong purcell effect for inas quantum boxes in three-dimensional solid-state microcavities. *Journal of Lightwave Technology* **17**, 2089–2095 (1999).

[7] Ding, X. *et al.* On-demand single photons with high extraction efficiency and near-unity indistinguishability from a resonantly driven quantum dot in a micropillar. *Physical Review Letters* **116**, 020401 (2016).

[8] Vahala, K. J. Optical microcavities. *nature* **424**, 839–846 (2003).

[9] Kuhn, A. & Ljunggren, D. Cavity-based single-photon sources. *Contemporary Physics* **51**, 289–313 (2010).

[10] Heinzen, D. J., Childs, J., Thomas, J. & Feld, M. Enhanced and inhibited visible spontaneous emission by atoms in a confocal resonator. *Physical Review Letters* **58**, 1320 (1987).

[11] Aharonovich, I., Englund, D. & Toth, M. Solid-state single-photon emitters. *Nature Photonics* **10**, 631 (2016).

[12] Dory, C. *et al.* Complete coherent control of a quantum dot strongly coupled to a nanocavity. *Scientific reports* **6**, 1–8 (2016).

[13] Sun, S., Kim, H., Solomon, G. S. & Waks, E. A quantum phase switch between a single solid-state spin and a photon. *Nature nanotechnology* **11**, 539–544 (2016).

[14] Santori, C., Pelton, M., Solomon, G., Dale, Y. & Yamamoto, Y. Triggered single photons from a quantum dot. *Physical Review Letters* **86**, 1502 (2001).

[15] Bennett, C. H. & Brassard, G. Proceedings of the ieee international conference on computers, systems and signal processing (1984).

[16] Knill, E., Laflamme, R. & Milburn, G. J. A scheme for efficient quantum computation with linear optics. *Nature* **409**, 46 (2001).

[17] Kok, P. *et al.* Linear optical quantum computing with photonic qubits. *Reviews of Modern Physics* **79**, 135 (2007).

[18] Lund, A. P. *et al.* Boson sampling from a gaussian state. *Physical review letters* **113**, 100502 (2014).

[19] Aaronson, S. A linear-optical proof that the permanent is #p-hard. *Proceedings of the Royal Society A: Mathematical, Physical and Engineering Sciences* **467**, 3393–3405 (2011).

[20] Wang, H. *et al.* Boson sampling with 20 input photons and a 60-mode interferometer in a 1 0 14-dimensional hilbert space. *Physical review letters* **123**, 250503 (2019).

[21] Loredo, J. *et al.* Boson sampling with single-photon fock states from a bright solid-state source. *Physical review letters* **118**, 130503 (2017).

[22] Wang, H. *et al.* High-efficiency multiphoton boson sampling. *Nature Photonics* **11**, 361–365 (2017).

[23] Azuma, K., Tamaki, K. & Lo, H.-K. All-photonic quantum repeaters. *Nature Communications* **6**, 6787 (2015).

[24] Neville, A. *et al.* Classical boson sampling algorithms with superior performance to near-term experiments. *Nature Physics* **13**, 1153–1157 (2017).

[25] Loredo, J. C. *et al.* Scalable performance in solid-state single-photon sources. *Optica* **3**, 433–440 (2016).

[26] Wang, H. *et al.* Towards optimal single-photon sources from polarized microcavities. *Nature Photonics* **13**, 770–775 (2019).

[27] Tomm, N. *et al.* A bright and fast source of coherent single photons. *Nature Nanotechnology* **16**, 399–403 (2021).

[28] Brown, R. & Twiss, R. Q. Correlation between photons in two coherent beams of light. *Nature* **177**, 27–29 (1956).

[29] Hong, C.-K., Ou, Z.-Y. & Mandel, L. Measurement of subpicosecond time intervals between two photons by interference. *Physical Review Letters* **59**, 2044 (1987).

[30] Loudon, R. *The quantum theory of light* (OUP Oxford, 2000).

[31] Kiraz, A., Atatüre, M. & Imamoğlu, A. Quantum-dot single-photon sources: Prospects for applications in linear optics quantum-information processing. *Physical Review A* **69**, 032305 (2004).

[32] Kok, P. & Lovett, B. W. *Introduction to optical quantum information processing* (Cambridge university press, 2010).

[33] Loredo Rosillo, J. Enabling multi-photon experiments with solid-state emitters: a farewell to downconversion (2016).

[34] Nowak, A. *et al.* Deterministic and electrically tunable bright single-photon source. *Nature Communications* **5**, 3240 (2014).

[35] Pelton, M. *et al.* Efficient source of single photons: a single quantum dot in a micropost microcavity. *Physical Review Letters* **89**, 233602 (2002).

[36] Gérard, J. *et al.* Enhanced spontaneous emission by quantum boxes in a monolithic optical microcavity. *Physical Review Letters* **81**, 1110 (1998).

[37] Pelton, M. *et al.* Efficient source of single photons: a single quantum dot in a micropost microcavity. *Physical review letters* **89**, 233602 (2002).

[38] Solomon, G., Pelton, M. & Yamamoto, Y. Single-mode spontaneous emission from a single quantum dot in a three-dimensional microcavity. *Physical Review Letters* **86**, 3903 (2001).

[39] Kiraz, A. *et al.* Cavity-quantum electrodynamics using a single inas quantum dot in a microdisk structure. *Applied Physics Letters* **78**, 3932–3934 (2001).

[40] Englund, D. *et al.* Controlling the spontaneous emission rate of single quantum dots in a two-dimensional photonic crystal. *Physical review letters* **95**, 013904 (2005).

[41] Yoshie, T. *et al.* Vacuum rabi splitting with a single quantum dot in a photonic crystal nanocavity. *Nature* **432**, 200 (2004).

[42] Reithmaier, J. P. *et al.* Strong coupling in a single quantum dot–semiconductor microcavity system. *Nature* **432**, 197 (2004).

[43] Peter, E. *et al.* Exciton-photon strong-coupling regime for a single quantum dot embedded in a microcavity. *Physical Review Letters* **95**, 067401 (2005).

[44] Migdall, A., Polyakov, S. V., Fan, J. & Bienfang, J. C. *Single-photon generation and detection: physics and applications* (Academic Press, 2013).

[45] Park, H.-G. *et al.* Electrically driven single-cell photonic crystal laser. *Science* **305**, 1444–1447 (2004).

[46] Strauf, S. *et al.* Self-tuned quantum dot gain in photonic crystal lasers. *Physical review letters* **96**, 127404 (2006).

[47] Choi, Y.-S. *et al.* Evolution of the onset of coherence in a family of photonic crystal nanolasers. *Applied Physics Letters* **91**, 031108 (2007).

[48] Andreani, L. C., Panzarini, G. & Gérard, J.-M. Strong-coupling regime for quantum boxes in pillar microcavities: Theory. *Physical Review B* **60**, 13276 (1999).

[49] Michler, P. *Single semiconductor quantum dots*, vol. 28 (Springer, 2009).

[50] Michler, P. *Quantum dots for quantum information technologies*, vol. 237 (Springer, 2017).

[51] Buckley, S., Rivoire, K. & Vučković, J. Engineered quantum dot single-photon sources. *Reports on Progress in Physics* **75**, 126503 (2012).

[52] Press, D. *et al.* Photon antibunching from a single quantum-dot-microcavity system in the strong coupling regime. *Physical Review Letters* **98**, 117402 (2007).

[53] Scully, M. O. & Zubairy, M. S. Quantum optics (1999).

[54] Hood, C., Chapman, M., Lynn, T. & Kimble, H. Real-time cavity qed with single atoms. *Physical Review Letters* **80**, 4157 (1998).

[55] Mabuchi, H. & Doherty, A. Cavity quantum electrodynamics: coherence in context. *Science* **298**, 1372–1377 (2002).

[56] McKeever, J., Boca, A., Boozer, A. D., Buck, J. R. & Kimble, H. J. Experimental realization of a one-atom laser in the regime of strong coupling. *Nature* **425**, 268–271 (2003).

[57] McKeever, J. *et al.* State-insensitive cooling and trapping of single atoms in an optical cavity. *Physical Review Letters* **90**, 133602 (2003).

[58] Thompson, R., Rempe, G. & Kimble, H. Observation of normal-mode splitting for an atom in an optical cavity. *Physical Review Letters* **68**, 1132 (1992).

[59] Greentree, A. D., Cole, J. H., Hamilton, A. & Hollenberg, L. C. Coherent electronic transfer in quantum dot systems using adiabatic passage. *Physical Review B* **70**, 235317 (2004).

[60] Kaldewey, T. *et al.* Coherent and robust high-fidelity generation of a biexciton in a quantum dot by rapid adiabatic passage. *Physical Review B* **95**, 161302 (2017).

[61] Gerard, J. & Gayral, B. Inas quantum dots: artificial atoms for solid-state cavity-quantum electrodynamics. *Physica E: Low-dimensional Systems and Nanostructures* **9**, 131–139 (2001).

[62] Kleppner, D. Inhibited spontaneous emission. *Physical Review Letters* **47**, 233 (1981).

[63] Goy, P., Raimond, J., Gross, M. & Haroche, S. Observation of cavity-enhanced single-atom spontaneous emission. *Physical Review Letters* **50**, 1903 (1983).

[64] Gabrielse, G. & Dehmelt, H. Observation of inhibited spontaneous emission. *Physical Review Letters* **55**, 67 (1985).

[65] Hulet, R. G., Hilfer, E. S. & Kleppner, D. Inhibited spontaneous emission by a rydberg atom. *Physical review letters* **55**, 2137 (1985).

[66] Flagg, E. B., Polyakov, S. V., Thomay, T. & Solomon, G. S. Dynamics of nonclassical light from a single solid-state quantum emitter. *Physical Review Letters* **109**, 163601 (2012).

[67] Fischer, K. A., Müller, K., Lagoudakis, K. G. & Vučković, J. Dynamical modeling of pulsed two-photon interference. *New Journal of Physics* **18**, 113053 (2016).

[68] Gold, P. *et al.* Two-photon interference from remote quantum dots with inhomogeneously broadened linewidths. *Physical Review B* **89**, 035313 (2014).

[69] Huber, T., Predojević, A., Solomon, G. S. & Weihs, G. Effects of photo-neutralization on the emission properties of quantum dots. *Optics Express* **24**, 21794–21801 (2016).

[70] Gazzano, O. *et al.* Effects of resonant-laser excitation on the emission properties in a single quantum dot. *Optica* **5**, 354–359 (2018).

[71] Majumdar, A., Kim, E. D., Gong, Y., Bajcsy, M. & Vučković, J. Phonon mediated off-resonant quantum dot–cavity coupling under resonant excitation of the quantum dot. *Physical Review B* **84**, 085309 (2011).

[72] Glässl, M., Barth, A. M. & Axt, V. M. Proposed robust and high-fidelity preparation of excitons and biexcitons in semiconductor quantum dots making active use of phonons. *Physical review letters* **110**, 147401 (2013).

[73] He, Y. *et al.* Indistinguishable tunable single photons emitted by spin-flip raman transitions in ingaas quantum dots. *Physical review letters* **111**, 237403 (2013).

[74] Bounouar, S. *et al.* Phonon-assisted robust and deterministic two-photon biexciton preparation in a quantum dot. *Physical Review B* **91**, 161302 (2015).

[75] Gazzano, O. *et al.* Bright solid-state sources of indistinguishable single photons. *Nature Communications* **4**, 1425 (2013).

[76] Ates, S. *et al.* Post-selected indistinguishable photons from the resonance fluorescence of a single quantum dot in a microcavity. *Physical Review Letters* **103**, 167402 (2009).

[77] Muller, A. *et al.* Resonance fluorescence from a coherently driven semiconductor quantum dot in a cavity. *Physical Review Letters* **99**, 187402 (2007).

[78] Vamivakas, A. N., Zhao, Y., Lu, C.-Y. & Atatüre, M. Spin-resolved quantum-dot resonance fluorescence. *Nature Physics* **5**, 198–202 (2009).

[79] Arcari, M. *et al.* Near-unity coupling efficiency of a quantum emitter to a photonic crystal waveguide. *Physical review letters* **113**, 093603 (2014).

[80] Uppu, R. *et al.* Scalable integrated single-photon source. *Science advances* **6**, eabc8268 (2020).

[81] Lodahl, P., Mahmoodian, S. & Stobbe, S. Interfacing single photons and single quantum dots with photonic nanostructures. *Reviews of Modern Physics* **87**, 347 (2015).

[82] Wang, H. *et al.* Near-transform-limited single photons from an efficient solid-state quantum emitter. *Physical Review Letters* **116**, 213601 (2016).

[83] Kuhlmann, A. V. *et al.* Charge noise and spin noise in a semiconductor quantum device. *Nature Physics* **9**, 570–575 (2013).

[84] Somaschi, N. *et al.* Near-optimal single-photon sources in the solid state. *Nature Photonics* **10**, 340 EP – (2016).

[85] Dousse, A. *et al.* Ultrabright source of entangled photon pairs. *Nature* **466**, 217–220 (2010).

[86] Walther, C. *et al.* Characterization of electron trap states due to inas quantum dots in gaas. *Applied Physics Letters* **76**, 2916–2918 (2000).

[87] Mazzucato, S. *et al.* Defect passivation in strain engineered inas/(inga) as quantum dots. *Materials Science and Engineering: C* **25**, 830–834 (2005).

[88] Chahboun, A. *et al.* Further insight into the temperature quenching of photoluminescence from in as/ ga as self-assembled quantum dots. *Journal of Applied Physics* **103**, 083548 (2008).

[89] Högele, A. *et al.* Voltage-controlled optics of a quantum dot. *Physical review letters* **93**, 217401 (2004).

[90] Atatüre, M. *et al.* Quantum-dot spin-state preparation with near-unity fidelity. *Science* **312**, 551–553 (2006).

[91] Houel, J. *et al.* Probing single-charge fluctuations at a gaas/alas interface using laser spectroscopy on a nearby ingaas quantum dot. *Physical review letters* **108**, 107401 (2012).

[92] Reigue, A. *et al.* Resonance fluorescence revival in a voltage-controlled semiconductor quantum dot. *Applied Physics Letters* **112**, 073103 (2018).

[93] Vural, H., Portalupi, S. L. & Michler, P. Perspective of self-assembled ingaas quantum-dots for multi-source quantum implementations. *Applied Physics Letters* **117**, 030501 (2020).

[94] Kistner, C. *et al.* Demonstration of strong coupling via electro-optical tuning in high-quality qd-micropillar systems. *Optics express* **16**, 15006–15012 (2008).

[95] Laucht, A. *et al.* Electrical control of spontaneous emission and strong coupling for a single quantum dot. *New Journal of Physics* **11**, 023034 (2009).

[96] Laucht, A. *et al.* Dephasing of exciton polaritons in photoexcited ingaas quantum dots in gaas nanocavities. *Physical review letters* **103**, 087405 (2009).

[97] Gevaux, D. *et al.* Enhancement and suppression of spontaneous emission by temperature tuning inas quantum dots to photonic crystal cavities. *Applied physics letters* **88**, 131101 (2006).

[98] Dousse, A. *et al.* Controlled light-matter coupling for a single quantum dot embedded in a pillar microcavity using far-field optical lithography. *Physical review letters* **101**, 267404 (2008).

[99] Hilaire, P. *et al.* Deterministic assembly of a charged-quantum-dot–micropillar cavity device. *Physical Review B* **102**, 195402 (2020).

BRIGHT SOURCE FOR MULTIPHOTON EXPERIMENT

Two-photon interference is an important figure of merit for quantifying the degree of indistinguishability of single-photon source. This is especially true for quantum information protocols that requires qubits to interact to perform gate operations. Maximum interference will occur when photons with the same polarisation and frequency components are overlapped spatially and temporally. However, it is challenging to achieve maximum interference, while simultaneously maintaining low multi-photon suppression and high absolute brightness. The degree of indistinguishability drops [1] when photons are separated more than few nanoseconds highlighting that whether the emitter is able to produce long stream of indistinguishable photons.

This chapter presents our approach in producing multiple indistinguishable single-photons [2], using our first generation device discussed in Chapter 2. We designed and implemented an optical collection system to increase the collection efficiency of single photons emitted by our first generation device. Our single-photons demonstrate excellent multiphoton suppression and an absolute brightness of 14%. This means about one in seven laser pulses creates a high-purity single photon at the end of single-mode fiber. We establish a device generating a stream of long consecutive photons separated by 400 ns, whilst remaining above the classical limit of 50%, even with high excitation powers.

3.1 Experimental

Our first generation device is a self-assembled InGaAs quantum dot grown by using molecular beam epitaxy, positioned in between two layers of GaAs/AlAs distributed Bragg reflectors, consisting of 16 (36) pairs acting as a top (bottom) mirror. The pillar of the device is the same as [3] and was employed in low-temperature *in situ* lithography [4] with micropillar centered around a single quantum dot with accuracy of 50 nm. The device is kept in a closed-cycle cryostat at a few Kelvin, and optically pumped by 5 ps laser pulses at an 80 MHz. The excitation wavelength is centred at 905.3 nm to create carriers in the p-shell. After excitation, the emission photons passed through two cryostat windows and a microscope objective before split from the laser path using a dichroic mirror (Alluxa filters). Any residual scattered laser light is filtered using FWHM band-pass filter. Table 3.1 depicts the efficiency of the experimental setup. The emission of the single photons are then sent into an unbalanced Mach-Zehnder interferometer.
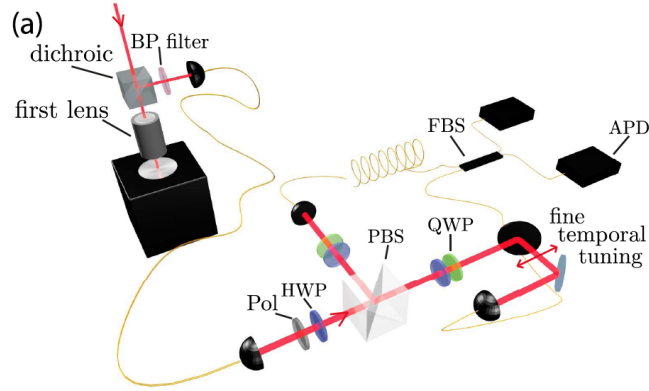
Figure 3.1: A simple unbalanced Mach-Zehnder interferometer with a path-length difference of $\Delta\tau_e$ probes the indistinguishability of two photons emitted with the same $\Delta\tau_e$ temporal separation.

Table 1	Efficiency	Error bar
a) Two cryostat windows, η_{cryo}	96	$\pm$ 1%
b) Microscope objective, η_{obj}	91	$\pm$ 1%
c) Dichroic mirror, η_{ml}	95	$\pm$ 1%
d) FWHM band pass filter, η_{bp}	91	$\pm$ 1%
e) Fiber-coupling efficiency, η_{fc}	65	$\pm$ 4%
f) Overall transmission, η_{setup}	49	$\pm$ 3%

Table 3.1: a) Set-up efficiency and transmission. b) Microscope objective lens (Olympus LM-PLN10XIR with N.A = 0.3). c) 6 mirrors and 2 lenses; Dichroic mirror (Alluxa filters) to remove photon emission from the excitation laser with > 60dB extinction while no appreciable loss is recorded at wavelength corresponding to photon-emission. d) 0.85nm Alluxa filters (FWHM) to remove residual scattered excitation laser. f) The fiber-coupling efficiency is estimated by comparing our collection with multimode fiber assumed to have a unity coupling efficiency.

Variable length of fiber is used to match the arrival time delay of two photons between two interferometer arms. The half-wave plate (HWP) and the polarizing beam splitter behave as a tuneable reflectivity beamsplitter. We tune this to match the fiber beam splitter, and forming a Mach-Zehnder interferometer. Quarter-wave plates and HWPs are used to tune the polarization of interfering photons to parallel or orthogonal configurations.

3.2 Absolute brightness and multi-photon suppression

In quantum-dots community, most of the works define brightness as the number of photons collected per excitation pulse into the first lens [15]. It allows one to compare the performance of the device independently from the efficiency of the optical setup during the experiment. Somaschi and co-workers [15] demonstrated a near-optimal single photons sources with visibilities reaching unity as well extraction efficiency of 65% and polarised brightness at the first lens approximately 16%. Whilst the reported value is impressived, the brightness is defined at the first lens with poor optical collection resulting a low photon count rates available in practice. Therefore, absolute source efficiencies remain close to 1% level, which is too low for practical scalable applications [5]. Further details for characterising brightness can be found in Chapter

2 (Section 2.2.3). In this work, we measure absolute brightness as the probability-per-laser-per-pulse of finding a spectrally isolated high-purity single photon at the output of a single-mode fiber.

Figure 3.2 presents the absolute brightness of our device. The output photon flux is detected on silicon avalanche photodiode (APD) as a function of saturation power. The saturation curves are fitted to $R_0(1-exp(-P/P_0))$, where R_0 is an asymptotic rate value and P_0 is the saturation power. The inset figure shows the spectra with respect to varying temperature T. Varying the temperature allows us to tune the dot-cavity system into resonance. The energy of the dot transition varies like the band gap of the semiconductor with temperature [6], whereas the cavity mode energy follows the temperature variation of the refractive index. A bright and sharp emission line corresponding to neutral exciton (X) line is seen in resonance at $T = 15$ K and we operate here.

The photon flux rates reach values as high as 3.6 MHz. For high rates, a known loss must be introduced in the optical path in order to properly quantify the available count rates, as they are beyond the APD's (Perkin-Elmer SPCM-AQR-14-FC) linear regime. High count rates allow us to accumulate a high amount of statistics with notably short integration times.
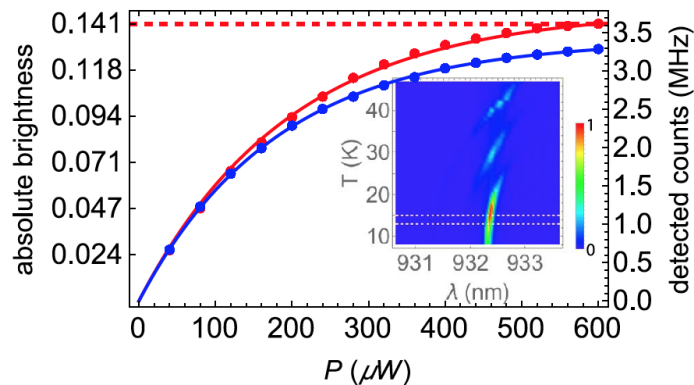
Figure 3.2: Absolute brightness and detected count rates of first generation device at $T = 15$ K (red), with the QD in resonance with the cavity mode, and 13 K (blue), with the QD slightly detuned from the cavity. Solid curves represent fits to $R_0(1-exp(-P/P_0))$ with $P_0 = 197\mu$W and $R_0 = 3.8$ MHz for $T = 13$ K, and $R_0 = 3.4$ MHz for $T = 15$ K. Inset: QD spectra with varying temperature.

The inset shows a $g^2(\Delta t)$ measurement—the second-order autocorrelation function where $g^{(2)}(0)$=0 corresponds to an ideal single-photon state—at P=P_0, yielding a value of $g^{(2)}(0)$=0.0130± 0.0002, where the small error is reached with an integration time of only 29 s. In fact we used about half the available counts after selecting one linear polarization emitted by our device. Thus, in our setup, the same amount of statistics will be achieved twice times faster when the polarizer is removed.

Remarkably, we observe low multi-photon suppression at all pump powers, with a measured maximum value of $g^{(2)}(0)$=0.0288 ± 0.0002 at P=$3P_0$. In Figure 3.3, we observe single-photon purity $1 - g^{(2)}(0) > 97\%$, even at maximum brightness. These values were extracted from integrating raw counts in a 2 ns window—sufficiently larger than the < 0.5 ns lifetime [7]—around the peak at zero delay compared to the average of the 10 adjacent lateral peaks, without

any background subtraction. The error bars in this work are deduced from assuming Poissonian statistics in the detected events.

The detected 3.6MHz photon flux rate, with the APD efficiency of 32% measured using the approach of Ref. [8] and a 80 MHz pump rate. The absolute brightness of our device– the probability-per-laser-pulse of finding a spectrally isolated high-purity single photon at the output of a single-mode fiber—is 14%, the highest reported to that date [2]. At the time of publication, there was no clear definition of brightness and hence a significant variation in source efficiency that depends on the various scientific communities. For instance, until now a drastic contrast between the performance at the first lens and the actual detected count rates has been common, e.g., reporting a brightness as high as 72% while detecting 65 kHz [9], or 143 MHz collected on the first lens but only 72 kHz available on detection [10]. Detected rates of 4.0 MHz at the single-photon level have been reported [8], but without coupling into a single-mode fiber and at the cost of high multi-photon contribution with $g^{(2)}(0) = 0.4$.
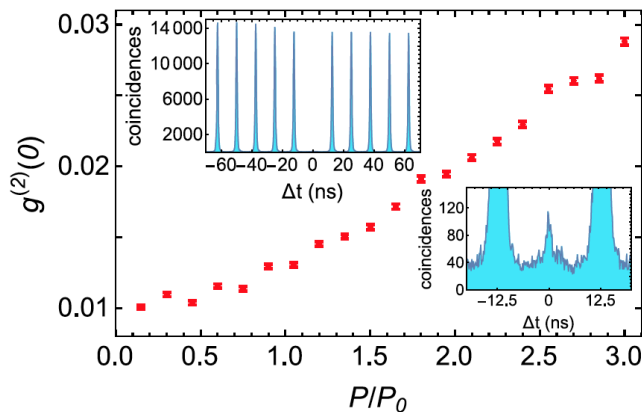
Figure 3.3: Power-dependent of first generation device $g^{(2)}(0) = 0$ at $T = 15$ K. Note that even three times above the saturation pump power, the photon purity remains $> 97\%$. Top inset shows the autocorrelation measurement for $P = 1P_0$ and bottom inset zooms into the zero delay resolving the nonzero $g^{(2)}(0)$ from experimental noise.

Based on the brightness value plotted in Figure 3.2, our device greatly exceeds, in terms of absolute brightness, the performance of any other single-photon source from any physical system, including the well-established spontaneous parametric down-conversion source—so far considered as the premier photon source—where the equivalent (triggered) absolute brightness is well below 1%. We note that, given our setup collection efficiency of $\eta_{setup} = 49\%$, our first generation device exhibits for the neutral exciton (X) state a brightness at the first lens of 29%. Deducing the exciton lifetime from the correlation curves at a low excitation power, we estimate the Purcell factor of the device to be around $F_p = 2$ and the fraction of emission into the cavity mode to be around 66%. Considering an output coupling efficiency of 90%, the measured brightness in the first lens could reach 60% with a unity probability to find the QD in the neutral exciton state. However, as is evident in the inset of Fig. 3.2, the present QD also presents an non-negligible probability to emit from the positively or negatively charged exciton transitions that are brought in resonance at higher temperatures. As a result, the

probability of the quantum dot to be in the neutral exciton is reduced, leading to the measured 29% brightness at the first lens. Note that this instability of the charge state was not observed originally in the devices under study (see Ref. [7]), but appeared after accidentally freezing the sample.

3.3 Consecutive streams of indistinguishable photons

Next, we investigate the indistinguishability of photons emitted by our first generation device with various temporal distances ranging from 12.5ns to 400ns. The measurement is done at at $T = 13$ K in order to reduce phonon-induced dephasing [11], which is sufficiently close to the quantum dot cavity resonance at $T = 5$ K. Note that contrary to most reports, the phonon sideband here is not filtered out by the 0.85 nm bandpass filter used to further suppress the laser light. Time-correlation histograms from the output of this interferometer (Figure 3.1) reveals the indistinguishability of photons emitted with a temporal distance, $\Delta\tau_e$. Fully distinguishable photons—e.g., with orthogonal polarisation—meeting at a 50:50 beam splitter and results in a 50% probability of being detected simultaneously at the outputs of the beam splitter. This result in the peak at $\Delta t = 0$ of the time-correlation measurement being about half of the height those at $\Delta t > 0$, with the exception of peaks at $\Delta t = \Delta\tau_e$, where the larger suppression indicates that the interfering photons were emitted with a temporal distance, $\Delta\tau_e$. Details for indistinguishability measurement will be discuss in the next section.

3.3.1 Areas in time-correlation histograms

This section is to deduce the area distribution of time-correlation histograms. For simplicity, we first consider two (fully-distinguishable) single-photons distributed in time-bins $\{t_1, t_2\}$, entering an unbalanced Mach-Zehnder interferometer composed of a first $50:50$ beamsplitter and a second beamsplitter with reflectance $\mathcal{R}$ (transmittance $\mathcal{T}=1-\mathcal{R}$). Our task is to find all possible output distributions leading to a coincidence detection between events separated in time by Δt. There are two timescales relevant in such coincidence measurements: the difference in occupied time-bins $\delta t=|t_2-t_1|$, and the temporal delay inside the unbalanced interferometer Δ. By inspecting this reduced scenario, we can find that there are 8 events leading to a coincidence detection, as depicted in Figure 3.4.

This results in local patterns of peak areas $A_{\Delta t}$ given by: $A_{-\delta t-\Delta}=\mathcal{R}^2$, $A_{-\delta t}=2\mathcal{R}\mathcal{T}$, and $A_{-\delta t+}\Delta=\mathcal{T}^2$, the local pattern around $-\delta t$; and $A_{\delta t-\Delta}=\mathcal{R}^2$, $A_{\delta t}=2\mathcal{R}\mathcal{T}$, and $A_{\delta t+\Delta}=\mathcal{T}^2$, the local pattern around δt. From this, we find simple rules for the time-correlation measurement of an array of single-photons distributed in arbitrary time-bins $\{t_i\}$ passing through a Δ-unbalanced Mach-Zehnder:

rule 1: Find all possible temporal delays δt relating each pair of photons within the given time-bin distribution.

rule 2 : $\pm\delta t$ assign the relative frequency of events $\{\mathcal{R}^2, 2\mathcal{R}\mathcal{T}, \mathcal{T}^2\}$ at temporal delays at $\Delta t = \{\pm\delta t - \Delta, \pm\delta t, \pm\delta t + \Delta\}$.
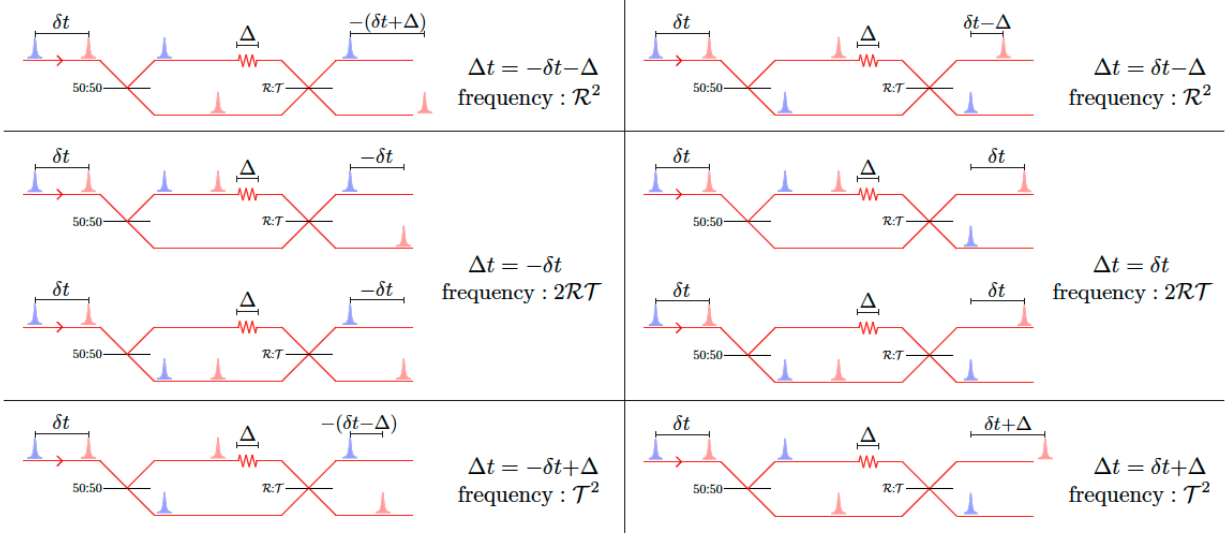
Figure 3.4: Two consecutive single-photons separated by δt passing through a Δ-unbalanced Mach-Zehnder interferometer. 8 outcome distributions, occurring with a given relative frequency, lead to a coincidence signal between events separated in time by Δt. The relative delay Δt is positive if a detector in the upper output fires first, and it is negative in the opposite case.

We note that these two simple rules describe different interesting histograms relevant in the literature. For instance, by simply identifying the involved parameters, one can find histograms of $g^{(2)}(\Delta t)$ measurements of arbitrary $|n\rangle$ Fock states by considering n single-photons occupying the same time-bin, resulting in distributions agreeing with $g^{(2)}(0)=1-1/n$, or the well known 5-peak structures in two-photon interference experiments involving pairs of photons separated by $\Delta\tau_e < 12.5$ ns repeated every 12.5 ns.

Since the experiment performed is the particular case of an infinitely long stream of single-photons separated by a fixed δt=12.5ns, and passing through an unbalanced interferometer with $\Delta = \Delta\tau_e$. Under this consideration, and following $rule1$ and $rule2$, we derive the distribution of areas $A_{\Delta t}$, given by: $A_k = N, A_{-\Delta\tau e} = N(1 - \mathcal{R}^2), A_{\Delta\tau e} = N(1 - \mathcal{T}^2)$, and $A_0 = N((\mathcal{R}^2 + \mathcal{T}^2) - 2\mathcal{R}\mathcal{T}V)$, with $k = \pm 12.5$ ns, ± 25 ns, ..., excluding peaks at $\pm\Delta\tau_e$ and N an integration constant. The visibility term V in A_0 appears from noticing (in virtue of $rule1$ and $rule2$) that the area at $\Delta t = 0$ for fully-distinguishable photons is $A_0^{V=0} = N(\mathcal{R}^2 + \mathcal{T}^2)$, and then one simply uses the well-known relation $V = (1 - A_0/A_0^{V=0})(\mathcal{R}^2 + \mathcal{T}^2)/(2\mathcal{R}\mathcal{T})$, with A_0 relating the coincidence rate at zero delay of photons with non-zero V indistinguishability.

We use the visibility V to quantify the degree of indistinguishability of the source. Since the measured visibility depends both on the photon source and on the apparatus used to characterize it, the latter must be accounted for. Ideally, the apparatus is a beam splitter of reflectivity $\mathcal{R} = 0.5$; in our experiment $\mathcal{R} = 0.471$, $\mathcal{T} = 0.529$, and the visibility V is thus,

$$V = \frac{\mathcal{R}^2 + \mathcal{T}^2 - A_0/A}{2\mathcal{R}\mathcal{T}} \tag{3.1}$$

where A is taken as the average value of A_k. Note that since the $g^{(2)}(0)$ values are intrinsic to the source, and hence affect any process in which we wish to use it, we do not correct for nonzero $g^{(2)}(0)$ in Eq. (3.1). The deduced V therefore corresponds to the raw two-photon

interference visibility and quantifies the degree of photon indistinguishability.

Figure 3.5 shows histograms for the indistinguishability of orthogonally (completely distinguishable) and parallel polarized (photon bunching) photons at $\Delta\tau_e$=50 ns and $P=P_0$. From Eq. (3.1) and the measured value $\mathcal{R}$=0.471, we obtain $V_{50ns}^{P_0}=(0.71\pm0.01)\%$ in the orthogonal configuration (red histogram) and $V_{50ns}^{P_0}=(60.31\pm0.60)\%$ parallelly polarized photons (blue histogram), where $V_{\tau_e}^P$ denotes the visibility taken at a power P and temporal delay $\Delta\tau_e$. We observe higher visibilities at lower powers and shorter delays. For instance, the measurements in Figure 3.5 were taken at $P = 0.5P_0$ and reveal $V_{12.5ns}^{0.5P_0} = (67.52 \pm 0.78)\%$ at a temporal delay (blue histogram) of $\Delta\tau_e = 12.5$ ns. Remarkably, we find that indistinguishability is robust in the temporal domain. Even after 33 consecutive emitted photons (orange histogram) at $\Delta\tau_e = 400$ ns, the value only decreases to $V_{400ns}^{0.5P_0} = (59.97\pm0.76)\%$. That is, there is a less than 8% visibility decrease in ~ 400 ns. All V values with the non resonant schemes are obtained without any background correction.
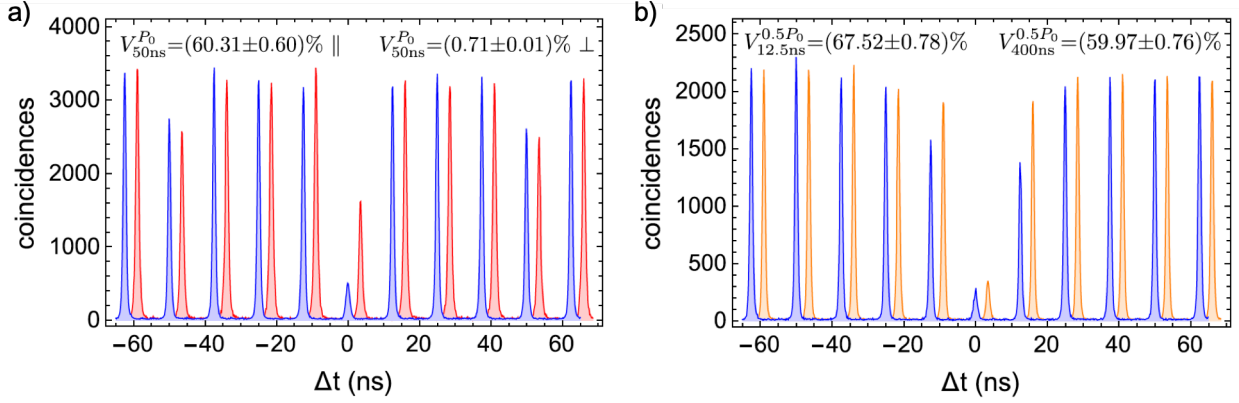
Figure 3.5: a) Interference histograms of orthogonally (red) and parallelly polarized (blue) photons with $\Delta\tau_e = 50$ns at the saturation of the quantum dot. (Note the suppression at $\Delta\tau_e$; see text for details). (c) Interference of parallelly polarized photons with $\Delta\tau_e = 12.5$ ns (blue) and $\Delta\tau_e = 400$ ns (orange), taken at $P = 0.5P_0$. A temporal offset of 3.5 ns has been introduced between histograms for clarity.

To thoroughly examine the indistinguishability properties of our first generation device, we carried out power- and temporal-dependent measurements, see Fig. 3.6. All the measured visibilities are within the 50%–70% range, thus showing conclusive quantum interference at all measured powers and timescales. The large available photon flux allows us to gather more than 100 visibility values with measurement errors sufficiently small to identify an interesting behavior in this narrow visibility range.

The interference visibility V of two photons separated in time by $\Delta\tau e$ exhibits a linear-dependence in the pump power P. For a given $\Delta\tau e$, we measure V at various values of P, up to three saturation powers $P = 3P_0$, and fit the data to $\overline{V} = V_{\Delta\tau e}^{max} + m\Delta\tau_e P$. Figure 3.7 shows the power-dependence of V for $\Delta\tau e = 12.4$ ns, $\Delta\tau e = 50$ ns, and $\Delta\tau e = 400$ ns. The fitted parameters are $V_{12.5ns}^{max} = (70.3 \pm 0.3)\%$, $m_{12.5ns} = -(6.1 \pm 0.2)\%$ at short time scales; $V_{50ns}^{max} = (65.0 \pm 0.3)\%$, $m_{50ns} = -(4.4\pm0.2)\%$ at moderate timescales; and $V_{400ns}^{max} = (60.8\pm0.3)\%$, $m_{400ns} = -(3.6\pm0.2)\%$ at the longest timescales explored in this work. Conversely, for fixed power, the visibility decreases
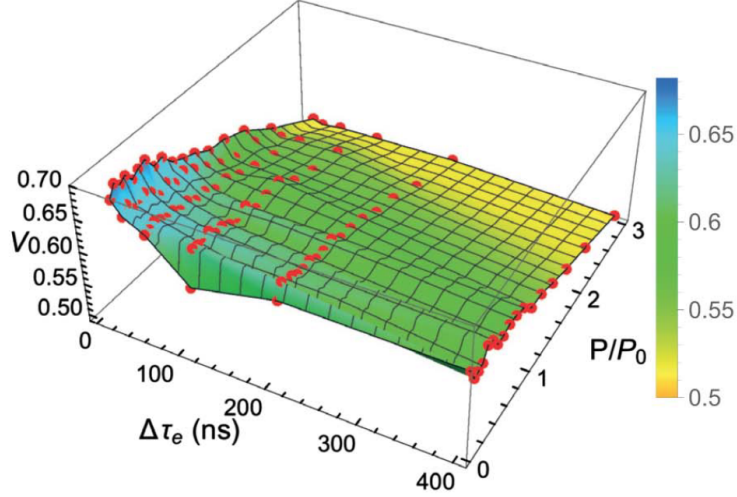
Figure 3.6: Power- and temporal-dependent two-photon interference. Over > 100 measured visibilities (red points) showing conclusive quantum interference,i.e., $V > 0.5$, at all measured powers and timescales. Colored surface is an interpolation to the data.

monotonically and asymptotically in $\Delta\tau_e$, flattening to fixed values at longer timescales. We model this behavior by considering a time-dependent wandering of the spectral line as the origin of the temporal modulation. That is, the frequency of every emitted photon $\omega(t)=\omega_0+\delta\omega(t)$ varies in time according to some wandering function $\delta\omega(t)$ occurring in timescales much longer than the photon lifetime.
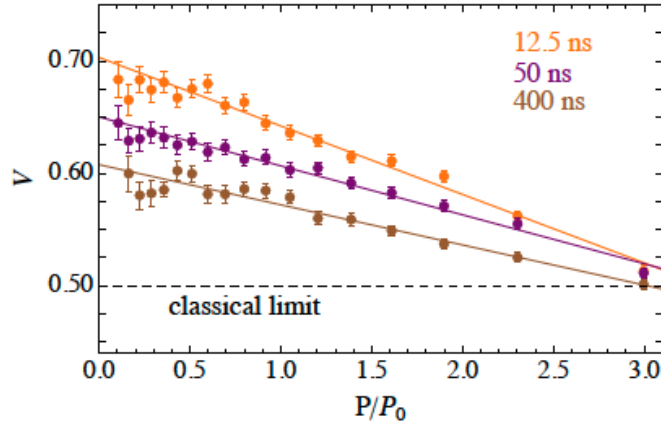
Figure 3.7: Power-dependence of V for $\Delta\tau_e = 12.5$ ns (orange), $\Delta\tau_e = 50$ ns (purple), and $\Delta\tau_e = 400$ ns (brown). Curves are fits $\overline{V} = V_{\Delta\tau e}^{max} + m\Delta\tau_e P$. V is above 50% (the classical limit) at all powers and timescales here explored.

Our problem is then equivalent to finding the mutual interference visibility between independent sources with finite frequency detuning [12]. The interference visibility of two photons from two sources a and b reads [12]:

$$V = \left(\frac{\gamma_a\gamma_b}{\gamma_a + \gamma_b}\right)\frac{(\gamma_a + \gamma_n + \gamma_a^* + \gamma_b^*)}{[(\gamma_a + \gamma_n + \gamma_a^* + \gamma_b^*)/2]^2 + \delta\omega^{2\prime}} \tag{3.2}$$

where the γ_i are the radiative rates, γ_i^* the pure dephasing rates, and $\delta\omega$ the frequency detuning between the two sources. If the interfering photons are emitted by the same quantum dot, we

assume that $\gamma_a = \gamma_b = \gamma$ and $\gamma_a^* = \gamma_b^* = \gamma^*$ are constant, but only the frequency $\omega = \omega_0 + \gamma\omega(t)$ varies over time (i.e. spectral wandering) around a central value ω_0. This model makes sense here as the timescale over which ω varies is much larger than the radiative lifetime. Then Eq. (3.2) reduces to:

$$V = \left\langle \frac{V(0)}{1 + \delta\omega_r^2} \right\rangle \tag{3.3}$$

which is given by $V(0)/(1 + \delta\omega_r^2)$ in the case where $V(0)$ is the degree of indistinguishability for each source alone (equal value for both) and $\delta\omega_r$ is the ratio of the frequency detuning to the spectral linewidth of the sources (equal linewidth for both). If this mismatch arises due to spectral wandering within the same source, then the time-averaged relative detuning squared is given by $2\delta\omega_r^2(1 - exp(-\Delta\tau_e/\tau_c))$, with τ_c a characteristic wandering timescale We thus derive the visibility of temporally distant photons as follows:

$$V(\Delta\tau_e) = \frac{V(0)}{1 + 2\delta\omega_r^2(1 - e^{-\Delta\tau_e/\tau_c})} \tag{3.4}$$

where we have used $V(0) = \gamma/(\gamma + \gamma^*)$ the "intrinsic" degree of indistinguishability, and $\delta\omega_r = \delta\omega/(\gamma + \gamma^*)$ the ratio between the frequency detuning and the spectral linewidth $\gamma + \gamma^*$. One can define a time correlation function for the frequency fluctuations as

$$F(\Delta\tau_e) = <\delta\omega(f)\delta\omega(t + \Delta\tau_e)> = <\delta\omega^2 > f(\delta\omega^2), \tag{3.5}$$

then, the frequency difference as a function of the delay $\Delta\tau_e$ can be expressed as

$$< \delta\omega^2(\delta\omega^2) >= < (\delta\omega(t + \Delta\tau_e) - \delta\omega(t))^2 > \tag{3.6}$$

$$=2 < \delta\omega^2 > (1 - f(\Delta\tau_e)). \tag{3.7}$$

A common assumption is to assume an exponential correlation function

$$f(\Delta\tau_e) = e^{-\Delta\tau_e/\tau_c}, \tag{3.8}$$

with τ_c a characteristic wandering timescale. Which is expected for a Markovian dynamics of the environment. An additional input which is required is the distribution for $\delta\omega$. Generally one assumes a Gaussian distribution, but for simplicity, and without loss of generality, we take a two-value distribution $\delta\omega = \pm\sqrt{< \delta\omega^2 >}$, so that:

$$V = \left\langle \frac{V(0)}{1 + \delta\omega_r^2(\Delta\tau_e)} \right\rangle = \frac{V(0)}{1 + \langle\delta\omega_r^2(\Delta\tau_e)\rangle} = \frac{V(0)}{1 + \langle\delta\omega_r^2(1 - e^{-\Delta\tau_e/\tau_c})\rangle} \tag{3.9}$$

To obtain a statistically meaningful temporal behavior, we used the fitted values of $\overline{V}$ at different $\Delta\tau_e$ for powers $P=0$, $P=P_0$, and $P=2P_0$. These values are plotted in Fig. 3.8 and are in good agreement with our model in Eq. (3.2). In the limit of low powers, we obtain $V(0) = (72.8 \pm 2.4)\%$, $\tau_c = (45.4 \pm 19.1)$ ns, and $\delta\omega_r = (29.4 \pm 3.1)\%$ whereas at high powers, at

$P = 2P_0$, these parameters are $V(0) = (59.0 \pm 2.0)\%$ and $\delta\omega_r = (19.3 \pm 4.5)\%$.
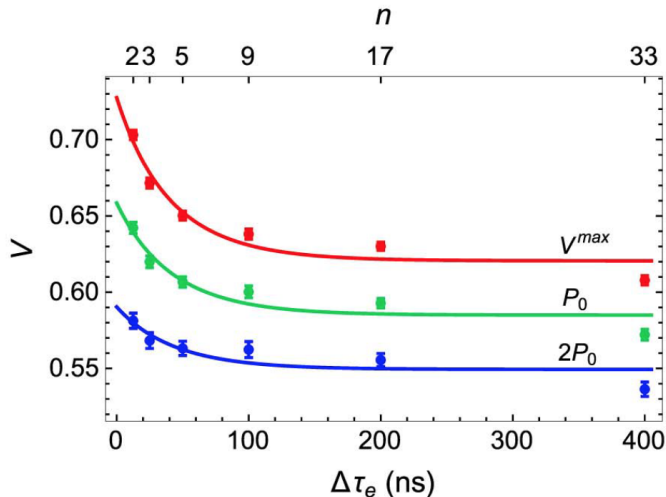
Figure 3.8: Fitted values of $\overline{V}$ at different $\Delta\tau_e$ (bottom axis), for $P = 0$ (red), $P = P_0$ (green), and $P = 2P_0$ (blue), showing interference between a first and n-th consecutive emitted photon (top axis). Curves are fits to our model in Eq. (3.4).

The maximum degree of indistinguishability $V(0)$ decreases only by 13.8% with increasing power, evidencing a slight increase of pure dephasing of the exciton transition. On the contrary, the relative amplitude of the spectral wandering decreases by 34% evidencing that spectral diffusion is significantly reduced at higher powers, as recently observed in nanowire-based devices [13]. Note that the large relative error in τ_c is due to a small relative decay in V, an uncertainty that increases with increasing power. Thus, although it is reasonable to assume that τ_c itself is power dependent, we extracted τ_c only at $P = 0$ and used it as a fixed parameter for the fits at higher powers. The decrease of the indistinguishability by a few percents for temporally distant photons demonstrates a very limited spectral diffusion in our micropillar devices.

This observation is in striking contrast to previous measurements on single-photon sources based on alternative approaches for efficient photon extraction, such as nanowires [13], or micro lenses [1]. A significantly lower stability of the electrostatic environment of the QD can reasonably be attributed to the close proximity of free surfaces in the latter. Indeed, as indicated by the observation of three emission lines from the same QD, even the micropillar devices under study do not provide a fully stable charge state for the QDs, an effect that we observe to be dependent on the quality of the etched surfaces. This makes strictly resonant spectroscopy difficult without an additional nonresonant excitation, a situation also observed in other micropillar devices [14].

Therefore, to explore the indistinguishability of temporally distant photons under strictly resonant excitation, we turn to electrically controlled micropillars and present data on two devices, *Device 2* and *Device 3* by our collaborators in France. These devices consist of quantum dots deterministically coupled to micropillars embedded in cylindrical gated structures with p- and n-contacts, respectively, defined on the top and bottom sides of the device, resulting in an effective p-i-n diode structure onto which an electric field can be applied (see Ref. [15]) for a detailed description of the device). The measurement were performed at $T = 9$ K and

the emission was tuned into cavity resonance via via an applied bias voltage of 0.3 V. The device was cooled by gas exchange in a closed-cycle cryostat and was pumped by shaped 15 ps laser pulses at an 82 MHz repetition rate. The experimental setup used for photon collection is reported in Ref. [15], and the apparatus used for the temporal-dependent measurements is conceptually identical to that in Fig. 3.1.
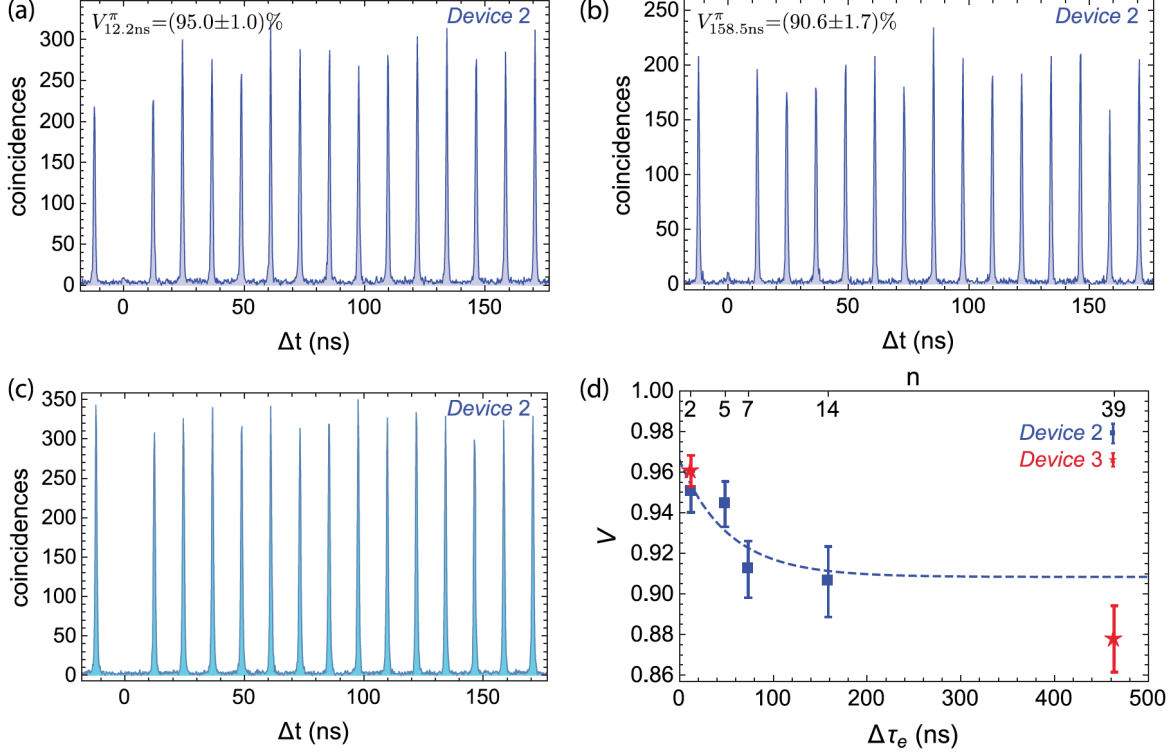
Figure 3.9: Temporal-dependent indistinguishability under strictly resonant excitation. Two-photon interference histograms with *Device 2* of parallelly polarized photons at (a) $\Delta\tau_e$ = 12.2 ns and (b) $\Delta\tau_e$ = 158.5 ns, under a π-pulse preparation. (c) Second-order autocorrelation measurement at π-pulse. (d) Indistinguishability between a first and n-th consecutive emitted photon from *Device 2* (blue) and *Device 3* (red). Indistinguishability remains robust in the temporal domain, decreasing only by 4.4% in ~159 ns (down to 90.6%) for *Device 2*, and by 8.3%in ~463 ns (down to 87.8%) for *Device 2*. The curve is a fit of the data from *Device 2* to Eq. 3.2.

Resonant excitation allows us to probe two-photon interference in a regime with excellent indistinguishability. Indeed, for *Device 2*, we obtain $V^{\pi}_{12.2ns}$ = $(95.0 \pm 1.0)\%$ at a short temporal separation, decreasing only to $V^{\pi}_{158.5ns}$ = $(90.6 \pm 1.7)\%$ at long timescales (see Figs. 3.9(a) and 3.9(b)). We observe a high single-photon purity quantified by $g^{(2)}(0)$ = 0.015 ± 0.007 at the π-pulse, (see Fig. 3.9(c)) where the nonvanishing $g^{(2)}(0)$ primarily consists of background noise and thus a value $1 - g^{(2)}(0)$ of 98.5% represents a lower bound on the intrinsic single-photon purity. Indistinguishability measurements at various temporal distances (see Fig. 3.9(d)), reveal plateaus at high values: up to a first and fourteenth photon, separated by ~ 150 ns, exhibit an indistinguishability greater than 90%. The curve is a fit to Eq. 3.2 with a maximum indistinguishability value of $V(0)$=96.6%, τ_c=54.4 ns, and $\delta\omega_r$=17.8%. The reproducibility of our results, is evidenced by similar indistinguishability values obtained on *Device 3*: $V^{\pi}_{12.2ns}$=$(96.1\pm0.8)\%$ a short temporal delay and V^{π}_{463ns}=$(87.8\pm1.6)\%$ for a first and thirty-ninth photon separated by
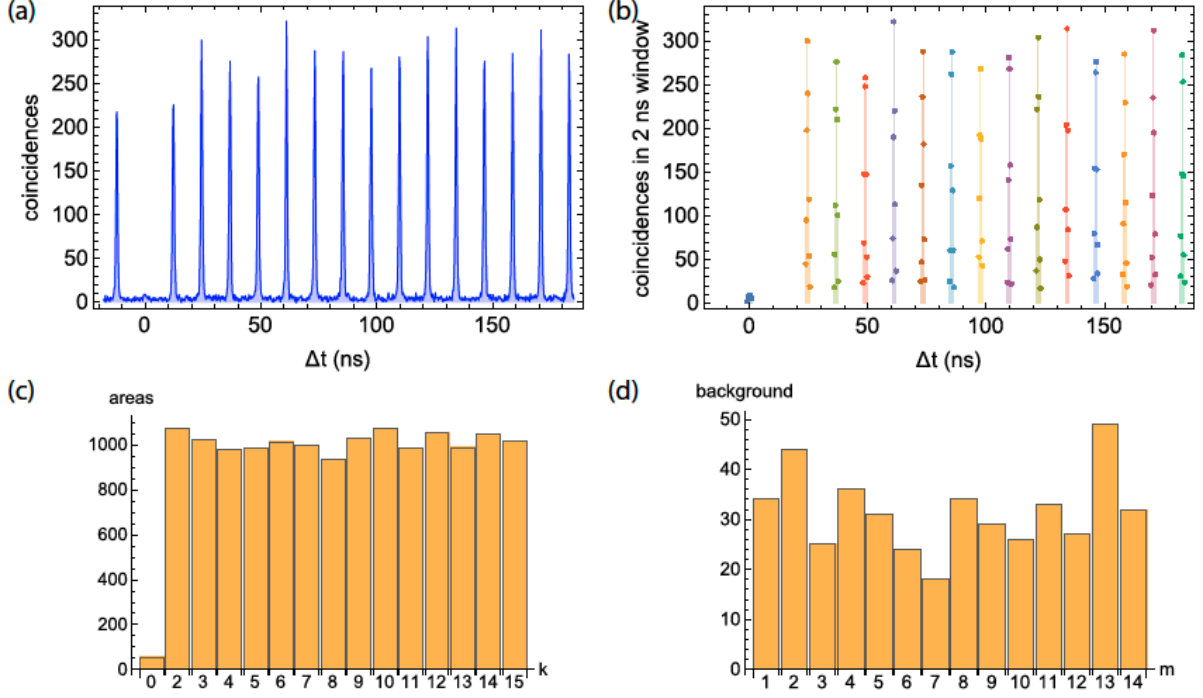
Figure 3.10: Method to extract the raw and corrected interference visibilities. a) Interference histogram of two photons separated by $\Delta\tau_e = 12.2$ ns. b) Subset of data involved in the evaluation of V. c) Integrated counts from data in b). d) Measured background in between peaks

463 ns. These values of indistinguishability are corrected for the measured background noise arising from detector dark counts since the experimental setup used for these resonant excitation measurements has a low collection efficiency and dark counts become significant. Thus, an integration of detected raw counts that includes the background noise, which at zero delay is as large as nonvanishing counts due to photon indistinguishability, would underestimate the intrinsic degrees of indistinguishability in our devices.

3.3.2 Resonant Excitation : Visibility extraction

Here we describe the methods to extract the raw and corrected two-photon interference visibilities under strictly-resonant excitation and π-pulse preparation, see Fig. 3.10. Figure 3.10a shows the interference histogram of two photons separated by $\Delta\tau_e = 12.2$ ns, from which a visibility is extracted via

$$V = \frac{\mathcal{R}^2 + \mathcal{T}^2 - A_0/A}{2\mathcal{R}\mathcal{T}}, \tag{3.10}$$

where A_0 is the area of the peak around $\Delta t = 0$, and A is taken as the average area of 14 adjacent peaks (excluding the peak at $\Delta\tau_e$). These areas are taken as the integrated counts within a temporal window of 2 ns (considerably longer than the subnanosecond lifetimes) around $\Delta t = k \times 12.2$ nswith $k = 0, 2, 3, ..., 15$, see Fig. 3.10b. The resulting integrated areas are shown in Fig. 3.10c, from which we extract a raw $V^\pi_{12.2\text{ns}} = (89.0 \pm 1.5)\%$. As described in the main text, the remaining non-vanishing area at $\Delta t = 0$ is indeed quite small and it is on the order of experimental noise. We take into account this noise by integrating coincidence counts within

a 2 ns window but now located in between peaks, that is at $\Delta t = (m + 1/2) \times 12.2$ ns, with $m = 1, 2, ..., 14$, see Fig. 3.9d. After subtracting the average of these background counts to the areas in Fig. 3.10(c), we obtained the corrected visibility $V_{12.2\text{ns}}^{\pi} = (95.0 \pm 1.0)\%$. These same methods were employed for all measurements under strictly-resonant excitation. Figure 3.11 shows both raw and corrected visibilities for two devices (Device 2 and 3) extracted with this method.Measurements under quasi-resonant excitation, as described in the main text, exhibit a noise level $< 1\%$, and therefore no noise-correction was employed.
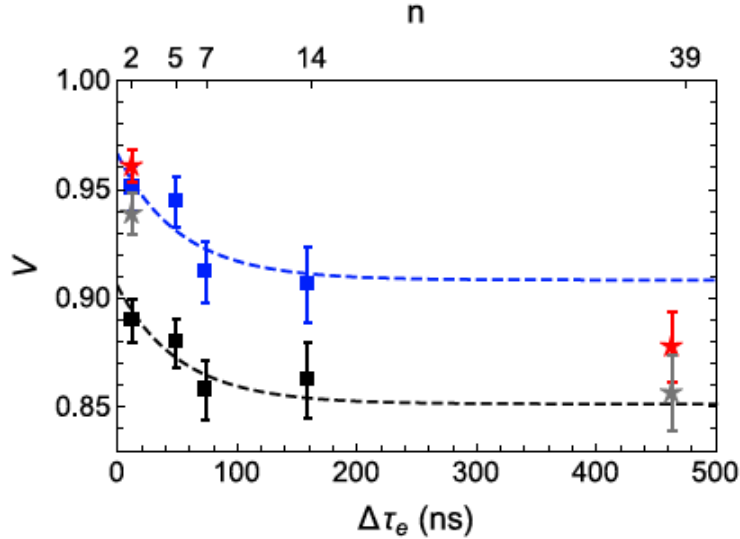
Figure 3.11: Indistinguishability vs temporal distance. Blue squares are corrected indistinguishabilities taken with *Device*2, and red stars are the corrected values taken with *Device*3. Black squares are raw values from *Device*2, and gray stars are raw values from *Device*3.

No correction for nonvanishing $g^{(2)}(0)$ was included. Note that a high absolute brightness with this recently developed technology is yet to be achieved. However, since the mode profile of connected pillars is the same as isolated ones [16] and a photon extraction efficiency at the first lens of 65% has been reported on this sample [17], the same experimental methods as before should allow even higher absolute efficiencies than the 14% reported here.

3.4 Discussion and conclusion

We provided here strong evidence that our sources emit long streams of indistinguishable photons. Under non-resonant excitation, even the first and thirty-third consecutive photon, separated by 400 ns, display conclusive quantum interference, $V > 50\%$. For a fixed pump power, photon indistinguishability decreases by only a few percent—about 8% at low powers and less than 4% at higher powers—before flattening to fixed values at longer timescales. This contrasts favourably to previous works, where photon indistinguishability has been observed to decrease by 40% in only 10 ns [1]. Moreover, under strictly resonant excitation, photon indistinguishability between the first and thirty-ninth photon remained at 88%.

Interestingly, the observation of only small reductions in the temporal domain indicate that nonunity indistinguishability under nonresonant excitation is mainly caused by homogenous broadening of the spectral linewidth (governing coherence times at short temporal delays) and a limited inhomogeneous broadening (governing effective coherence times at longer temporal delays). The relative amplitude of the spectral diffusion at saturation is similar for both resonant and non resonant excitation. However, *Device 1* operated in a limited Purcell regime, whereas *Device* 2 and 3 operated with a Purcell factor of around 7-10, leading to an increased radiative exciton linewidth. From this, we conclude that, although the application of an electrical bias in p-i-n diode structures allows a good control of the dot charge states, it does not lead to a significant decrease in the spectral wandering phenomena. The excellent indistinguishability observed in *Devices* 2 and 3 arises mainly from reduced pure dephasing of the exciton state, increased Purcell factor, and reduced time jitter in a resonant excitation scheme. Our reported indistinguishability values correspond to the longest temporal delays here studied at a particular pump repetition rate of 80 MHz. This value only represents a lower bound on the number of photons we can generate—limited by radiative lifetimes in the order of a few hundred picoseconds—that can be further used in quantum information processing protocols with solid-state sources [18].

Previous works investigating noise spectra in resonance fluorescence have shown evidence of long streams of near transform-limited photons [19] in timescales potentially reaching seconds [20]. In fact, *Device* 2 has recently been shown to emit photons with near transform-limited linewidth on a millisecond timescale [21], in which case we would expect that our devices are producing at least hundreds of thousands of highly indistinguishable single photons. Our findings are especially relevant in implementations with time-bin encoded degrees of freedom, such as some recently proposed schemes of linear-optics quantum computing with time-bin encoding [22, 23], where the indistinguishability of temporally distant photons will directly determine quantum fidelities of the implemented protocols.

Scaling solid-state multi-photon sources by combining multiple independent emitters remains challenging, as atomic growth accuracy or complex individual electric control over multiple devices is needed. These requirements can be circumvented by making use of a single photon source emitting a long temporal stream of highly indistinguishable photons that can be demultiplexed by fast active optics, see Chapter 4. A high absolute brightness will be critical for successfully implementing multi-photon experiments with these sources, where their down-conversion counterparts currently require experimental runs of hundreds of hours [24, 25]. The key role of high emission yields in these devices has been made explicit in the recent demonstration of a solid-state based multi-photon experiment [26], realized with *Device* 1, where integration times outperformed those in equivalent down-conversion implementations by two-orders of magnitude. Achieving high absolute efficiencies, and thus allowing the scaling of multi-photon experiments to larger photon numbers, becomes feasible due to the Purcell enhancement of deterministically coupled quantum dot-micropillar devices [7, 12, 15, 16, 27]. This necessary condition is unlikely to be found by chance with nondeterministic approaches which

here reported [27] device yields as high as of 1% [14]. Thus, the deterministic fabrication, high absolute brightness, and long timescale indistinguishability of our devices will enable large-scale applications that have been heretofore impossible.

3.5 Comparison between QD and SPDC single-photon sources

Table 3.2 is presented to further highlight the comparison between QD and SPDC single-photon sources. The sources are characterised by three main figure of merit; the purity($g^2(0)$), the indistinguishability (V_{HOM}), and the brightness. SPDC has been leading as a conventional heralded source for single-photons with high indistinguishability prior to 2000s period of quantum dot community. However, the high indistinguishability always at cost of brightness to typically 2% [28]. Despite of that, SPDC leads any new single-photon source technology. Aside from that, they are robust and operate at room temperature. Numbers of work has been done to constantly improved the efficiency [29] of the SPDC and integrating photonics optics [30] from bulk resources overhead. Another critical aspect of SDPC which is worth to highlight here the probability of creating n pairs scales up with pump intensity to the nth power. Pan and co-workers [31] show that the visibility, V_{HOM} close to unity but the brightness decreases significantly. This is because the heralding process does not alter the probability of generating more than one pair. One obviously can increase the pump power in order to increase the probability of heralding an event thus resulting more photons. Subsequently, it leads to reduce it purity to 0.2 for a source that contains only one pair for every 20 pulse.

Since 2017, the progress in developing single-photon sources based on semiconductor quantum dots has set a significant benchmark in optical quantum technologies. Despite of accelerating progress, QD-based source still struggle with limited overall efficiency of around 25%, which is three times out of four, the expected clocked single photon is missing. The overall probability to obtain the single photon per clock cycle at the end of the fiber output is $P_{\text{fiber}} = P_{\text{out}}\eta_{\text{set-up}}$. Several techniques have been demonstrated by quantum dots community to enable near unity coupling such as rapid adiabatic passage [32] or bullseye cavity [33]. Resonant excitation technique allows one to obtain single photon with indistinguishability up tp 0.995 [14, 15] but at cost of 50% polarisation filtering. The losses in polarisation filtering fundamentally limiting the scaling photonic quantum technologies. In 2019, Wang and co-workers [34] mitigate this with birefringent cavity and demonstrate a polarised single-photon efficiency up to 60%.

Tomm and co-workers [35] successfully achieved 57% end-to-end efficiency while maintaining source purity. This is achieved by designing an open cavity [36, 37] structure where the cavity bottom mirror is grown below the cavity spaces that embeds the quantum dots. The top mirror of the cavity has a concave shape and is micro-machined into a silica substrate while the bottom mirror contains a highly reflective planar mirror to minimise unwanted loss rate from the cavity. The main advantage of the open cavity is the flexibility to fine tune the cavity frequency in the orthogonal direction to match the dot transition. The polarised cavities enable controlled

coupling to quantum dots and used enhance spontaneous emission into one linear polarisation resulting nearly a factor of 2 gain in the source efficiency.

A different approach was made recently by Thomas [38] and co-workers to achieve a state-of-the-art quantum performance by harnessing the intrinsic linear dipole in a neutral quantum dot via phonon-assisted excitation. An off-resonant phonon-assisted excitation technique uses a laser which is spectrally detuned from the wavelength emission and that can be easily separated. It relies on detuned strong optical pulse that dresses frequency optical transition. During the pulse duration, the system relaxes between the dresses states through the emission of longitudinal-acoustic (LA) phonons. During the switch-off excitation pulse, a strong occupation of the excited state is obtained following an adiabatic undressing. The indistinguishability of phonon-assisted excitation is in the range of $90\% - 95\%$, at the same level as resonant excitation but with higher occupation probability and major increase the brightness. The increase in brightness could attribute to the fact that the emission of the single photons from LA-phonon-assisted excitation is less sensitive compared to resonant excitation. It can therefore concluded LA-phonon-excitation scheme is more experimentally robust against experimental drifts and instabilities.

Source	Excitation/Material	$g^2(0)$	$V_{\text{HOM}}(\%)$	Brightness	Efficiency, $\eta(\%)$
Tomm[35][QD]	Resonant	0.979 ± 0.01	97.5 ± 0.5	-	57
Thomas[38][QD*]	Phonon-assisted	0.954 ± 0.002	90.9 ± 0.4	50 ± 1[a]	65
Wang[34][QD]	Resonant	0.75 ± 0.005	97.5 ± 0.6	56 ± 2[b]	60
Kaneda[39][SPDC]	PPKTP	0.91 ± 0.02	91.2	1.1×10^4[c]	$90(91)$[d]
Bruno[40][SPDC]	PPKTP	0.91 ± 0.04	98.7	≈ 4000[e]	95
Zhong[41][SPDC]	BBO	0.96	96 ± 0.01	≈ 1100	97

Table 3.2: Comparison of SPDC and quantum-dots including a current state-of-the-art* for single photon sources. [a]Polarised first lens brightness corresponds to a detected cou5nt rate of 6 MHz with 69% single photon detector at 81 MHz of laser repetition rate. [b] Wang estimated $\approx 56\%$ of the polarised single photons are extracted by the first objective lens. Note for SPDC; [c] The brightness is characterised as the photon generation per unit pump power (e.g., cps/mW). The efficiency for SPDC is determined by heralding efficiency. [d] $\eta_s = 90 \pm 3\%$ and $\eta_i = 91 \pm 4\%$ [e] The crystal generates 0.01 photons per pulse at repetition rate of 80 MHz with pump power of 200 mW. Brightness as the fiber output without the detector efficiency.

REFERENCES

[1] Thoma, A. *et al.* Exploring dephasing of a solid-state quantum emitter via time-and temperature-dependent hong-ou-mandel experiments. *Physical review letters* **116**, 033601 (2016).

[2] Loredo, J. C. *et al.* Scalable performance in solid-state single-photon sources. *Optica* **3**, 433–440 (2016).

[3] Gazzano, O. *et al.* Bright solid-state sources of indistinguishable single photons. *Nature communications* **4**, 1425 (2013).

[4] Dousse, A. *et al.* Controlled light-matter coupling for a single quantum dot embedded in a pillar microcavity using far-field optical lithography. *Physical review letters* **101**, 267404 (2008).

[5] O'brien, J. L., Furusawa, A. & Vučković, J. Photonic quantum technologies. *Nature Photonics* **3**, 687 (2009).

[6] Grilli, E., Guzzi, M., Zamboni, R. & Pavesi, L. High-precision determination of the temperature dependence of the fundamental energy gap in gallium arsenide. *Physical Review B* **45**, 1638 (1992).

[7] Gazzano, O. *et al.* Bright solid-state sources of indistinguishable single photons. *Nature communications* **4**, 1425 (2013).

[8] Strauf, S. *et al.* High-frequency single-photon source with polarization control. *Nature photonics* **1**, 704 (2007).

[9] Claudon, J. *et al.* A highly efficient single-photon source based on a quantum dot in a photonic nanowire. *Nature Photonics* **4**, 174 (2010).

[10] Schlehahn, A. *et al.* Single-photon emission at a rate of 143 mhz from a deterministic quantum-dot microlens triggered by a mode-locked vertical-external-cavity surface-emitting laser. *Applied Physics Letters* **107**, 041105 (2015).

[11] Unsleber, S. *et al.* Two-photon interference from a quantum dot microcavity: Persistent pure dephasing and suppression of time jitter. *Physical Review B* **91**, 075413 (2015).

[12] Giesz, V. *et al.* Cavity-enhanced two-photon interference using remote quantum dot sources. *Physical Review B* **92**, 161302 (2015).

[13] Reimer, M. E. *et al.* Overcoming power broadening of the quantum dot emission in a pure wurtzite nanowire. *Physical Review B* **93**, 195316 (2016).

[14] Ding, X. *et al.* On-demand single photons with high extraction efficiency and near-unity indistinguishability from a resonantly driven quantum dot in a micropillar. *Physical review letters* **116**, 020401 (2016).

[15] Somaschi, N. *et al.* Near-optimal single-photon sources in the solid state. *Nature Photonics* **10**, 340 (2016).

[16] Nowak, A. *et al.* Deterministic and electrically tunable bright single-photon source. *Nature communications* **5**, 3240 (2014).

[17] Somaschi, N. *et al.* Near-optimal single-photon sources in the solid state. *Nature Photonics* **10**, 340 EP – (2016).

[18] Gazzano, O. *et al.* Entangling quantum-logic gate operated with an ultrabright semiconductor single-photon source. *Physical review letters* **110**, 250501 (2013).

[19] Kuhlmann, A. V. *et al.* Charge noise and spin noise in a semiconductor quantum device. *Nature Physics* **9**, 570 (2013).

[20] Kuhlmann, A. V. *et al.* Transform-limited single photons from a single quantum dot. *Nature communications* **6**, 8204 (2015).

[21] Giesz, V. *et al.* Coherent manipulation of a solid-state artificial atom with few photons. *Nature communications* **7**, 11986 (2016).

[22] Humphreys, P. C. *et al.* Linear optical quantum computing in a single spatial mode. *Physical review letters* **111**, 150501 (2013).

[23] Rohde, P. P. Simple scheme for universal linear-optics quantum computing with constant experimental complexity using fiber loops. *Physical Review A* **91**, 012306 (2015).

[24] Bentivegna, M. *et al.* Experimental scattershot boson sampling. *Science advances* **1**, e1400255 (2015).

[25] Zhang, C. *et al.* Experimental greenberger-horne-zeilinger-type six-photon quantum nonlocality. *Physical review letters* **115**, 260402 (2015).

[26] Loredo, J. *et al.* Boson sampling with single-photon fock states from a bright solid-state source. *Physical review letters* **118**, 130503 (2017).

[27] Unsleber, S. *et al.* Highly indistinguishable on-demand resonance fluorescence photons from a deterministic quantum dot micropillar device with 74% extraction efficiency. *Optics express* **24**, 8539–8546 (2016).

[28] Senellart, P., Solomon, G. & White, A. High-performance semiconductor quantum-dot single-photon sources. *Nature Nanotechnology* **12**, 1026 EP – (2017).

[29] U'Ren, A. B., Silberhorn, C., Banaszek, K. & Walmsley, I. A. Efficient conditional preparation of high-fidelity single photon states for fiber-optic quantum networks. *Physical review letters* **93**, 093601 (2004).

[30] Harder, G. *et al.* An optimized photon pair source for quantum circuits. *Optics express* **21**, 13975–13985 (2013).

[31] Pan, J.-W. *et al.* Multiphoton entanglement and interferometry. *Reviews of Modern Physics* **84**, 777 (2012).

[32] Simon, C.-M. *et al.* Robust quantum dot exciton generation via adiabatic passage with frequency-swept optical pulses. *Physical review letters* **106**, 166801 (2011).

[33] Liu, J. *et al.* A solid-state source of strongly entangled photon pairs with high brightness and indistinguishability. *Nature nanotechnology* **14**, 586–593 (2019).

[34] Wang, H. *et al.* Towards optimal single-photon sources from polarized microcavities. *Nature Photonics* **13**, 770–775 (2019).

[35] Tomm, N. *et al.* A bright and fast source of coherent single photons. *Nature Nanotechnology* **16**, 399–403 (2021).

[36] Barbour, R. J. *et al.* A tunable microcavity. *Journal of Applied Physics* **110**, 053107 (2011).

[37] Wang, D. *et al.* Turning a molecule into a coherent two-level quantum system. *Nature Physics* **15**, 483–489 (2019).

[38] Thomas, S. *et al.* Bright polarized single-photon source based on a linear dipole. *Physical Review Letters* **126**, 233601 (2021).

[39] Kaneda, F., Garay-Palmett, K., U'Ren, A. B. & Kwiat, P. G. Heralded single-photon source utilizing highly nondegenerate, spectrally factorable spontaneous parametric down-conversion. *Optics express* **24**, 10733–10747 (2016).

[40] Bruno, N., Martin, A., Guerreiro, T., Sanguinetti, B. & Thew, R. T. Pulsed source of spectrally uncorrelated and indistinguishable photons at telecom wavelengths. *Optics express* **22**, 17246–17253 (2014).

[41] Zhong, H.-S. *et al.* 12-photon entanglement and scalable scattershot boson sampling with optimal entangled-photon pairs from parametric down-conversion. *Physical review letters* **121**, 250505 (2018).

CHAPTER 4

MUCHOS PHOTONS

In the Chapter 3, I have shown our device can successfully generate a bright long stream of single-photons from a single quantum-dot with robust and conclusive indistinguishability. In addition to that, I displayed extraction efficiencies outperforming downconversion with equivalent levels of multi-photon suppression as well as indistinguishability. This gives us one-in-seven pulses at the end of a single-mode fiber which can be utilised as a multiphoton sources. Such properties are keys for enabling large-scale quantum photonic technologies.

To circumvents the limitations of downconversions single-photons sources, such as unwanted multiple-photon terms, schemes have been introduced with active spatial [1, 2], temporal [3, 4] and, spatio-temporal [5, 6], multiplexing that combine the output of many downconversion sources to create one bright source without deteriorating single-photon purity or indistinguishability [4]. However, the experimental setup commonly comes at a great cost both in terms of increasing size and complexity, and using bulk optical components that result in poor stability and scalability [7]. This is where integrated quantum photonics comes into the picture for demultiplexing. This platform allows photons to travel at longer delays without having a spectral diffusion overlap at different times. In 2017, Loredo and co-workers [8] reported Boson Sampling measurements at a much faster rate with up to five photons — higher rate than heralded N-fold photon sources based on downconversion [9].

The aim of this chapter is to realise a scalable multi-photon source from a single emitter using the latest integrated photonics. In order to achieve our goal, I first used a train of single-photons from our first generation device to create a multi-photon source. Then used active spatial and temporal photonic demultiplexing to create a multi spatial-mode photon source. device that is compatible with solid-state sources operating at 932 nm. I work closely with M. Lobino group from Griffith University to realise this scheme [10] where the fabrication and development of the demultiplexer is taken place.

4.1 Demultiplexing concept

I demultiplex a source with a single spatial mode and single photons. Lithium niobate (LN) separate temporal modes into a source within a single temporal mode and single photons in N separable spatial modes. The concept of multiplexing and demultiplexing is well known from classical optical communication, where the techniques are utilised to increase communication

bandwidth of an optical fiber. Multiplexing entails having multiple channels in some degree of freedom, typically frequency, combined into a single channel. This requires the multiple modes be orthogonal to avoid crosstalk. Demultiplexing is the reverse process where information from a single channel is distributed into multiple channels. In classical communication, frequency-division multiplexing is used, where the different information channels have different frequencies and are separated using an array waveguide grating [11]. Frequency-division multiplexing is unsuitable for demultiplexing of single-photons in the context of quantum information processing, as the photonic qubits are required to have the same frequency for application in quantum information gates.

Spatial multiplexing can modify N inefficient probabilistic sources into a single near-deterministic photon source [12]. N inefficient sources are connected to a main channel through an active switch. When the creation of a single photon in one source is heralded that source is switched to the main channel and the remaining sources are blocked. By having sufficient sources the success probability of single-photon creation per pulse approaches unity. Spatial multiplexing was used to improve the performance of a SPDC source: by using two sources the heralded count rate was enhanced by 63% [12].

4.2 The MuCHOs

The demultiplexer device is known as the Multiple Channel Optical Switch (MuChOS) and depicted in Figure 4.1. It consists of a network of reconfigurable directional couplers with electro-optically tunable splitting ratios.
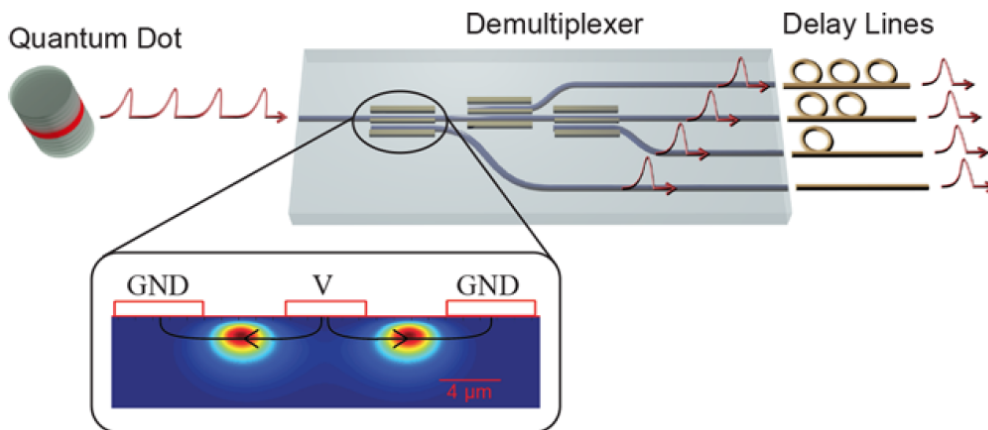
Figure 4.1: Schematic for ideal active spatial-temporal demultiplexing. A stream of single-photons emitted at successive time intervals from a quantum dot-micropillar cavity system are actively routed into different spatial channels by an optical demultiplexer. A set of delay lines at the output can be used to match the arrival times of the single photons. The colormap (a.u.) represents the waveguides intensity mode profiles at 932 nm and the black arrows show the direction of the applied electric field.

Figure 4.2 presents the integrated waveguide with one input and four output channels fabricated using annealed proton exchange technique [13] on an X-cut lithium niobate substrate. The splitting ratio can be tuned between $0 - 100\%$ using electrodes that are patterned on
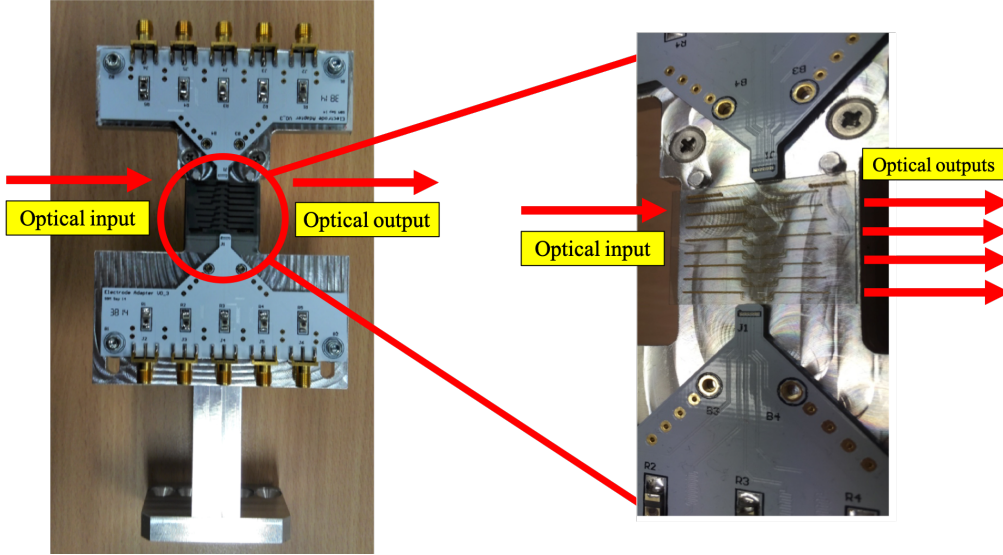
Figure 4.2: Electro-optical device (MuCHOS) in the lab consist one inputs and four output channels. Zoom out : Close up the electrode array.

the top of the waveguides by changing the phase mismatch, $\triangle\beta$ between interacting modes [14]. Monolithic integration of the directional coupler network on a single chip is necessary for reduced insertion losses, and with our technology it allows up to 10 output channels in a 5 cm long device. The output of an n-channel demultiplexer can be expressed by n-photon count rate $^c\mathrm{DM}^{(n)}$ as below:

$$^C\mathrm{DM}^{(n)} = R[\eta_{SD}\eta_{det}]^n S_{DM}{}^{(n)} \tag{4.1}$$

where $\eta_{SD} = \eta_{QD}T$ is the product of the source brightness η_{QD}, defined as the probability of emitting one photon at the input of the demultiplexer for each excitation pulse, times the total transmission of the device T. R is the pump rate of the source and η_{det} is the detector efficiency. $S_{DM}(n)$ is a parameter which accounts for how the efficiency of the demultiplexing scheme scales with increasing number of photons and it represents the limit of what can be achieved by the demultiplexer with a lossless and deterministic source. Note that the term $[\eta_{SD}\eta_{det}]^n$ is intrinsically probabilistic, and will unavoidably result in an exponential decay with photon number. In a probabilistic scheme [8]—made of a network of passive beam splitters— the demultiplexing parameter scales as $S_{DM}{}^{(n)} = (1/n)^n$, super-exponentially decreasing with n—certainly a non-scalable approach! In contrast, in an active demultiplexing scheme the scaling is

$$S_{DM}{}^{(n)} = \frac{1}{n}\Big[\eta_{DM}^n + (n-1)\Big(\frac{1-\eta_{DM}}{n-1}\Big)^n\Big] \tag{4.2}$$

where η_{DM} is the "switching efficiency", defined as the average probability of routing a single photon in the desired channel in each time bin. In the limit of deterministic demultiplexing, i.e. $\eta_{\mathrm{DM}} \to 1$, the scaling becomes polynomial in n—thus constituting a *scalable* approach.

The waveguides were fabricated with a 6 μm channel width and a proton exchange [13] depth of 0.47 μm followed by annealing in air at 328 °C for 15 h. These parameters are chosen in order to ensure good overlap with single mode fiber and single-mode operation at ~ 930 nm,
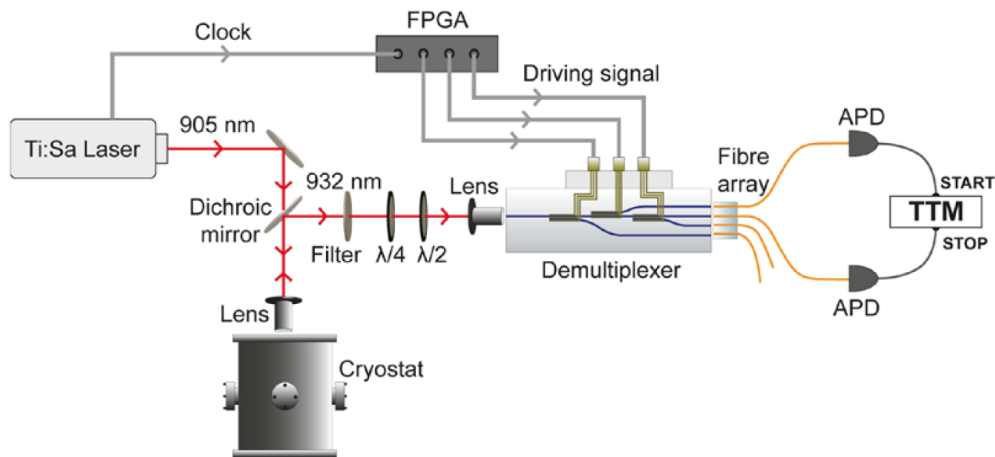
Figure 4.3: Setup for the experimental implementation of the demultiplexing scheme (detailed description is given in the main text).

the emission wavelength of our InGaAs dot. Each directional coupler has a distance between waveguide centres of 8.84 μm and a 4.5 mm length (equal to three coupling lengths), resulting in complete transmission of light into the coupled waveguide when no voltage to the corresponding switching electrodes is applied. The discussion of details design and fabrication is not in the context of this chapter, however can be found in Ref [13]. Difference from this ideal behaviour is from non-uniform waveguide channel widths, caused by the resolution of the photolithography.

4.3   Experimental setup

I investigated the performance of the MuCHOS with a single-photon source based from our first generation device—a QD deterministically coupled to a micropillar cavity [15, 16]. In the Fig. 4.4, I excite the dot quasi-resonantly with 5 ps pulsed Ti: Sapphire laser centred wavelength at 905 nm at 80 MHz repetition rate.

The single-photons are emitted with a wavelength at 932 nm and are collected by microscope objective lens (Olympus LMPLN10XIR with N.A = 0.3). A FWHM bandpass filter (0.85 nm) is used to filter the single-photons emission from the pump excitation. Quarter- and half-wave plates are used at the input for polarisation alignment as the waveguides within the demultiplexer guide one polarisation (horizontal, H). Since our source is only weakly polarised [16], this reduced the photon flux by ~ 50%, an issue absent if operated with sources engineered to exhibit a large degree of polarization. Following the input injection to the MuCHOS with a lens of NA = 0.55, the output modes are collected with a fibre V-Groove array.

The detection is measured using avalanche photodiodes (APDs) with 30% average quantum efficiency, and a time-tagging module (TTM) connected with single-mode fiber. The electrodes of the demultiplexer are driven with a custom-made pulse generator based on a field programmable gate array (FPGA) [17]. The FPGA produces a preset sequence of pulses with varying amplitude voltages that are used to tune the splitting ratio of the directional couplers

between on and off values. The driving pulses are synchronized with the clock signal of the Ti:Sapphire laser using internal phase-locked loops (PLL) of the FPGA which provide an adjustable time delay with a low time jitter (300 ps)[17]. By changing the programming of the pulse generator, I can actively drive the MuCHOS into any configuration. It needs to be highlighted here that the reconfiguration is not event-ready since the clocking is derived from the pump laser rather than the emission of the single-photons from the QD. Driving voltages were optimized by maximizing the coincidence counts between the different channels. As imperfections in the fabrication may cause non-ideal performance, it is necessary to apply a nonzero voltage. To verify the correct operation of the MuCHOS, as well as synchronization with the master laser, I first reconstruct the time histograms of two-photon coincidence counts between the first output of the demultiplexer and all other channels. The MuCHOS is cyclically operated such that the first photon is sent to output one, the second to output two, and so on, and coincidences are measured between all four outputs simultaneously.

4.4 Discussion

The histograms from the photon-coincidences detected by all four APDs are presented in Fig 4.4. Enhanced peaks are clearly observed in coincidences at the corresponding delays of our demultiplexer, together with suppressed counts at different delays—indicating the MuCHOS is functioning. The non-vanishing coincidence counts (smaller peaks) in the histograms arise from imperfect operation of the modulated couplers. From the data in Fig. 4.4 I calculated the splitting ratios of the three switches for both settings using a least-squares fitting procedure (see Table 4.1). The presence of non-zero *off* values and non-unity *on* values reveals the non-ideal operation of the device. The absence of counts at zero time delay (at the same level of accidental counts) is due to the low $g^2(0)$ value of the source, measured as $g^2(0) = 0.029 \pm 0.00$ at $P = 3P_0$ in [15].

switch	1	2	3
on	0.87 ± 0.06	0.94 ± 0.05	0.90 ± 0.06
off	0.06 ± 0.02	0.13 ± 0.03	0.13 ± 0.05

Table 4.1: Splitting ratios of the directional couplers calculated from the data in Fig. 4.3, with uncertainty from the fit confidence. Non-zero off values are caused by incorrect voltages from the pulse generator. Non-unity on values are caused by incorrect driving voltages and deviations from the desired coupling rate due to waveguide imperfections.

I measure the relationship between the power-dependent rate of two-photon coincidences $c_{DM}(2) = c_{max}(2)[1 - exp(-P/P_0)]^2$ at outputs 1 and 2 of our demultiplexer (inset Fig. 4.5). As expected for a QD pumped under quasi-resonant excitation it follows a saturation function quadratic in the P-dependance of the single-photon brightness. A fit to the data results in a maximum detected 2-photon rate of $c_{max}(2) = 70.9 \pm 3.0$ Hz, and the saturation power of $P_0 = 348 \pm 16 \mu$W. The rate of two-fold and three-fold photon coincidences are respectively 65 ± 10s^{-1} and 0.11 ± 10s^{-1} at the output for a pump power $P = 660 \mu$W. The switching efficiency η_{DM} is
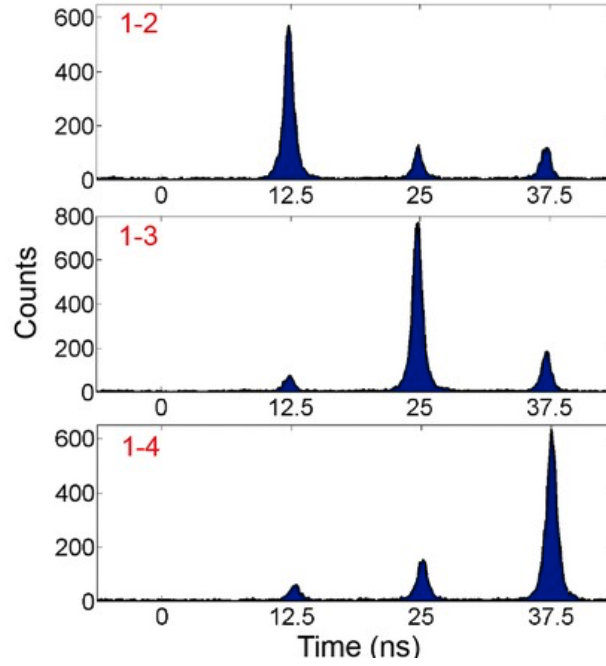
Figure 4.4: Two-photon coincidences between the first output (1) and other outputs (2, 3, 4) for a pump power $P = 660\mu$W and a two minute acquisition time

finally estimated by fitting all ten combinations of two and three photon coincidence rates with Eq. 4.1, with $R = 80$ MHz, $\eta_{det} = 30\%$, and $\eta_{SD} = 0.76\%$ is calculated from the total number of counts measured with the four detectors. I find an average switching efficiency $\eta_{DM} = 0.78\pm0.06$, in good agreement with the value $\eta_{DM} = 0.80\pm0.09$ predicted from the measured splitting ratios. Four-fold coincidences were predicted to be 0.18 ± 0.06 mHz due to the low value of T in the current system, producing insufficient statistics in the acquisition time of 87 min. Dark counts of our detectors were ~300 Hz per detector, giving no significant contribution to coincidence measurements.

To investigate the potential of our technology for the realisation of a multi-photon source with larger numbers I calculate the expected photon rates at the output of the demultiplexer for a state-of-the-art QD with 15% polarised brightness pumped under resonant-excitation [18].

The transmission of waveguide is tested at 932 nm on the first and fourth on two central inputs. The total transmission of our demultiplexer is tested by coupling the waveguide with a gaussian mode from a single-mode optical fibre, and is found to be T=30%. This value is compatible with an overlap with the waveguide mode $\simeq 85\%$ as measured from mode imaging at the output of the waveguide, 14% Fresnel losses at the input and output facet, and propagation losses $\simeq 0.65$ dBcm, and is the same value measured from a straight waveguide fabricated on the same chip, meaning that the couplers and electrodes did not introduce extra losses. In Fig. 4.5 I report the expected photon rates for increasing photon numbers calculated for a pump rate $R = 80$ MHz, $\eta_{DM} = 78\%$, and a transmission $T = 0.3/(0.86 \times 0.86)$ corrected for Fresnel losses, that can be eliminated with an anti-reflection coating at the input and output facets. The QD brightness is corrected by an additional loss factor 65% that takes into account the coupling efficiency of the QD emission mode to a single mode fibre [15]. The proposed system with these parameters is expected to outperform a probabilistic demultiplexing scheme—made

of a network of passive beam splitters with zero propagation losses—or a number of photons $n>4$ and would enable a brightness which is three orders-of-magnitude larger than what could be obtained with six heralded SPDC sources with equivalent quality and brightness of 0.075 [18] (see Fig. 4.5). The same calculation for a resonantly-excited QD with a 14% brightness measured at the output of a single-mode fibre [19], shows that would enable, a 6-photon rate of $\simeq 0.1$ Hz.
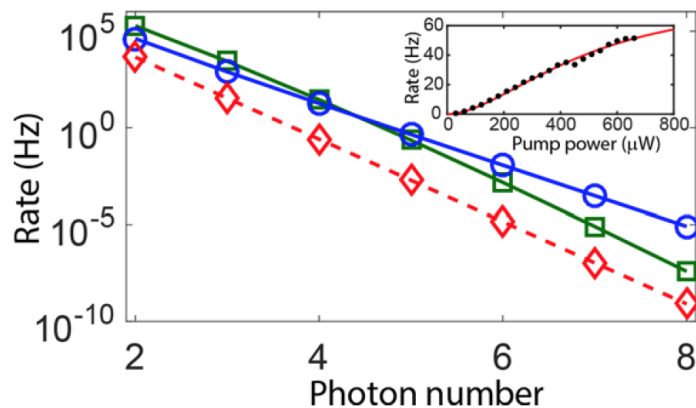
Figure 4.5: Comparison between the estimated photon rates at the output of the demultiplexer of an active (○) and probabilistic (□) demultiplexing schemes for a state-of-the-art QD pumped [18] under resonant excitation. (◇) shows the rate of n heralded single photon sources with brightness of 0.75%. Inset shows the measured two-photon coincidence rates $c_p(2)$ as a function of the pump power P. Red line is the fit made with the saturation function given in the main text. Error bars are smaller than data points.

This technology offers great potential for further improvement, in particular by the use of the Reverse Proton exchange (RPE) technique [13] for an improved coupling with optical fibres, and reduced surface-scattering losses. APE technique implemented in this work generates an asymmetry in the measured intensity profile of the waveguides due to the asymmetry in the refractive index profile. One of the main impact is reduces the coupling efficiency with the optical fiber and the mode overlap in the frequency conversion process. For example the non-vanishing coincidence counts in the histograms peak (Fig. 4.4). To overcome the device imperfection, RPE technique is proposed which H+ near the LN surface are removed while other proton are annealed deeper into the substrate. The significant component for effective coupling mode is the anisotropic diffusion because the lateral H+ plays a crucial role in fabricating waveguides. Lenzini and co-workers [13] show the changes in the peak of the mode profile of the RPE waveguide symmetrically while reducing the surface scattering component of the losses and demonstrates 90% coupling efficiency. As for this work, I estimate that I can achieve insertion losses, lower than 3 dB. Furthermore the switching efficiency of the couplers can be increased with an optimised driving voltage and waveguide fabrication process. Such upgrades will enable the scaling of this platform to a larger number of photons.

4.5 Conclusion

I have proposed, and experimentally implemented, active demultiplexing of single-photons from a solid-state source with a single integrated device. The performance of the demultiplexer has been analysed in conjunction with a quantum-dot micropillar device pumped under quasiresonant excitation, and I have discussed the potential of our technology for state-of-the-art quantum dots. The proposed demultiplexing device is of general interest for any bright, temporally distributed single-photon source and provides a scalable approach for the realisation of multiphoton sources of larger photon numbers. Our platform thus constitutes a very promising approach for scalable quantum photonics, in particular for protocols of intermediate—i.e., non-universal—quantum computation, such as Boson Sampling [20–22] with multiphotons states up to $N = 14$ even at low photon rate [23].

REFERENCES

[1] Ma, X.-s., Zotter, S., Kofler, J., Jennewein, T. & Zeilinger, A. Experimental generation of single photons via active multiplexing. *Physical Review A* **83**, 043814 (2011).

[2] Collins, M. J. *et al.* Integrated spatial multiplexing of heralded single-photon sources. *Nature communications* **4**, 2582 (2013).

[3] Kaneda, F. *et al.* Time-multiplexed heralded single-photon source. *Optica* **2**, 1010–1013 (2015).

[4] Xiong, C. *et al.* Active temporal multiplexing of indistinguishable heralded single photons. *Nature communications* **7**, 10853 (2016).

[5] Meany, T. *et al.* Hybrid photonic circuit for multiplexed heralded single photons. *Laser & photonics reviews* **8**, L42–L46 (2014).

[6] Mendoza, G. J. *et al.* Active temporal and spatial multiplexing of photons. *Optica* **3**, 127–132 (2016).

[7] O'brien, J. L. Optical quantum computing. *Science* **318**, 1567–1570 (2007).

[8] Loredo, J. *et al.* Boson sampling with single-photon fock states from a bright solid-state source. *Physical review letters* **118**, 130503 (2017).

[9] Wang, H. *et al.* High-efficiency multiphoton boson sampling. *Nature Photonics* **11**, 361–365 (2017).

[10] Lenzini, F. *et al.* Active demultiplexing of single photons from a solid-state source. *Laser & Photonics Reviews* **11**, 1600297 (2017).

[11] Takahashi, H., Suzuki, S., Kato, K. & Nishi, I. Arrayed-waveguide grating for wavelength division multi/demultiplexer with nanometre resolution. *Electronics letters* **26**, 87–88.

[12] Collins, M. J. *et al.* Integrated spatial multiplexing of heralded single-photon sources. *Nature communications* **4**, 2582 (2013).

[13] Lenzini, F., Kasture, S., Haylock, B. & Lobino, M. Anisotropic model for the fabrication of annealed and reverse proton exchanged waveguides in congruent lithium niobate. *Optics express* **23**, 1748–1756 (2015).

[14] Taylor, H. Optical switching and modulation in parallel dielectric waveguides. *Journal of Applied Physics* **44**, 3257–3262 (1973).

[15] Loredo, J. C. *et al.* Scalable performance in solid-state single-photon sources. *Optica* **3**, 433–440 (2016).

[16] Gazzano, O. *et al.* Bright solid-state sources of indistinguishable single photons. *Nature communications* **4**, 1425 (2013).

[17] Haylock, B. *et al.* Nine-channel mid-power bipolar pulse generator based on a field programmable gate array. *Review of Scientific Instruments* **87**, 054709 (2016).

[18] Somaschi, N. *et al.* Near-optimal single-photon sources in the solid state. *Nature Photonics* **10**, 340 (2016).

[19] Ding, X. *et al.* On-demand single photons with high extraction efficiency and near-unity indistinguishability from a resonantly driven quantum dot in a micropillar. *Physical review letters* **116**, 020401 (2016).

[20] Aaronson, S. & Arkhipov, A. The computational complexity of linear optics. In *Proceedings of the forty-third annual ACM symposium on Theory of computing*, 333–342 (ACM, 2011).

[21] Aaronson, S. A linear-optical proof that the permanent is# p-hard. *Proceedings of the Royal Society A: Mathematical, Physical and Engineering Sciences* **467**, 3393–3405 (2011).

[22] Huh, J., Guerreschi, G. G., Peropadre, B., McClean, J. R. & Aspuru-Guzik, A. Boson sampling for molecular vibronic spectra. *Nature Photonics* **9**, 615 (2015).

[23] Li, M., Garcia-Ripoll, J. J. & Ramos, T. Scalable multiphoton generation from cavity-synchronized single-photon sources. In *APS March Meeting Abstracts*, vol. 2021, V28–001 (2021).

OPTICAL ENTANGLING GATES

5.1 Introduction to entanglement

Entanglement is a phenomena at the heart of foundation for quantum mechanics [1] and an essential building block for quantum technologies. Quantum entanglement refers to correlations between the results of measurements made on distinct subsystems of a composite system. These correlations cannot be explained in terms of standard statistical correlations between classical properties inherent in each subsystem [2]. Famously, early discussion of entanglement was led by Schrödinger [3] and Einstein, Podolsky and Rosen in 1935 [4]. Quantum entanglement has moved from a "spooky theory" to a key phenomena enabling tasks such as quantum cryptography [5], quantum teleportation [6, 7] as well as quantum information [8]. In the 1960s, attention was refocused on entanglement by Bell [9], and the subsequent CHSH inequality [10].

Previously, researchers realised entanglement either from a single source where two entangled particles emerge, or interfering two particles with each other. In the early 1980s, Aspect and co-workers created entanglement by an atomic cascade transition [1]. In the experiment, calcium atoms excite into higher energy levels and emit photon pairs. The photons are polarisation entangled, however the process is slow and happens in random directions. Ever since then, innumerable experiments had been carried out to explore the mystery of entanglement involving protons [11, 12], atoms [13], trapped ions [14, 15] and photons [16–20].

In the late 1980s, the most popular and conventional technique to generate pairs of entangled photons was spontaneous parametric downconversion [16, 17, 21–23]. In this, a pair of correlated photons is generated when a nonlinear crystal $\chi^{(2)}$ is optically pumped and the pairs are naturally entangled in frequency [17, 24] and transverse spatial mode, and can be made entangled in polarisation [25]. This technique has shown the highest fidelity entangled photon pairs [26]. In recent works, Pan and co-workers successfully demonstrated up to ten entangled photons [27], at a count rate that is three orders of magnitude higher than any other down-conversion source at that time. Despite this success, SPDC has an inherent problem, in that the generation of entangled pairs is probabilistic and follows Poissonian statistics [28]. This means that the photon pairs are generated at random times with a low efficiency [29]; the resulting multiple pairs leads to errors when performing quantum gates. In order to boost gate performance, one needs to pump with lower power intensity, although this has the undesirable effect of reducing the count rate of the gate [30]. Although this technique has proven

very useful for demonstrating the viability of small quantum circuits, it is difficult to scale to larger applications. Furthermore, it is very difficult to maintain the stability of the experiment involving bulk optical elements. Photonic scalability is what we need in the future as we push forward with experiments require more complex tasks [31–35]. In attempt to realise scalable photonic technologies, quantum dots have risen as a major contender in this league.

Recently times have seen multiple observations of entangled photon pairs by quantum dots [36–38]. Among the first reported were Benson and co-workers [39] and Moreau's groups [40], via radiative decay of biexciton-exciton-ground state emission. During this process, two radiative recombination paths are possible through two exciton states of orthogonal polarisation. The emitted photons are entangled if the two states are degenerate and the recombination paths are indistinguishable [39, 41]. Since then, strong efforts has been made to generate entangled photon pairs from the dots [42–45] for photonic quantum information processing. Akopian et al. [36] entangled photon pairs by selecting them with spectral filtering. This method allowed photon pairs within a narrow spectral overlap of the two fine structure components and erases the information path contained in the photons. The photon pairs were entangled, violate Bell's inequality, but the method is not event-ready since it used cw lasers and the pairs are generated randomly. An example of event-ready polarisation-entangled photon pairs was demonstrated by Benson et al. [39], using p-i-n junction surrounded by a microcavity. The dot was electrically driven producing pairs of photons polarised either horizontally or vertically that violates Bell's inequality. Although the above mentioned methods generate highly entangled photons, further improvements are needed in order to solve the fine-structure splitting (FSS) caused by the imperfect degenerate energy during recombination process. One way is to grow the dot on higher symmetry substrates [46, 47], another is to apply various tuning schemes involving electric [48] or magnetic [49] fields, strain [50] or optical [51] fields.

A promising alternative we explore here is to generate entangled photons by manipulating the highly indistinguishable, on-demand, photons from a QD using linear optical elements [52–55]. Ideally, when two indistinguishable photons are interfered at a beam splitter—input labelled as a and b—quantum interference effect ensures that when photons are detected at different output ports—labelled as c and d—of the beam splitter should be entangled in polarisation [21, 22]. The output state is expected to be EPR-Bell state:

$$|\psi^-\rangle = \frac{1}{\sqrt{2}}\left(|H\rangle_c|V\rangle_d - |V\rangle_c|H\rangle_d\right), \tag{5.1}$$

where H and V is horizontal and vertical polarisation respectively. This scheme relies on coincidence detection, since it also generates two photons in one mode. Fattal et al. [52] observed a clear violation of Bell's inequality with a high fidelity of 0.69, beyond the classical limit of 0.5. However, due to its low quantum extraction efficiency, the entanglement produced from this method does not allow the creation of event-ready entangled photon pair. In fact, the post-selection suggests that the entangled photons are destroyed when this method succeeds. Current advanced in a deterministic fabrication technologies has improved the inherent collection efficiency of single photons based on semiconductor quantum dots, achiving efficiencies

as high as 65% [56–60]. Such sources are very suitable for use in linear optics, where entangling gates consist of linear optical elements such as beam splitters and wave-plates as well as detectors. This shall be further discussed in details in Section 5.3.

5.2 Photons as qubits

In the classical information, the basic unit of information is known as a bit. A bit has two states—it can only be either 0 or 1. For example, a flipped coin can land on heads or tails, but not heads and tails at the same time. On the other hand, quantum information can be presented by a quantum bit—qubit—that can be in other state than the basis states $|0\rangle$ and $|1\rangle$. A two-level quantum systems, qubits can occupy any superposition of these two basis states as follows;

$$|\psi\rangle = \alpha|0\rangle + \beta|1\rangle = \alpha \begin{pmatrix} 1 \\ 0 \end{pmatrix} + \beta \begin{pmatrix} 0 \\ 1 \end{pmatrix}, \tag{5.2}$$

where $|0\rangle$ and $|1\rangle$ are the two basis states that form the qubit while α and β are complex numbers which satisfy $|\alpha|^2 + |\beta|^2 = 1$. The absolute square of the probability amplitude $|\psi|^2$, give the probability of measuring the qubit in states $|0\rangle$, $|\alpha|^2$ and $|1\rangle$, $|\beta|^2$. All the states in Eq. 5.2 can be represented in Bloch-sphere as illustrated in Figure 5.1. The pole of the sphere corresponds to the classical bit values $|0\rangle$ and $|1\rangle$, or *computational basis states*, and all other states are *quantum superposition states*.
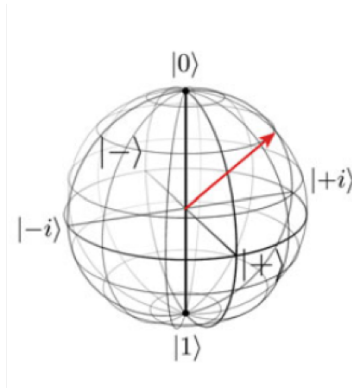
Figure 5.1: Bloch sphere representation of a qubit in pure quantum states i.e with the computational basis states

While ideally the states are assumed to be pure, in reality during the experiments noise is inevitable. Thus, *mixed quantum states*, which lie within the sphere, can be represented by the density-matrix operator:

$$\hat{\rho} = \sum_i p_i |\psi_i\rangle\langle\psi_i|, \tag{5.3}$$

where p_i represents the probability that the light field occupies state $|\psi_i\rangle$. For pure states, p_i is $p_{i\neq0} = 0$ and $p_0 = 1$. The ensemble average of an observable $\hat{O}$ can be found from the trace of

its product with the density matrix [61]:

$$\langle \hat{O} \rangle = \text{Tr}\{\hat{\rho}\hat{O}\}, \tag{5.4}$$

when the photon number states are used as basis states, the diagonal elements of $\hat{\rho}$ contain the photon number probabilities:

$$P(n) = \text{Tr}\{\hat{\rho}|n\rangle\langle n|\} = \langle n|\hat{\rho}|n\rangle, \tag{5.5}$$

where $P(n)$ is the probability that a source emits n photons. The photon number probabilities are normalised such that:

$$\sum_{n=0}^{\infty} P(n) = \text{Tr}\{\hat{\rho}\} = 1, \tag{5.6}$$

which satisfies the usual density-matrix normalisation condition.

Arguably, the simplest way to realise quantum states is with photons. They are ideal carriers to encode the information over long distance due to their low interaction with the environment. Bennet and Brassard [62] proposed in 1984 that photons can be used to encode messages via secret key-distribution to avoid eavesdropping. More recently, photons have been used to realise in efficient quantum-logic gates based on linear optics [63, 64]. In the early days of quantum information, there were several difficulties in manipulating photonic qubits. Initially, it thought that entangling photons required a deterministic interaction between two independent photons in order to achieved a strong nonlinearities during well-defined intervals [65, 66]. However, in a breakthrough paper Knill and co-workers [63] showed that it is possible to realise entangled photons using only linear optical elements. A key challenge is realising source of highly indistinguishable deterministic single photons in quantum computation [67, 68] and in quantum repeaters [69, 70]. Quantum teleportation has been realised with probabilistic gates [64, 71], but this type of scheme has massive resource overhead and does not stable, hence is a major roadblock for quantum photonics.

5.3 Non-deterministic entangling gates

Qubits can be encoded in various degrees-of-freedom of photons, such as polarisation [72], orbital angular momentum [73], time-bin [74, 75], and spatial mode [76]. In this chapter we will manipulate the polarisation of the photons. This is an excellent encoding due to the availability of high efficiency polarisation-control elements, and the relative insensitivity of most materials to birefringent thermally-induced drifts [17, 77]. Early sources of polarisation-entangled photons suffered low brightness and low efficiency [17–20]. With our second second-generation device, we obtain single-photon with high brightness and efficiency, and are able to generate pairs of entangled polarisation photons using linear optical entangling gates. In this section, we will briefly discuss the theory behind such optical entangling gates.

Beam splitters play a critical role in a range of devices: interferometers [78]; quantum entan-

gler [79]; and Bell measurement device [22]. We present a single photon by the bosonic creation operator, $\hat{a}^\dagger$, as $|1\rangle = \hat{a}^\dagger|0\rangle$ where $|0\rangle$ is the vacuum state of the field. The corresponding annihilation operator, $\hat{a}$, removes the photon $|0\rangle_U = \hat{a}|1\rangle_U$. These operators obey the commutation relation $[\hat{a}, \hat{a}^\dagger] = 1$ which implies that $\hat{a}|n\rangle = \sqrt{n}|n-1\rangle$ and $\hat{a}^\dagger|n\rangle = \sqrt{n+1}|n+1\rangle$. Now the transformation from input to output in a beam splitter is [80]:

$$\hat{a}_U \rightarrow t\hat{a}_U + ir\hat{a}_R \quad , \quad a_R \rightarrow t\hat{a}_R + ir\hat{a}_U, \tag{5.7}$$

where U and R signify the mode upward and downward modes, and,

$$[\hat{a}_U, \hat{a}_U^\dagger] = [\hat{a}_D, \hat{a}_D^\dagger] = 1, \tag{5.8}$$

with all other commutation relations equal to zero.

Ideally, a lossless 50% beam splitter [81] is characterised by following transformation:

$$\hat{a} \rightarrow (\hat{c} + i\hat{d})/\sqrt{2}, \quad \hat{b} \rightarrow (i\hat{c} + \hat{d})/\sqrt{2}. \tag{5.9}$$

For polarising beam splitter (PBS), the transformation is as follows:

$$\hat{a}_H \rightarrow \hat{c}_H \quad \text{and} \quad \hat{a}_V \rightarrow i\hat{d}_V, \tag{5.10}$$

$$\hat{b}_H \rightarrow \hat{d}_H \quad \text{and} \quad \hat{b}_V \rightarrow i\hat{c}_V. \tag{5.11}$$

The transmission and reflection of beam splitters is illustrated in Fig. 5.2 where two incoming modes on either side of the beam splitter be denoted by a and b and the outgoing modes by c and d. When two single photons interfere at the beam splitters, they can be entangled. The relationship between the input and output can be described as follows:

$$\begin{pmatrix} \hat{a}_1^\dagger \\ \hat{a}_2^\dagger \end{pmatrix}_{in} \rightarrow U \begin{pmatrix} \hat{a}_1^\dagger \\ \hat{a}_2^\dagger \end{pmatrix}_{out} \tag{5.12}$$

where the 50/50 beam splitter matrix is defined by $U = \frac{1}{\sqrt{2}} \begin{pmatrix} 1 & i \\ i & 1 \end{pmatrix}$.

Under this transformation, the Bell states is given by:

$$|\psi^+\rangle = \frac{1}{\sqrt{2}}(\hat{h}_1^\dagger \hat{v}_2^\dagger + \hat{v}_1^\dagger \hat{h}_2^\dagger)_{in}|0\rangle \rightarrow \frac{i}{\sqrt{2}}(\hat{h}_1^\dagger \hat{v}_1^\dagger + \hat{v}_2^\dagger \hat{h}_2^\dagger)_{out}|0\rangle, \tag{5.13}$$

$$|\psi^-\rangle = \frac{1}{\sqrt{2}}(\hat{h}_1^\dagger \hat{v}_2^\dagger - \hat{v}_1^\dagger \hat{h}_2^\dagger)_{in}|0\rangle \rightarrow \frac{1}{\sqrt{2}}(\hat{h}_1^\dagger \hat{v}_1^\dagger - \hat{v}_2^\dagger \hat{h}_2^\dagger)_{out}|0\rangle, \tag{5.14}$$

$$|\phi^\pm\rangle = \frac{1}{\sqrt{2}}(\hat{h}_1^\dagger \hat{h}_2^\dagger \pm \hat{v}_1^\dagger \hat{h}_2^\dagger)_{in}|0\rangle \rightarrow \frac{1}{\sqrt{2}}(\hat{h}_1^\dagger \hat{h}_2^\dagger \pm \hat{v}_1^\dagger \hat{v}_2^\dagger)_{out}|0\rangle, \tag{5.15}$$

Our goal in this chapter is to generate entanglement between independent single photons emitted by single QD of our second generation device QD in our lab. In principle, entanglement
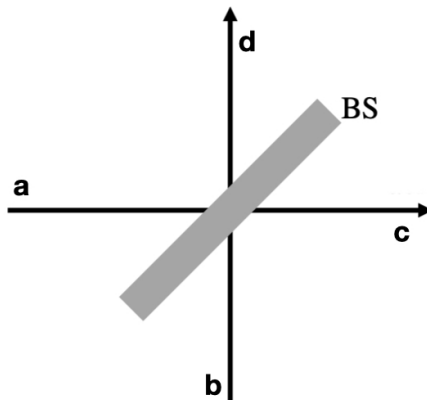
Figure 5.2: The beam splitter with two input modes ; a and b and two output modes c and d

can be induced between noninteracting single-photons, provided they are quantum mechanically indistinguishable [52]. Taking advantages of our deterministic and indistinguishable single-photons [56], we create polarisation-entangled photon-pairs by measurement [21, 22]. This type of entanglement can be easily produced and manipulated with basic optical elements e.g., polarising beam splitters, polarisers and wave plates [29]. The most significant advantage is that this scheme does not require photon-number resolving detectors. Furthermore, the photons are sent through a Hong-Ou-Mandel setup instead of a Mach-Zechnder interferometer, thus removing the requirement of maintaining phase stability on the order of the photon's wavelength. This stabilisation will produce a better visibility at HOM interference [82].

5.4 Event-ready entangling gates

Browne and Rudolph [83] proposed using linear optical elements such as beam splitters and wave plates, to boost success probability of the probabilistic gates by replacing the teleportation gate [84] with a fusion mechanism [85, 86]. This fusion gate scheme produces an entangled states with a probability of 50%, reduces resource overhead by heralding on successful events, and recycling already entangled photons in the event of a failed detection when attempting to produce more. Fig. 5.3 illustrates the fusion gate with four inputs each a single photon, half-wave plates (HWP), the polarising beam splitters (PBS), with the output sent to a rotating polarizing beam splitter (RPBS) and detectors. The framework of theory allowing for non-perfect visibility in our experiment is developed by Nicolas Quesada [87]. We will be dealing with linear optics calculations involving spatial modes, polarisation degrees of freedom and partially distinguishable photons. The following notation: $a_{i,\sigma,k}$ is a destruction operator for a photon in path i, polarisation σ, and frequency profile k. These operators satisfy commutation relations:

$$[a_{i,\sigma,k}, a^{\dagger}_{i',\sigma',k'}] = \delta_{i,i'}, \delta_{\sigma,\sigma'}\delta_{k,k'}, \tag{5.16}$$

$$[a_{i,\delta,k}, a_{i',\delta',k'}] = 0, \tag{5.17}$$

$$[a^{\dagger}_{i,\sigma,k}, a^{\dagger}_{i',\sigma',k'}] = 0 \tag{5.18}$$

The values $\sigma = 1$ for horizontal polarisation and $\sigma = 2$ for vertical polarisation. Polarising beam splitters (PBS) and half wave plates (HWP) in the operators. For each of these operations one can introduce a unitary operators, $\mathcal{U}_{i,j}$ (for a PBS between paths i and j) and $\mathcal{V}_k$ (for a HWP in path k) whose action in the canonical operators is as follows

$$\mathcal{U}_{ij}a_{i,1,k}\mathcal{U}_{ij}^\dagger = a_{i,1,k} \quad , \quad \mathcal{U}_{ij}a_{i,2,k}\mathcal{U}_{ij}^\dagger = a_{j,2,k}, \tag{5.19}$$

$$\mathcal{V}_k a_{k,1,l}\mathcal{V}_k^\dagger = \frac{a_{k,1,l} + a_{k,2,l}}{\sqrt{2}} = d_{k,1,l} \quad , \quad \mathcal{V}_k a_{k,1,l}\mathcal{V}_k^\dagger = \frac{a_{k,1,l} - a_{k,2,l}}{\sqrt{2}} = d_{k,2,l}. \tag{5.20}$$

The operators $d_{k,\sigma,l}$ satisfy commutation relations analogous to Eq. 5.16 and can be identified with destruction operators for the diagonal ($\sigma = 1$) and antidiagonal ($\sigma = 2$) polarisations. PBS and HWPs do not modify the frequency profile of the modes, i.e., they leave unchanged the third index of the operators.

The inputs of the gates are prepared as follows:

$$|\psi_{in}\rangle = d_{1,1}^\dagger d_{2,1}^\dagger d_{3,1}^\dagger d_{4,1}^\dagger |\text{vac}\rangle = |D\rangle_1 |D\rangle_2 |D\rangle_3 |D\rangle_4, \tag{5.21}$$

where four inputs ($d = 1, 2, 3, 4$) in the paths $1-4$ are prepared in the diagonal polarisation state $|D\rangle_i = \frac{1}{\sqrt{2}}(|H\rangle_i + |V\rangle_i)$. Each pair of photons are interfered at respective PBS as follows—Photon 1 and Photon 2 at PBS1, while Photon 3 and Photon 4 at PBS2. This yields:

$$|\psi_{PBS}\rangle = \mathcal{U}_{12}\mathcal{U}_{34}|\Psi_{in}\rangle = \mathcal{U}_{12}d_{1,1}^\dagger d_{2,1}^\dagger \mathcal{U}_{34}^\dagger d_{3,1}^\dagger d_{4,1}^\dagger \mathcal{U}_{34}^\dagger |\text{vac}\rangle \tag{5.22}$$

$$= \frac{1}{4}\left(a_{2,2}^\dagger a_{2,1}^\dagger + a_{1,1}^\dagger a_{1,2}^\dagger + a_{1,1}^\dagger a_{2,1}^\dagger + a_{2,2}^\dagger a_{1,2}^\dagger\right)$$

$$\times \left(a_{4,2}^\dagger a_{4,1}^\dagger + a_{3,1}^\dagger a_{3,2}^\dagger + a_{3,1}^\dagger a_{4,1}^\dagger a_{4,2}^\dagger a_{3,2}^\dagger\right)|\text{vac}\rangle$$

$$= \frac{1}{4}\left(|0\rangle_1 |HV\rangle_2 + |HV\rangle_1 |0\rangle_2 + |H\rangle_1 |H\rangle_2 + |V\rangle_1 |V\rangle_2\right) \tag{5.23}$$

$$\times \left(|0\rangle_3 |HV\rangle_4 + |HV\rangle_3 |0\rangle_4 + |H\rangle_3 |H\rangle_4 + |V\rangle_3 |V\rangle_4\right)$$

$$= |\phi_{12}\rangle |\phi_{34}\rangle$$

The total states are sent to a rotated PBS (RPBS) which consist of PBSs with HWPs in each inputs and outputs. Finally one looks at the state of modes 2 and 3 conditioned on two clicks in polarisation sensitive detectors placed in paths 1 and 4. It is direct to calculate the effect of the rotated PBS in the state ψ. However, the projected states after RPBS are complicated and extensive, hence we will consider two paths — path with a vacuum component and path contain one photon.
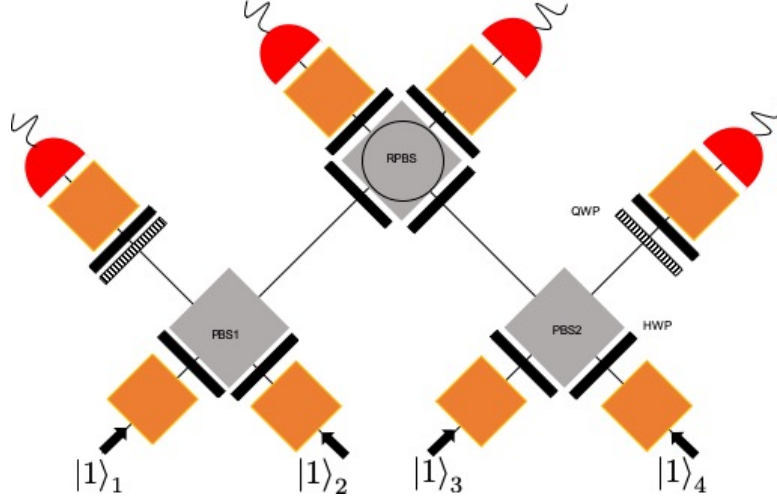
Figure 5.3: Four single photons are sent to the fusion gate as input to two PBS's as shown. The HWPs rotate the outputs of these PBS's. Two of the outputs are then interfered again at the third PBS and successful events are detected by polarisation discriminating single-photon detectors.

5.4.1 One path with a vacuum component

This is where at least one of the paths has zero photons:

$$
\prod{}_0|\psi_{PBS}\rangle = \frac{1}{4}\Bigg((|0\rangle_1|HV\rangle_2 + |HV\rangle_1|0\rangle_2)(|0\rangle_3|HV\rangle_4 + |HV\rangle_3|0\rangle_4)
$$
$$
+ (|0\rangle_1|HV\rangle_2 + |HV\rangle_1|0\rangle_2)(|H\rangle_3|H\rangle_4 + |V\rangle_3|V\rangle_4) \tag{5.24}
$$
$$
+ (|H\rangle_1|H\rangle_2 + |V\rangle_1|V\rangle_2)(|0\rangle_3|HV\rangle_4 + |HV\rangle_3|0\rangle4)\Bigg)
$$

By eliminating terms that does not have two photons in modes 1 and 4 and two photons in modes 2 and 3, we have:

$$
|\psi_{RPBS}\rangle = \frac{1}{4}(|0\rangle_1|HV\rangle_2|0\rangle_3|HV\rangle_4 + |HV\rangle - 1|0\rangle_2|HV\rangle_3|0\rangle_4) \tag{5.25}
$$

The probability of getting this state 1/8. The state after RPBS can be shown as

$$
\mathcal{U}_{RPBS}|0\rangle_1|HV\rangle_4 = \frac{1}{4}\Big(\sqrt{2}(|0\rangle_1|2H\rangle_4 - |2H\rangle_1|0\rangle_4 - |2V\rangle_1|0\rangle_4 + |0\rangle_1|2V\rangle_4)
$$
$$
+2|HV\rangle_1|0\rangle_4 + 2|0\rangle1|HV\rangle_4\Big) \tag{5.26}
$$

$$
\mathcal{U}_{RPBS}|HV\rangle_4|0\rangle_1 = \frac{1}{4}\Big(-\sqrt{2}(|0\rangle_1|2H\rangle_4 - |2H\rangle_1|0\rangle_4 - |2V\rangle_1|0\rangle_4 + |0\rangle_1|2V\rangle_4)
$$
$$
+2|HV\rangle_1|0\rangle_4 + 2|0\rangle1|HV\rangle_4\Big) \tag{5.27}
$$

Above equations show that if there are photons in orthogonal polarisation in either path 1 or 4, we will have two clicks with the probability of getting two clicks at once is 1/2. Hence, the overall probability of going to the state is $1/8 \times 1/2 = 1/6$. If these clicks occur the state will

collapse into

$$|\psi_D\rangle = \frac{1}{\sqrt{2}}(|HV_2\rangle_2|0\rangle_3 + |0\rangle_2|HV\rangle_3), \tag{5.28}$$

This states can be turned into an entangled state by sending photons 2-3 to a PBS that transforms into

$$|\psi_E\rangle = \mathcal{U}_{2,3}|\psi_D\rangle = \frac{1}{\sqrt{2}}(|H\rangle_2|V\rangle_3 + |V\rangle_2|H\rangle_3). \tag{5.29}$$

5.4.2 One photon in each path

Now we look at paths with one photon each. It is given by

$$|\psi_3^1\rangle = (\mathbb{I} - \Pi_0)|\psi_2\rangle = \frac{1}{4}(|H\rangle_1|H\rangle_2 + |V\rangle_1|V\rangle_2)(|H\rangle_3|H\rangle_4 + |V\rangle_3|V\rangle_4) \tag{5.30}$$

The probability of obtaining this state is 1/4. If now one introduces the four (normalised) Bell states

$$|\phi^\pm\rangle = \frac{1}{\sqrt{2}}(|H\rangle|H\rangle \pm |V\rangle|V\rangle), \quad |\psi^\pm\rangle = \frac{1}{\sqrt{2}}(|H\rangle|V\rangle \pm |V\rangle|H\rangle) \tag{5.31}$$

It can be written as

$$|\psi_3^1\rangle = \frac{1}{4}(|\psi^+\rangle_{1,4}|\psi^+\rangle_{2,3} + |\psi^-\rangle_{1,4}|\psi^-\rangle_{2,3} + |\phi^+\rangle_{1,4}|\phi^+\rangle_{2,3} + |\phi^-\rangle_{1,4}|\phi^-\rangle_{2,3}) \tag{5.32}$$

Now, the RPBS with detectors is a Bell state analyser that works half the time (i.e can discriminate only the 2 symmetric Bell states) hence the overall probability for this sector of the ket Eq. 5.22 to generate entangled states is $1/2 \times 1/4 = 1/8$. Adding the probabilities from the two previous subsections we find an overall probability of $1/8 + 1/16 = 3/16$ of preparing a maximally entangled state.

Click pattern $(1_H, 1_V, 4_H, 4_V)$	Projected state $|\psi\rangle_{(1_H,1_V,4_H,4_V)}$	Probability $\rho(1_H, 1_V, 4_H, 4_V)$
(1,0,1,0)	$\frac{1}{8}(|V\rangle_2|V\rangle_3 + |H\rangle_2|H\rangle_3)$	$\frac{1}{32}$
(1,1,0,0)	$\frac{1}{8}(|0\rangle_2|HV\rangle_3 + |HV\rangle_2|0\rangle_3)$	$\frac{1}{32}$
(1,0,0,1)	$\frac{1}{8}(|V\rangle_2|H\rangle_3 + |H\rangle_2|V\rangle_3)$	$\frac{1}{32}$
(0,1,1,0)	$\frac{1}{8}(|V\rangle_2|H\rangle_3 + |H\rangle_2|V\rangle_3)$	$\frac{1}{32}$
(0,0,1,1)	$\frac{1}{8}(|0\rangle_2|HV\rangle_3 + |HV\rangle_2|0\rangle_3)$	$\frac{1}{32}$
(0,1,0,0)	$\frac{1}{8}(|V\rangle_2|V\rangle_3 + |H\rangle_2|H\rangle_3)$	$\frac{1}{32}$

Table 5.1: Different patterns in paths 1 and 4 that can generate a maximally entangled state in paths 2 and 3. This table is assuming that photon number resolving detectors are available and they can distinguish between zero, one and more than one photons.

5.4.3 A simple model of partially indistinguishable photons

So far the calculation assumes fully indistinguishable single photons. Now let us consider partially indistinguishable single-photons [88] initial input state entering the gate:

$$|D_i\rangle = (\sqrt{1-\eta}d^\dagger_{i,1,0} + \sqrt{\eta}d^\dagger_{i,1,i})|\text{vac}\rangle, \tag{5.33}$$

where we can distinguish two term here; the photon entering path i will have a component shared with the other photons $(\sqrt{1-\eta}d^\dagger_{i,1,0}|\text{vac}\rangle$ and a component that is different an orthogonal to all others given by $(\sqrt{1-\eta}d^\dagger_{i,1,i}|\text{vac}\rangle$. The overlap between photons i and j is given by

$$\langle 1_i|1_i\rangle = 1 - \eta \tag{5.34}$$

If they were sent to a Hong-Ou-Mandel (HOM) setup with zero delay then the probability of getting simultaneous clicks in the two output ports is

$$v_{min} = \eta - \frac{\eta^2}{2} \tag{5.35}$$

This is the minimum click probability in a HOM experiment. The maximum click probability is obtained by putting a huge delay between photons i and j and equals $v_{max} = 1/2$. With this two pieces of information we can construct the visibility

$$V = \frac{v_{max} - v_{min}}{v_{max}} = (1 - \eta)^2 = |\langle 1_i|1_j\rangle|^2 \tag{5.36}$$

We can finally write

$$\eta = 1 - \sqrt{V} \tag{5.37}$$

5.4.4 Expected outcome

In this section we will discuss the outcome of entangled photons from partially distinguishable photons. The calculations will be more extensive as we need to consider photons in 4 paths, 2 polarisation and 5 frequency profiles (1 shared profile + 4 different and mutually orthogonal). As a results, this gives 40 different operators. The state after the PBS and RPBS contains 10^4 different components. Since the photons are partially distinguishable, the state of the photons in mode 2 and 3 will no longer be maximally entangled. However, the overall probability of getting the event distribution considered in Table 5.1 does not change and still each event has a probability equal to 1/32. Hence, the normalised density matrices in the basis $|H\rangle_2|H\rangle_3.|H\rangle_2|V\rangle_3, |V\rangle_2|H\rangle_3, |V\rangle_2|V\rangle_3$ are

$$\rho_1 = \begin{pmatrix} \frac{V+1}{4} & 0 & 0 & \frac{V^2}{2} \\ 0 & \frac{1-V}{4} & 0 & 0 \\ 0 & 0 & \frac{1-V}{4} & 0 \\ \frac{V^2}{2} & 0 & 0 & \frac{V+1}{4} \end{pmatrix} \tag{5.38}$$

$$\rho_2 = \begin{pmatrix} \frac{1-V}{4} & 0 & 0 & 0 \\ 0 & \frac{V+1}{4} & \frac{V^2}{2} & 0 \\ 0 & \frac{V^2}{2} & \frac{V+1}{4} & 0 \\ 0 & 0 & 0 & \frac{1-V}{4} \end{pmatrix} = (\mathbb{I} \otimes \sigma_x)\rho_1(\mathbb{I} \otimes \sigma_x) \tag{5.39}$$

The concurrence C of these two states is the same since they are related by a local unitary transformation and can be denotes as [89, 90] :

$$C(V) = \max[0, (2V^2 + V - 1)/2] \tag{5.40}$$

The concurrence function as visibility can be illustrated in Fig. 5.4 where for visibility, V below 0.5, the concurrence $C = 0$, while $V > 0.5$ the concurrence increase near linearly until $C = 1$ for $V = 1$.
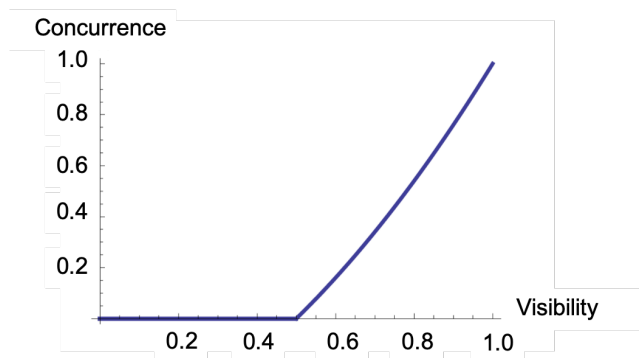
Figure 5.4: Concurrence, *(C)* as a function of visibility, *(V)*

5.5 Experimental setup

5.5.1 Single photon source

Our single photons are generated by our second-generation quantum-dot device at the Quantum Technology Laboratory at The University of Queensland. These devices are InGasAs quantum-dots deterministically coupled to electrically-tuned pillar cavities [57, 91]. The devices are kept in a low vibration closed-cycle, cryostat at 7 Kelvin. The experimental setup is shown in Fig 6.2 where the QD is excited resonantly at its p-shell by a Ti:Sapphire laser wavelength centred at 925.5nm, with a repetition rate of 82 MHz: ie every 12.5ns. The p-i-n diode structure is embedded to the pillar cavity and electrical contacts are defined to control the QD resonance through the confined Stark effect. Photons are preferentially emitted into the cavity mode because of enhanced spontaneous emission. The experiments are performed with a neutral exciton in resonance with the cavity mode, which yields single-photon lifetimes of 160ps and a wavelength 925.47nm. This short single-photon lifetime allows increasing the laser repetition rate by a factor of 4—from 82 to 328 MHz—using a passive pulse multiplier composed of beam-splitters and delay lines. The single photons are collected by a microscope objective lens (Olympus LMPLN-IR/LCPLN-IR N.A $= 0.45$) and pass through a half-wave plate (HWP) and

a quarter-wave plate (QWP) before being separated from the pump excitation by a polarising beam splitter (PBS). The HWP and QWP are design to control the polarization with respect to the cavity and axes to correct any polarization ellipticity arise due to the electrical contact between the p-i-n diode and the pillar [92].
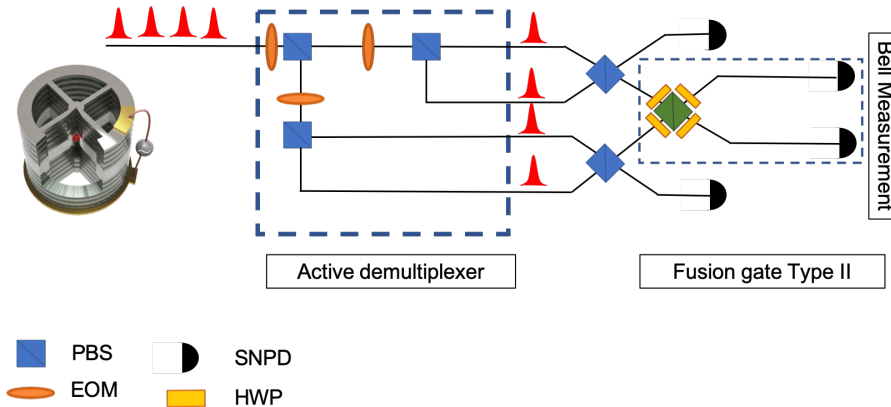

Figure 5.5: Experimental setup for optical entangling gates with single-photon source, active demultiplexer, fusion gate and detectors

5.5.2 Spatio-temporal demultiplexer

A stream of single photons are then collected using single-mode fibre and sent to the demultiplexer. The demultiplexer consist of three intensity electro-optic modulator (EOM) transforming temporal into four-spatial input mode for the entangling gate. This is to ensure that the inputs of the gate remains its indistinguishability even when they are separated more than few nanoseconds [93–95]. We construct a fast demultiplexer using a configurable customised resonance-enhanced QUBIG EOM (20 MHz) with low loss transmission, and a low-voltage control ($\sim 5V$). The demultiplexer four output modes are collected using single-mode fibres. The measured optical transmission of the switches is η_{demux}= 94.8%, 93.7% and 96.7%. By using half-waveplates (HWP) and polarising beam splitter (PBS), the photons are separated into four different spatial modes as input to the fusion gate—path 1 to 4. The polarised single photons are routed into four distinct spatial modes synchronously with the laser trigger. In order to make sure all the single photons arrive simultaneously, we varying appropriate path length of fibres and free space tuning.

5.5.3 Optical entangling gates

All four single photons with the same temporal mode from the demultiplexer are sent to the fusion gate, which we denote as $|1\rangle_1$, $|1\rangle_2$, $|1\rangle_3$ and $|1\rangle_4$. Each pair are then prepared in a diagonal polarisation as in Eq. 5.13. Photon 1 and 2 interfere at PBS1 and Photon 2 and 3 interfere at PBS2. The resulting state after PBS1 and PBS2 interfere at a rotating polarising beam splitter (RPBS) where the Type-II fusion mechanism happens. This can be accomplished by inserting HWPs in both input and output of the PBS. By detecting both output modes, 2

66

and 3, the input state is projected into a maximally entangled Bell state. This will be projected onto one of the four Bell states, which form a complete basis for the combined state of photon 2 and 3 [96]. The advantage of this scheme is once we detect photons at out 2 and 3, we can confirm the entangled pairs at output 1 and output 4. This prepares event-ready entangled pairs of photons for other experiments that require entangled photons.

The polarisation analysis can be read in details in Ref.[82]: the configuration allows one to distinguish between the Bell states due to the different outcomes of the interference at the beam spitter and the subsequent polarisation analysis. The spatial part of the state determines the photon statistics behind the (polarisation insensitive) beam splitter. This result either in both photons leaving the beam splitter via the same output beam for symmetric spatial part or in one photon exiting into each output for antisymmetric spatial component of the state—where a photon state has to be bosonic. ie. symmetric upon exchange of the particle. Thus the symmetry of the spatial part of the wave function will be changed together with the spin part. This is the case when switching to and from ψ^-. For changing between other three Bell states the spatial part of the wave function remains unchanged, giving the characteristic interference effects. Mattle also mentioned that since only the state ψ^- has an antisymmetric spatial part, only this state will be registered by coincidence detection between the different outputs of the beam splitter for instance coincidence between detector D_h and D'_v or between D'_h and D_v).

5.5.4 Quantum tomography

In order to get a comprehensive study of the polarisation entangled state of our system, we perform quantum state tomography by reconstruct the reduced density matrix of the two output photons [97, 98]. To fully characterise the polarisation states, we performed measurement in either the linear basis linear basis $\{|V\rangle, |H\rangle\}$, the diagonal basis $\{|D\rangle, |A\rangle\}$ or the circular basis $\{|R\rangle, |L\rangle\}$ [99]. The setup includes half-and quarter wave-plates, a polarising beam-splitter and single-photon detectors at outputs 2 and 3. The polarisation transformation between the different bases is performed by the two wave-plates. The polarization of the photon is then projected onto the $\{|V\rangle, |H\rangle\}$ basis by the PBS and detected. The tomography for single-qubit is constructed by three linearly independent measurements. If two detectors are utilized at each output, then there are three measurement settings needed to obtain a full description. Assuming the input state is a superposition of the two linear polarizations states $|\psi\rangle = \frac{1}{\sqrt{2}}(|H\rangle + |V\rangle)$, the detected count rates of the two detectors are expected to be equal and half of the total count rate when measuring in the linear polarization basis. But as a eigenstate of the other basis generates the same detection pattern, the chosen measurement setting is not sufficient to faithfully reconstruct the input state. By measuring projection onto the six basis states a detection pattern emerges that is reconciled uniquely by the input state. If the state of interest is a two qubit state, e.g. a Bell state, the tomography is performed by permuting between the two outputs setups to generate nine different measurement settings [100]. The detection events in the different bases are correlated between the two detection setups to achieve a description of the two-qubit state. The fidelity, $\mathcal{F}$ is defined as the overlap with a maximally entangled

state. $|\varphi_e\rangle = (|0\rangle_A|1\rangle_B - |1\rangle_A|0\rangle_B) \sqrt{2}$ as $\mathcal{F} = \langle\varphi_e|\rho|\varphi_e\rangle$. A fidelity $\mathcal{F} > 0.5$ shows that the state ρ is entangled [15]. The fidelity is dependent on the choice of expected state.

The measurement of entanglement of a bipartite system is quantified by the tangle $\tau_{AB}=[\max\{0, \lambda_1 - \lambda_2 - \lambda_3 - \lambda_4\}]^2$ [101] where λ_i is the eigenvalues of the density matrix ρ_{AB} for bipartite system consisting of qubits A and B.

5.6 Results and discussions

5.6.1 QD performance

In order to test the performance of our gates, we characterise our device in terms of multi-photon suppression, which corresponds to the purity of the single photon state, $g^{(2)}$ and its indistinguishability, V_{HOM}. The experiments are performed with only neutral-charged dots. Fig 5.3 (a) depicts the source with $g^{(2)} = 5.9\%$ under integration windows for 2 ns for each peak. Note the value is quite higher than the source reported in [57] due to poor filtering of light scattered from the excitation laser. As previously mentioned, the entanglement depends on the visibility of the two-photon interference. The photon-photon interference is performed between two inputs passing through our entangling gates. The extracted visibility is shown in Fig. 5.3 (b) with $V_{12.5ns} = (85.1 \pm 0.48)\%$. (without background correction) and $V_{12.5ns} = (91.0\%$ (with background correction). From the value we are expecting a concurrence of $\simeq 0.65$ (see Fig. 5.4). As we are at the early installation stage, the experiment is performed without any spectral shaping of the pulse laser. According to [57], with spectral shaping the value approximately about 40 ps, indistinguishability can be observed about 90% and $g^{(2)}$ could be suppressed to 1%. It is interesting to note in this work, the value of V_{HOM} obtained from the experiment were done without any frequency manipulation—either pump shape [57] or filtering the output with an etalon [37]. Both [37, 57] had higher indistinguishability by using a filter to reduce the scattered laser light, and hence improve the indistinguishability of the device. Another way to suppress the scattered excitation laser is by controlling the crossed polarisation laser at the excitation path [92].

Based on Eq. 5.20, we measure the concurrence, C and obtained $C = 0.37 \pm 0.088$. However, one BS had lower $V_{BS2} = 67\%$ and this limits C. Although we have seen a better value of V_{HOM} [57], the photon flux produce by our source is worth to be highlighted as it is in a order of magnitude than reported by Zhang and co-workers [102]. Thus, we observe a clean and clear two-photon interference between single photons via optical entangling gates proven that our source is ready to overcome a proof-of-principle experiment done by [102] from the SPDC source. This scheme was developed assuming the photons are fully indistinguishable and interfered at a perfect beam splitters. If all beamsplitters have identical measured visibility, we expect the concurrence value obtained is higher than $C = 0.37 \pm 0.09$. However, after a thorough investigation we are able to identify the imperfect beam splitter in the setup with $V_{BS2} = 67\%$ and $V_{PBS3} = 95\%$.
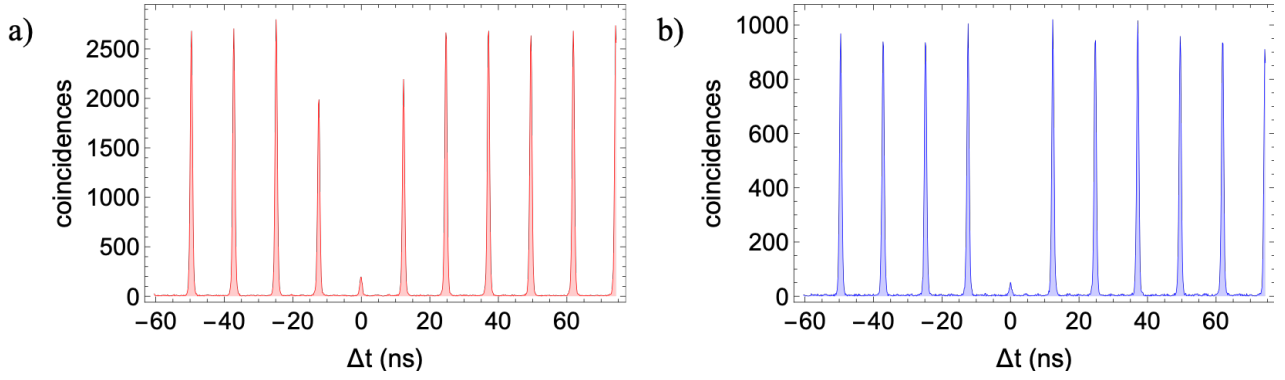
Figure 5.6: Performance of QD single-photon source **a)** Second-order correlation histogram, $g^{(2)}$ for QD under resonant excitation at T = 7 K **b)** Correlation histogram measuring the indistinguishability of single photons emitted at 12.5 ns under resonant excitation. Integration window around each peak = 2 ns.
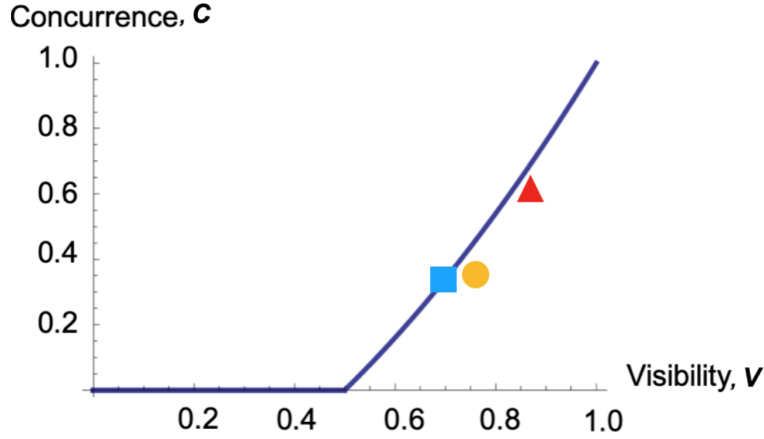

Figure 5.7: Concurrence, C versus visibility, V. The red triangle depicts the value for concurrence if all the beamsplitters have identical measured visibility, $V = 85\%$. The yellow circle is the measured concurrence in the experiment. The blue square is the value expected if the visibility, $V \approx 67\%$.

5.6.2 State tomography

Fig. 5.8 shows the reconstructed density matrix of a $|HV\rangle$ input state, the density matrix is dominated by $|HV\rangle\langle VH|$. The fidelity of the reconstructed density matrix with ideal density matrix is extracted to $F_{|\psi\rangle|HV\rangle} = 0.59 \pm 0.01$. Table 5.1 summaries the measured state of the system.

While in section 5.4.4 predicts the polarisation entangled photons, i.e., stronger outer diagonal element in the real part demonstrate the high probability that the photon pairs have the same linear polarisation. Most significant are the outer-diagonal elements, which are present due to superposition in the two-photon wave function and are clear indictors of entanglement [98]. However, the reconstructed matrix obtained from this work shows otherwise. There are several unwanted contributions that leads to low entanglement. According to Peres [103], the state is inseparable if the partial transpose of $\hat{\rho}$ has nonpositive eigenvalue. Although it does not imply in this particular density matrix, since $\rho_{HV,VH}\rho_{VH,HV}$ contains nonzero, the density matrix already measure a very small amount of entanglement from distinguishable photons.

69

The fidelity value obtained slightly exceeds the classical limit of 0.5 showing a weak entanglement regime obtained from our proposed scheme. The reason behind the weak entanglement value from the density matrix analysis could arise from the imperfect optical elements such the beam-splitters and wave-plates. It has been suggested by Rezai [104] that with the imperfect optical elements, the unitary transformation has been compromised. Furthermore, the optical elements are generally made of dielectric media which have a small absorption amplitude [105] and Scheel [106] proved that imperfect mode matching interference by the beam splitters for instance is non-trivial in entangling gates. This has been proven by a multimode analysis that the imperfect interference is responsible in generating polarisation entangled photons [52]. Furthermore, the degree of entanglement could be improved significantly by reducing the laser background scattered from resonant excitation [51, 107].
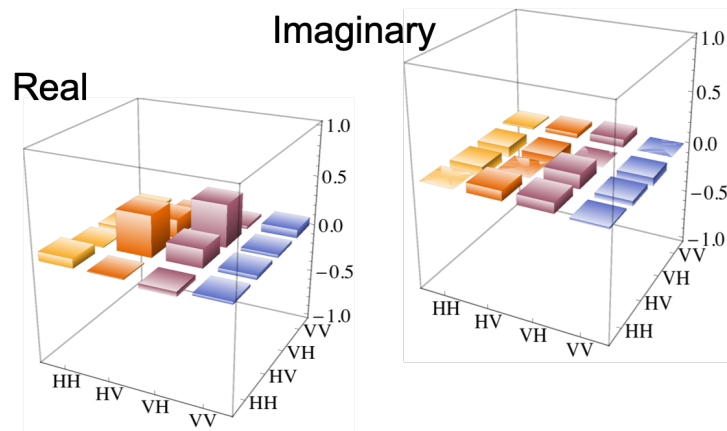
Figure 5.8: State tomography of the projected output detection 1 and 4 a) Real part of the density matrix b) Imaginary part of the density matrix

Measured state	Value
a) Fidelity	0.595 ± 0.02
b) Purity	0.518 ± 0.04
c) Concurrence	0.369 ± 0.09
d) Tangle	0.13 ± 0.07
e) Quantum discord	0.2 ± 0.1

Table 5.2: Summary of the measured entangled photons state fidelities, purity, concurrence, tangle and quantum discord.

REFERENCES

[1] Aspect, A., Grangier, P. & Roger, G. Experimental realization of einstein-podolsky-rosen-bohm gedankenexperiment: a new violation of bell's inequalities. *Physical Review Letters* **49**, 91 (1982).

[2] Walls, D. F. & Milburn, G. J. *Quantum Optics* (Springer Science & Business Media, 2007).

[3] Schrödinger, E. Die gegenwärtige situation in der quantenmechanik. *Naturwissenschaften* **23**, 823–828 (1935).

[4] Einstein, A., Podolsky, B. & Rosen, N. Can quantum-mechanical description of physical reality be considered complete? *Physical Review* **47**, 777 (1935).

[5] Gisin, N., Ribordy, G., Tittel, W. & Zbinden, H. Quantum cryptography. *Reviews of Modern Physics* **74**, 145 (2002).

[6] Bouwmeester, D. *et al.* Experimental quantum teleportation. *Nature* **390**, 575–579 (1997).

[7] Furusawa, A. *et al.* Unconditional quantum teleportation. *Science* **282**, 706–709 (1998).

[8] Edamatsu, K. Entangled photons: generation, observation, and characterization. *Japanese Journal of Applied Physics* **46**, 7175 (2007).

[9] Bell, J. S. On the einstein podolsky rosen paradox. *Physics Physique Fizika* **1**, 195 (1964).

[10] Clauser, J. F., Horne, M. A., Shimony, A. & Holt, R. A. Proposed experiment to test local hidden-variable theories. *Physical Review Letters* **23**, 880 (1969).

[11] Lamehi-Rachti, M. & Mittig, W. Quantum mechanics and hidden variables: A test of bell's inequality by the measurement of the spin correlation in low-energy proton-proton scattering. *Physical Review D* **14**, 2543 (1976).

[12] Sakai, H. *et al.* Spin correlations of strongly interacting massive fermion pairs as a test of bell?s inequality. *Physical Review Letters* **97**, 150405 (2006).

[13] Hagley, E. *et al.* Generation of einstein-podolsky-rosen pairs of atoms. *Physical Review Letters* **79**, 1 (1997).

[14] Turchette, Q. *et al.* Deterministic entanglement of two trapped ions. *Physical Review Letters* **81**, 3631 (1998).

[15] Sackett, C. A. *et al.* Experimental entanglement of four particles. *Nature* **404**, 256–259 (2000).

[16] Kwiat, P. G., Waks, E., White, A. G., Appelbaum, I. & Eberhard, P. H. Ultrabright source of polarization-entangled photons. *Physical Review A* **60**, R773 (1999).

[17] Kwiat, P. G. *et al.* New high-intensity source of polarization-entangled photon pairs. *Physical Review Letters* **75**, 4337 (1995).

[18] Santos, E. Critical analysis of the empirical tests of local hidden-variable theories. *Physical Review A* **46**, 3646 (1992).

[19] Kwiat, P. G., Eberhard, P. H., Steinberg, A. M. & Chiao, R. Y. Proposal for a loophole-free bell inequality experiment. *Physical Review A* **49**, 3209 (1994).

[20] De Caro, L. & Garuccio, A. Reliability of bell-inequality measurements using polarization correlations in parametric-down-conversion photon sources. *Physical Review A* **50**, R2803 (1994).

[21] Shih, Y. & Alley, C. O. New type of einstein-podolsky-rosen-bohm experiment using pairs of light quanta produced by optical parametric down conversion. *Physical Review Letters* **61**, 2921 (1988).

[22] Ou, Z. & Mandel, L. Violation of bell's inequality and classical probability in a two-photon correlation experiment. *Physical Review Letters* **61**, 50 (1988).

[23] Kiess, T., Shih, Y., Sergienko, A. & Alley, C. Einstein-podolsky-rosen-bohm experiment using pairs of light quanta produced by type-ii parametric down-conversion. *Physical Review Letters* **71**, 3893 (1993).

[24] Mair, A., Vaziri, A., Weihs, G. & Zeilinger, A. Entanglement of the orbital angular momentum states of photons. *Nature* **412**, 313 (2001).

[25] Hamel, D. R. *et al.* Direct generation of three-photon polarization entanglement. *Nature Photonics* **8**, 801 (2014).

[26] Rangarajan, R., Goggin, M. & Kwiat, P. Optimizing type-i polarization-entangled photons. *Optics Express* **17**, 18920–18933 (2009).

[27] Wang, X.-L. *et al.* Experimental ten-photon entanglement. *Physical Review Letters* **117**, 210502 (2016).

[28] Scarani, V., De Riedmatten, H., Marcikic, I., Zbinden, H. & Gisin, N. Four-photon correction in two-photon bell experiments. *The European Physical Journal D-Atomic, Molecular, Optical and Plasma Physics* **32**, 129–138 (2005).

[29] Pan, J.-W. *et al.* Multiphoton entanglement and interferometry. *Reviews of Modern Physics* **84**, 777 (2012).

[30] Shields, A. J., Stevenson, R. M. & Young, R. J. Entangled photon generation by quantum dots. In *Single Semiconductor Quantum Dots*, 227–265 (Springer, 2009).

[31] Vlastakis, B. *et al.* Deterministically encoding quantum information using 100-photon schrödinger cat states. *Science* **342**, 607–610 (2013).

[32] Gu, X., Kockum, A. F., Miranowicz, A., Liu, Y.-x. & Nori, F. Microwave photonics with superconducting quantum circuits. *Physics Reports* **718**, 1–102 (2017).

[33] Ozawa, T. *et al.* Topological photonics. *Reviews of Modern Physics* **91**, 015006 (2019).

[34] Wendin, G. Quantum information processing with superconducting circuits: a review. *Reports on Progress in Physics* **80**, 106001 (2017).

[35] Flamini, F., Spagnolo, N. & Sciarrino, F. Photonic quantum information processing: a review. *Reports on Progress in Physics* **82**, 016001 (2018).

[36] Akopian, N. *et al.* Entangled photon pairs from semiconductor quantum dots. *Physical review letters* **96**, 130501 (2006).

[37] Istrati, D. *et al.* Sequential generation of linear cluster states from a single photon emitter. *Nature communications* **11**, 1–8 (2020).

[38] Schimpf, C. *et al.* Quantum dots as potential sources of strongly entangled photons: Perspectives and challenges for applications in quantum networks. *Applied Physics Letters* **118**, 100502 (2021).

[39] Benson, O., Santori, C., Pelton, M. & Yamamoto, Y. Regulated and entangled photons from a single quantum dot. *Physical Review Letters* **84**, 2513 (2000).

[40] Moreau, E. *et al.* Quantum cascade of photons in semiconductor quantum dots. *Physical Review Letters* **87**, 183601 (2001).

[41] Dousse, A. *et al.* Ultrabright source of entangled photon pairs. *Nature* **466**, 217 (2010).

[42] Santori, C., Fattal, D., Pelton, M., Solomon, G. S. & Yamamoto, Y. Polarization-correlated photon pairs from a single quantum dot. *Physical Review B* **66**, 045308 (2002).

[43] Stevenson, R. M. *et al.* A semiconductor source of triggered entangled photon pairs. *Nature* **439**, 179–182 (2006).

[44] Young, R. J. *et al.* Improved fidelity of triggered entangled photons from single quantum dots. *New Journal of Physics* **8**, 29 (2006).

[45] Bayer, M. *et al.* Fine structure of neutral and charged excitons in self-assembled in (ga) as/(al) gaas quantum dots. *Physical Review B* **65**, 195315 (2002).

[46] Juska, G., Dimastrodonato, V., Mereni, L. O., Gocalinska, A. & Pelucchi, E. Towards quantum-dot arrays of entangled photon emitters. *Nature Photonics* **7**, 527–531 (2013).

[47] Kuroda, T. *et al.* Symmetric quantum dots as efficient sources of highly entangled photons: Violation of bell's inequality without spectral and temporal filtering. *Physical Review B* **88**, 041306 (2013).

[48] Bennett, A. *et al.* Electric-field-induced coherent coupling of the exciton states in a single quantum dot. *Nature Physics* **6**, 947–950 (2010).

[49] Stevenson, R. *et al.* Magnetic-field-induced reduction of the exciton polarization splitting in inas quantum dots. *Physical Review B* **73**, 033306 (2006).

[50] Zhang, J. *et al.* High yield and ultrafast sources of electrically triggered entangled-photon pairs based on strain-tunable quantum dots. *Nature communications* **6**, 1–8 (2015).

[51] Muller, A., Fang, W., Lawall, J. & Solomon, G. S. Creating polarization-entangled photon pairs from a semiconductor quantum dot using the optical stark effect. *Physical review letters* **103**, 217402 (2009).

[52] Fattal, D. *et al.* Entanglement formation and violation of bell's inequality with a semiconductor single photon source. *Physical Review Letters* **92**, 037903 (2004).

[53] Trebbia, J.-B., Tamarat, P. & Lounis, B. Indistinguishable near-infrared single photons from an individual organic molecule. *Physical Review A* **82**, 063803 (2010).

[54] Sanaka, K. *et al.* Entangling single photons from independently tuned semiconductor nanoemitters. *Nano letters* **12**, 4611–4616 (2012).

[55] Gazzano, O. *et al.* Entangling quantum-logic gate operated with an ultrabright semiconductor single-photon source. *Physical Review Letters* **110**, 250501 (2013).

[56] Loredo, J. C. *et al.* Scalable performance in solid-state single-photon sources. *Optica* **3**, 433–440 (2016).

[57] Somaschi, N. *et al.* Near-optimal single-photon sources in the solid state. *Nature Photonics* **10**, 340 EP – (2016).

[58] Ding, X. *et al.* On-demand single photons with high extraction efficiency and near-unity indistinguishability from a resonantly driven quantum dot in a micropillar. *Phys. Rev. Lett.* **116**, 020401 (2016).

[59] Wang, H. *et al.* Near-transform-limited single photons from an efficient solid-state quantum emitter. *Phys. Rev. Lett.* **116**, 213601 (2016).

[60] Ollivier, H. *et al.* Reproducibility of high-performance quantum dot single-photon sources. *ACS photonics* **7**, 1050–1059 (2020).

[61] Loudon, R. *The quantum theory of light* (OUP Oxford, 2000).

[62] Bennett, C. H. & Brassard, G. Proceedings of the ieee international conference on computers, systems and signal processing (1984).

[63] Knill, E., Laflamme, R. & Milburn, G. J. A scheme for efficient quantum computation with linear optics. *Nature* **409**, 46–52 (2001).

[64] Gottesman, D. & Chuang, I. L. Demonstrating the viability of universal quantum computation using teleportation and single-qubit operations. *Nature* **402**, 390–393 (1999).

[65] Turchette, Q. A., Hood, C. J., Lange, W., Mabuchi, H. & Kimble, H. J. Measurement of conditional phase shifts for quantum logic. *Physical Review Letters* **75**, 4710 (1995).

[66] Hofmann, H. F. & Takeuchi, S. Quantum phase gate for photonic qubits using only beam splitters and postselection. *Physical Review A* **66**, 024308 (2002).

[67] Nielsen, M. A. Optical quantum computation using cluster states. *Physical Review Letters* **93**, 040503 (2004).

[68] Barrett, S. D. & Kok, P. Efficient high-fidelity quantum computation using matter qubits and linear optics. *Physical Review A* **71**, 060310 (2005).

[69] Briegel, H.-J., Dür, W., Cirac, J. I. & Zoller, P. Quantum repeaters: the role of imperfect local operations in quantum communication. *Physical Review Letters* **81**, 5932 (1998).

[70] Azuma, K., Tamaki, K. & Lo, H.-K. All-photonic quantum repeaters. *Nature communications* **6**, 1–7 (2015).

[71] Bennett, C. H. *et al.* Teleporting an unknown quantum state via dual classical and einstein-podolsky-rosen channels. *Physical Review Letters* **70**, 1895 (1993).

[72] Zeilinger, A., Weihs, G., Jennewein, T. & Aspelmeyer, M. Happy centenary, photon. *Nature* **433**, 230–238 (2005).

[73] Stockill, R. *et al.* Phase-tuned entangled state generation between distant spin qubits. *Physical review letters* **119**, 010503 (2017).

[74] Brendel, J., Gisin, N., Tittel, W. & Zbinden, H. Pulsed energy-time entangled twin-photon source for quantum communication. *Physical Review Letters* **82**, 2594 (1999).

[75] De Riedmatten, H. *et al.* Tailoring photonic entanglement in high-dimensional hilbert spaces. *Physical Review A* **69**, 050304 (2004).

[76] Rossi, A., Vallone, G., Chiuri, A., De Martini, F. & Mataloni, P. Multipath entanglement of two photons. *Physical Review Letters* **102**, 153902 (2009).

[77] Takesue, H. & Inoue, K. Generation of polarization-entangled photon pairs and violation of bell?s inequality using spontaneous four-wave mixing in a fiber loop. *Physical Review A* **70**, 031802 (2004).

[78] Paris, M. G. Entanglement and visibility at the output of a mach-zehnder interferometer. *Physical Review A* **59**, 1615 (1999).

[79] Kwiat, P. G., Barraza-Lopez, S., Stefanov, A. & Gisin, N. Experimental entanglement distillation and hidden non-locality. *Nature* **409**, 1014–1017 (2001).

[80] Milburn, G. Photons as qubits. *Physica Scripta* **2009**, 014003 (2009).

[81] Zeilinger, A. General properties of lossless beam splitters in interferometry. *American Journal of Physics* **49**, 882–883 (1981). `https://doi.org/10.1119/1.12387`.

[82] Mattle, K., Weinfurter, H., Kwiat, P. G. & Zeilinger, A. Dense coding in experimental quantum communication. *Physical Review Letters* **76**, 4656 (1996).

[83] Browne, D. E. & Rudolph, T. Resource-efficient linear optical quantum computation. *Phys. Rev. Lett.* **95**, 010501 (2005).

[84] Yoran, N. & Reznik, B. Deterministic linear optics quantum computation with single photon qubits. *Physical Review Letters* **91**, 037903 (2003).

[85] Raussendorf, R. & Briegel, H. J. A one-way quantum computer. *Phys. Rev. Lett.* **86**, 5188–5191 (2001).

[86] Raussendorf, R., Browne, D. E. & Briegel, H. J. Measurement-based quantum computation on cluster states. *Phys. Rev. A* **68**, 022312 (2003).

[87] Quesada, N. Fusion gates with partially distinguishable photons. *Unpublished* (2016).

[88] Ralph, T. C., Langford, N. K., Bell, T. & White, A. Linear optical controlled-not gate in the coincidence basis. *Physical Review A* **65**, 062324 (2002).

[89] Wootters, W. K. Entanglement of formation of an arbitrary state of two qubits. *Physical Review Letters* **80**, 2245 (1998).

[90] Hill, S. & Wootters, W. K. Entanglement of a pair of quantum bits. *Physical Review Letters* **78**, 5022 (1997).

[91] Nowak, A. *et al.* Deterministic and electrically tunable bright single-photon source. *Nature communications* **5**, 3240 (2014).

[92] Hilaire, P. *et al.* Accurate measurement of a 96% input coupling into a cavity using polarization tomography. *Applied Physics Letters* **112**, 201101 (2018).

[93] Wang, H. *et al.* High-efficiency multiphoton boson sampling. *Nature Photonics* **11**, 361–365 (2017).

[94] Wang, H. *et al.* Toward scalable boson sampling with photon loss. *Physical Review Letters* **120**, 230502 (2018).

[95] Latmiral, L., Spagnolo, N. & Sciarrino, F. Towards quantum supremacy with lossy scattershot boson sampling. *New Journal of Physics* **18**, 113008 (2016).

[96] Pan, J.-W., Bouwmeester, D., Weinfurter, H. & Zeilinger, A. Experimental entanglement swapping: entangling photons that never interacted. *Physical Review Letters* **80**, 3891 (1998).

[97] White, A. G., James, D. F., Eberhard, P. H. & Kwiat, P. G. Nonmaximally entangled states: production, characterization, and utilization. *Physical Review Letters* **83**, 3103 (1999).

[98] James, D. F., Kwiat, P. G., Munro, W. J. & White, A. G. On the measurement of qubits. In *Asymptotic Theory of Quantum Statistical Inference: Selected Papers*, 509–538 (World Scientific, 2005).

[99] Altepeter, J. B., Jeffrey, E. R. & Kwiat, P. G. Photonic state tomography. *Advances in Atomic, Molecular, and Optical Physics* **52**, 105–159 (2005).

[100] Altepeter, J. B., James, D. F. & Kwiat, P. G. 4 qubit quantum state tomography. In *Quantum state estimation*, 113–145 (Springer, 2004).

[101] Coffman, V., Kundu, J. & Wootters, W. K. Distributed entanglement. *Physical Review A* **61**, 052306 (2000).

[102] Zhang, Q. *et al.* Demonstration of a scheme for the generation of "event-ready" entangled photon pairs from a single-photon source. *Physical Review A* **77**, 062316 (2008).

[103] Peres, A. Separability criterion for density matrices. *Physical Review Letters* **77**, 1413 (1996).

[104] Rezai, M., Wrachtrup, J. & Gerhardt, I. Polarization-entangled photon pairs from a single molecule. *Optica* **6**, 34–40 (2019).

[105] Kok, P. *et al.* Linear optical quantum computing with photonic qubits. *Reviews of Modern Physics* **79**, 135 (2007).

[106] Scheel, S. Lower bounds on the absorption probability of beam splitters. *Physical Review A* **73**, 013809 (2006).

[107] Huber, D. *et al.* Highly indistinguishable and strongly entangled photons from symmetric gaas quantum dots. *Nature Communications* **8**, 15506 (2017).

CHAPTER 6

CONCLUSIONS AND OUTLOOK

In this thesis, I have built a strong platform for producing multi-fold single photons at higher rates than those available based on spontaneous parametric down-conversion sources. By optimising the optical setup we successfully improve collection efficiency of the photon emission and couple it to a single mode fiber, allowing it to be further used in quantum experiments. The stream of photons are mutually indistinguishable even when separated by as long as 400 ns. The source is suitable for use with integrated photonics: here we used it with an integrated switch, realising an active demultiplexer: an important step on the route to scalable technologies. Taking advantage of our bright source, we realised a six-photon rate three orders-of-magnitude higher that the probabilistic source based on down conversion [1]. In future, the switching efficiency can be increased using Reverse Proton exchange technique [2]. The de-multiplexed first generation device can only be excited non-resonantly, creating time-jitter, and subsequently leading to dephasing of single photon emission. This limits the photons linewidth, and thus the photon indistinguishability.

Ultimately, we are in the pursuit of a device that can be driven coherently. To this end I installed a second generation device that is on electrically tunable. It was fabricated by our collaborator group at the CNRS in France using a new technique to couple electric contacts to the micropillar cavities. Applying voltage through these contact allows tuning of the dot transition via the Stark shift, and so the ability to excite the dot in resonance with its transition. In addition, the applied voltage stabilises the electrostatic environment surrounding the quantum dot, minimising variations in emission. This allows us to perform a resonant excitation on the dot. We developed a scheme to generate entangled pairs of photons from the stream of single photons emitted by our second generation device. The scheme is that proposed by Browne and Rudolph [3] and further modelled by N. Quesada [4] using only linear optical elements such as beam-splitters, phase-shifters and detectors. Although my measured value of indistinguishability $V_{HOM} = (85.1 \pm 0.48)\%$ is slightly lower than the same device in [5], the device out-performed the Bell and Rudolph scheme realised with donwncoversion [6], with greater photon flux over a short integration time.

In the near future, we aim to improve our entangled photon pairs by improving the indistinguishability of our single-photons. In order to improve the visibility, we need to improve its multiphoton suppressions. The first step is to completely eliminate the background laser scattering from the collection path [7, 8] and side excitation [9]. The side excitation is where

the pump path is orthogonal to the collection path. This optimises the indistinguishability of the single photon by reducing background scattering while preserving other characteristics. The second step is to design a pulse-shaper to adjust the temporal shape of the excitation pulse laser [10, 11]. This allows us to shape the pump pulses for optimal frequency match between the pump pulse and the cavity [12], further improving the indistinguishability of the single photons.

On the technical side, the on-demand experiment requires careful stabilisation of the laser energy and power, as small fluctuations in these parameters dramatically affect state tomography. The final step to improve device efficiency is to introduce an adaptive-optics to the collection path, to optimise free-space to single-mode fiber coupling. The adaptive-optics serves as a wavefront corrector by minimising wavefront aberrations simultaneously maximising the convex coupled-power [13]. The preliminary results from the on-demand entanglement experiment are very encouraging: in future there will be high quality entanglement available on-demand from solid-state photon sources. However, due to current pandemic COVID-19, the maintenance progress in order to get the system ready is double the length period time than pre-pandemic time.

REFERENCES

[1] Lenzini, F. *et al.* Active demultiplexing of single photons from a solid-state source. *Laser & Photonics Reviews* **11**, 1600297 (2017).

[2] Lenzini, F., Kasture, S., Haylock, B. & Lobino, M. Anisotropic model for the fabrication of annealed and reverse proton exchanged waveguides in congruent lithium niobate. *Optics Express* **23**, 1748–1756 (2015).

[3] Browne, D. E. & Rudolph, T. Resource-efficient linear optical quantum computation. *Phys. Rev. Lett.* **95**, 010501 (2005).

[4] Quesada, N. Fusion gates with partially distinguishable photons. *Unpublished* (2016).

[5] Somaschi, N. *et al.* Near-optimal single-photon sources in the solid state. *Nature Photonics* **10**, 340 EP – (2016).

[6] Zhang, Q. *et al.* Demonstration of a scheme for the generation of ?event-ready? entangled photon pairs from a single-photon source. *Physical Review A* **77**, 062316 (2008).

[7] Hilaire, P. *et al.* Accurate measurement of a 96% input coupling into a cavity using polarization tomography. *Applied Physics Letters* **112**, 201101 (2018).

[8] Tomm, N. *et al.* A bright and fast source of coherent single photons. *Nature Nanotechnology* **16**, 399–403 (2021).

[9] Ates, S. *et al.* Post-selected indistinguishable photons from the resonance fluorescence of a single quantum dot in a microcavity. *Physical Review Letters* **103**, 167402 (2009).

[10] Pursley, B., Carter, S., Yakes, M., Bracker, A. & Gammon, D. Picosecond pulse shaping of single photons using quantum dots. *Nature communications* **9**, 1–6 (2018).

[11] Béguin, L. *et al.* On-demand semiconductor source of 780-nm single photons with controlled temporal wave packets. *Physical Review B* **97**, 205304 (2018).

[12] Rohde, P. P., Ralph, T. C. & Nielsen, M. A. Optimal photons for quantum-information processing. *Physical Review A* **72**, 052332 (2005).

[13] Jobling, S., McCusker, K. & Kwiat, P. G. Adaptive optics for improved mode-coupling efficiencies. In *Laser Science*, JWA32 (Optical Society of America, 2008).